

Dissertation
submitted to the
Combined Faculties for Natural Sciences and for Mathematics
of the Ruperto-Carola University of Heidelberg, Germany
for the degree of
Doctor of Natural Sciences

Presented by
Ulrike Lemke
Diploma: Biochemistry, University of Leipzig, Germany
Date and Place of Birth: 14.03.1978 in Salzwedel, Germany

The role of transcriptional repressor Hes-1 in glucocorticoid-mediated fatty liver development

Referees:

Prof. Dr. Lutz Gissmann (University of Heidelberg/ DKFZ)

PD Dr. Ursula Klingmüller (University of Heidelberg/DKFZ)

Science is organized knowledge.

Immanuel Kant (German Philosopher, 1724 – 1804)

Abstract

Aberrant hepatic fat accumulation (“fatty liver”) represents a pathophysiological hallmark of obesity and is associated with extended glucocorticoid therapy, obesity, Type II diabetes, and starvation. Elevated glucocorticoid levels under these conditions are causative for the fatty liver phenotype, although the molecular mechanisms of their action remain largely unclear.

This study demonstrates that glucocorticoids (GCs) promote fatty liver development through facilitated fat transport into the liver and not due to increased *de novo* fat synthesis. Transient knock-down of hepatic GR was associated with decreased hepatic gene expression of the fat transporters CD36 and caveolin 1 and with decreased expression of peroxisome proliferation-activating receptor gamma (PPAR γ) – a transcription factor promoting CD36 and caveolin expression.

Moreover, glucocorticoids inhibited hepatic expression of transcriptional repressor Hairy and Enhancer of Split-1 (Hes-1) a previously identified anti-lipogenic factor. In fatty liver mouse models characterized by elevated GC levels diminished Hes-1 levels correlated with increased hepatic lipid stores. Genetic restoration of hepatic Hes-1 levels in obese mice normalized hepatic triglyceride levels and improved systemic insulin sensitivity. In mice injected with GCs for three weeks, genetically restored hepatic Hes-1 levels inhibited GC-induced liver fat accumulation. In both models, sustained Hes-1 was accompanied by increased oxidative consumption of triglycerides and decreased fat import into the liver. Hes-1 re-expression inhibited hepatic PPAR γ , CD36 and caveolin expression resembling effects in mice with transient GR knockdown. Loss of function analysis in primary hepatocytes confirmed PPAR γ and Cav1 as Hes-1 target genes. The data suggest that Hes-1 antagonizes GR-mediated transcriptional regulation of fat transport programs in the liver.

Mechanistically, glucocorticoid exposure of hepatocytes lead to the disassembly of a cAMP-dependent CREB transactivator complex on the proximal *Hes-1* gene promoter. The glucocorticoid receptor was shown here to decrease intracellular P-CREB levels and to interact with CREB via the bZIP domain of CREB. Furthermore, GR associated to glucocorticoid response elements in the proximal *Hes-1* promoter region.

Inhibition of hepatic Hes-1 provides a rationale for glucocorticoid-induced fatty liver development. Restoration of Hes-1 activity might, therefore, represent a new approach in the treatment of Non-Alcoholic Fatty Liver Disease and its associated complications such as hepatic insulin resistance.

Zusammenfassung

Die erhöhte Einlagerung von Neutralfetten in der Leber ("Fettleber") stellt ein pathophysiologisches Kennzeichen von Fettleibigkeit dar und korreliert mit Langzeit-Glucocorticoid-Therapie, Typ II Diabetes und Übergewicht aber auch mit Langzeithungern. Erhöhte Glucocorticoidwerte in den genannten Zuständen verursachen das Auftreten der Fettleber. Die zugrunde liegenden molekularen Mechanismen sind bisher jedoch nur wenig erforscht.

In der vorliegenden Arbeit konnte gezeigt werden, dass Glucocorticoide (GCs) die Entstehung einer Fettleber begünstigen, indem sie die Aufnahme von Fetten in die Leber über Fetttransporter erleichtern. Andererseits konnte keine erhöhte Neusynthese von Fetten als Ursache der Glucocorticoid-bedingten Fettleber belegt werden. Transiente Verminderung des hepatischen Glucocorticoid-Rezeptors (GR) mittels shRNAs wird von einer erniedrigten Genexpression der Fetttransporter CD36, Caveolin1 und von einer Unterdrückung der Expression von Peroxisome Proliferation-Activating Receptor gamma (PPAR γ) begleitet, der die Expression von CD36 und Cav1 anregt.

Darüber hinaus inhibieren GCs die hepatische Expression des anti-lipogenen transkriptionellen Repressors Hairy and Enhancer of Split (Hes-1). In Fettlebermodellen, in denen erhöhte Glucocorticoid-Konzentrationen auftreten, korrelieren erniedrigte hepatische Hes-1 Mengen mit erhöhten Leberfettwerten. Genetische Wiederherstellung der Leber-Hes-1-Mengen in übergewichtigen Mäusen hat eine Normalisierung der Leberfette zur Folge und verbessert gleichzeitig die systemische Insulinsensitivität. In mit GCs behandelten Mäusen inhibieren aufrechterhaltene Hes-1 Spiegel den Transport von Fetten in die Leber und damit deren Ansammlung in Hepatozyten. Hes-1 vermindert die Expression von PPAR γ , CD36 und Cav1, was dem Phänotyp in hepatischen GR Knock-down Mäusen gleicht. Hes-1 Erniedrigung durch shRNAs in primären Hepatozyten bestätigt Cav1 und PPAR γ als Hes-1 Zielgene.

In *in vivo* Hes-1-Promotorstudien destabilisieren GCs den cAMP-abhängigen CREB Transaktivatorkomplex. Der GR verringert intrazelluläre P-CREB Mengen und kann außerdem mit der bZIP-Domäne des CREB-Proteins interagieren. Schließlich bindet der GR direkt an Glucocorticoid Response Elemente in der proximalen Hes-1 Promotorregion.

Zusammengefaßt stellt die Inhibierung der hepatischen Hes-1 Mengen eine Ursache der Glucocorticoid-induzierten Fettleber dar. Die Aufrechterhaltung der Leber-Hes-1-Aktivität kann daher als neuer Ansatz in der Behandlung der Nicht-Alkohol-abhängigen Fettleber und deren Folgeerkrankungen wie zum Beispiel hepatische Insulinresistenz angesehen werden.

Acknowledgements

First of all I would like to thank my supervisor Dr. Stephan Herzig for offering me the opportunity to work in his lab and for the challenging and interesting project. I want to thank him for many scientific discussions that deeply broadened my knowledge, for critical suggestions and guidance through many technical and theoretical problems and most importantly for the encouraging and optimistic attitude, when I had lost faith in my work.

I also want to thank the other members of my thesis advisory committee, namely Prof. Dr. Günther Schütz and Prof. Dr. Lutz Gissmann for critical evaluation of the progress of my work and for assuring that my thesis stayed on the right track. In addition I want to thank Prof. Dr. Schütz for providing L-GRKO mice, that were invaluable for my project. Thanks to Dr. Efferth for his tremendous work in further improving the graduate training of PhD students and for being so open minded.

I want to thank Prof. Dr. Andrew Cato from the Forschungszentrum Karlsruhe for kindly supporting me with MKP-1 knock-out mice. Special thanks to Jana Maier who helped during the preparation of these mice even at impossible working hours. I want to mention Milen Kirilov, Gitta Erdmann and Daniel Habermehl from the Schütz lab for providing reagents, helping with mouse studies and for introducing me into the complex world of glucocorticoid biology. A big thank also to PD Dr. Ursula Klingmüller, Sebastian Bohl and Peter Nickel from the Department of “Systems Biology of Signal Transduction”, who provided primary hepatocytes.

Of course, I would like to thank all members of the Herzig lab for critical discussions, a lot of technical support and the scientific spirit. I owe special thanks to our lab technician Dagmar Metzger, who managed ordering of the most seldom reagents and continuously helped with experiments. Also very special thanks to Anja Ziegler, who injected the adenoviruses into my mice with perfection and thereby greatly contributed to the success of this work. Thanks to Anke, Anna, Evgeny, Inka, Nicola and Prachiti for sharing the fate of being a PhD student. Thanks to Ulrike Hardeland for sharing her indefinite methodological knowledge in biochemical assays that helped me to succeed in vitro. Special thanks to Anja Krones-Herzig for her outstanding scientific and personal support during the critical phase of the thesis work.

Most of all, I would like to thank Alexander Vegiopoulos, Mauricio Berriel-Diaz and Tessa Walcher for their continuous scientific support, their ingenious ideas, a lot of scientific and “science-related” discussions and for offering me their friendship. Without you guys, I would have gone crazy!

Finally, I would like to thank my mother, my sister and my friends for always supporting me with my plans, for distracting me and for cheering me up. Thanks to Claudia Kloth and Jeffrey Grenda, who critically reviewed this manuscript and encouraged me to start a PhD thesis. I will never forget the fun times we spent together! I especially want to thank Alexander for his patience and kindness during the sinusoidal course of my mood. I will never ever again postpone holidays.

Table of contents

Abstract	IV
Zusammenfassung	V
Acknowledgements	VI
Table of Contents	VIII
1 Introduction	12
1.1 Metabolic homeostasis and the liver	12
1.1.1 Regulation of Liver Metabolism	13
1.2 Transcription factors in metabolic control	14
1.2.1 Molecular mechanisms of metabolic control	14
1.3 Transcriptional regulation of liver metabolism	15
1.3.1 Transcriptional control mediated by glucagon	16
1.3.2 Glucocorticoids and the glucocorticoid receptor	17
1.3.3 Insulin signaling and transcriptional control	18
1.4 Obesity – a risk factor for metabolic disease	20
1.4.1 Non-alcoholic fatty liver disease	21
1.5 Metabolic disease and transcription factors	22
1.5.1 The implication of glucocorticoids in fatty liver development	23
2 Aim of the Study	24
3 Results	25
3.1 Generation of adenoviruses encoding for shRNAs against murine GR	25
3.2 Transient knock-down of hepatic GR in two fatty liver mouse models	27
3.2.1 shRNA-induced knockdown of GR	27
3.2.2 Target gene analysis after GR knockdown	29
3.3 Investigation of Hes-1 levels in different fatty liver mouse models	33

3.3.1	Starvation-induced fatty liver	33
3.3.2	Chronic fatty liver models	34
3.3.3	Model of diet-induced obesity (DOI)	36
3.3.4	Determination of serum glucocorticoids in fatty liver mouse models	37
3.4	The physiological signal causing decreased Hes-1 expression	38
3.4.1	Glucocorticoid treatment of C57BL/6J mice and its consequences on hepatic Hes-1 expression	38
3.4.2	Starvation experiment in mice with a hepatic glucocorticoid receptor knock-out	42
3.5	Rescue of Hes-1 levels during starvation and in a pathophysiological mouse model	44
3.5.1	Hepatic Hes-1 overexpression in wt C57BL/6J mice	44
3.5.2	Hepatic Hes-1 overexpression in db/db mice	47
3.5.3	Phenotype analysis of Hes-1 overexpression in db/db mice	50
3.5.4	Reconstitution of diminished Hes-1 in dexamethasone-treated mice	52
3.5.5	Generation of Hes-1 RNAi Adenoviruses	54
3.5.6	RNAi experiment in primary hepatocytes	55
3.5.7	Promoter analysis of new target genes for N-Box elements	57
3.6	Mechanism of GC/GR mediated Hes-1 repression	57
3.6.1	Glucocorticoids regulate Hes-1 expression on the transcriptional level	57
3.6.2	Direct interference of GR on the Hes-1 promoter	60
3.6.3	The GR binds to the proximal Hes-1 promoter region	61
3.6.4	The GR binds to two elements on the Hes-1 promoter	62
3.7	GR-mediated dephosphorylation of CREB	63
3.7.1	Dexamethasone treatment of MKP-1 ^{-/-} mice	63
3.7.2	Protein-protein interactions	67
3.7.3	p300 can reverse GR/GC-mediated inhibition of CREB	71
3.7.4	Consequences of CREB dephosphorylation for Hes-1 promoter activation	72
4	Discussion	74
4.1	Acute hepatic GR knockdown in fatty liver ameliorates steatosis by decreased fat import and increased fat utilization	74

4.2	Effects of transient hepatic GR knockdown on glucose metabolism	76
4.3	Transcriptional repressor Hes-1 represents an inhibitory GR target in steatotic liver	76
4.4	Role of Hes-1 in hepatic lipid metabolism	78
4.5	Genes regulated in Hes-1 loss-of function and gain-of-function models	79
4.6	GR-mediated regulation of the Hes-1 promoter	80
4.7	Outlook	83
5	Methods and Materials	84
5.1	Molecular Biology	84
5.1.1	DNA gel electrophoresis	84
5.1.2	Extraction of DNA fragments from agarose gels	84
5.1.3	Transformation of bacteria for plasmid amplification	84
5.1.4	Plasmid purification	85
5.1.5	Isolation of genomic DNA from murine tissue	85
5.1.6	RNA isolation with Qiazol™ Lysis Reagent	86
5.1.7	RNA isolation with RNeasy Mini purification kit	87
5.1.8	Evaluation of RNA quality and quantification	87
5.1.9	cDNA synthesis	88
5.1.10	Quantitative Real-Time PCR	89
5.2	Cell Biology	90
5.2.1	Cell line treatment and transfection	90
5.2.2	Harvest of transfected cells	91
5.2.3	Measurement of luciferase activity	91
5.2.4	Measurement of β -galactosidase activity	92
5.3	Biochemistry	92
5.3.1	Preparation of Protein Extracts from liver samples using PGC buffer	92
5.3.2	Preparation of Protein Extracts from liver samples using SDS lysis buffer	93
5.3.3	Protein determination with the BCA™ method	93
5.3.4	Protein determination with the 2D-Quant Kit	94
5.3.5	SDS-PAGE	94

5.3.6	Immunoblotting	95
5.3.7	Isolation of hepatic lipids	96
5.3.8	Isolation of hepatic glycogen	96
5.3.9	Colorimetric Assays	97
5.3.10	ABCD Assay	99
5.3.11	Chromatin Immunoprecipitation (ChIP-Assay)	102
5.3.12	Radioimmunoassay for corticosterone	105
5.4	Animal experiments	106
5.4.1	Glucose tolerance test	106
5.4.2	Insulin tolerance test	106
5.5	Generation and production of Adenoviruses	107
5.5.1	Cloning of adenoviruses	107
5.5.2	Virus harvest by Freeze-and-Thaw-Method	108
5.5.3	Virus production	109
5.5.4	Cesium chloride gradient	109
5.5.5	Virus titration	110
5.6	Buffers	111
5.7	Plasmids	112
6	Appendix	113
6.1	Abbreviations	113
6.2	Figures	115
6.3	Tables	116
7	Bibliography	117

1 Introduction

During 2.5 million years of human development, the principal evolutionary pressure to survival has been famine. The development of adipocytes as energy stores provided means for coping with the occurrence of undernutrition (1). With the industrial revolution, an unprecedented change in the availability of food took place in western countries. For the first time famine was replaced by unending overnutrition, the effects of which were furthermore amplified by permanent underexertion imposed by sedentary occupations and immobilizing technologies of modern life (1). Since compensatory mechanisms that buffer the metabolic consequences of short-term overnutrition were incapable of compensating for such chronic changes in caloric balance, diseases of overnutrition became increasingly prevalent. Nowadays, poor diet and physical inactivity are the second leading cause of preventable death in the United States and are predicted to be number one within the next decade (2).

Diseases associated with overnutrition and obesity include coronary artery disease and the so-called Metabolic Syndrome – an umbrella term summarizing complications such as dyslipidemia, hypertension, insulin resistance, fatty liver, non insulin-dependent diabetes mellitus (NIDDM) and heart disease (3-5). With regard to the prevalence of obesity in western societies and the steadily growing number of patients suffering from obesity the Metabolic Syndrome, and its consequences will be a major cause of morbidity and mortality in the so-called civilized countries. While it is no longer doubted that the excessive fat storage itself is not harmless, it remains unclear how much fat accumulation can be tolerated and whether an upper threshold for the absolute amount exists.

1.1 Metabolic homeostasis and the liver

Energy homeostasis is a prerequisite for a healthy organism and many tissues participate in the maintenance of it. Amongst them, the liver plays a unique role as it represents the largest gland of the organism. It is one of the main tissues involved in the regulation of protein-, lipid- and carbohydrate metabolism (6, 7), and secretes a number of essential proteins into the blood such as coagulation factors (fibrinogen), lipoproteins and albumins (8). The liver is also a major source of fatty acids, triglycerides, ketone bodies and cholesterol (9, 10). Additionally, it produces bile and secretes it through a duct system. Bile serves as an emulsifier of fats thereby increasing solubility of dietary fat and facilitating their subsequent enzymatic cleavage. Moreover, the liver detoxifies the organism by removing metabolic side products such as

bilirubin and excess hormones. It metabolises drugs and toxins to prepare them for secretion. Vitamin B12 and minerals are stored in the liver, vitamin A is synthesized. Specialized liver cells, so-called Kupffer cells clear particulate material from the blood stream by phagocytosis (11, 12).

Glucose homeostasis is achieved by the liver through removal of glucose from the blood after ingestion of food and storing it as glycogen. During fasting periods, liver glycogen is converted back into glucose and released into the serum to maintain blood glucose levels and to supplement extrahepatic tissues such as brain, erythrocytes and renal medulla (13). If glycogen stores are empty, the liver generates glucose from carbohydrate and amino acid precursors. Fats cannot be converted into glucose. The process of *de novo* glucose synthesis is called gluconeogenesis and solely occurs in liver and to a small degree in the cortex of the kidneys.

Lipids transported into the liver serve on one hand as energy source for the organ. Free fatty acids can be activated and oxidized to the C2-precursor acetyl-CoA and NADH via β -oxidation. Acetyl-CoA can subsequently be metabolized in the citrate cycle or used for cholesterol biosynthesis. Excess acetyl-CoA is used for the synthesis of ketone bodies, which are secreted into the blood and serve as energy source for peripheral tissues. Dietary fats, that are not consumed to generate energy are transformed into phospholipids and triacylglycerides and transported in lipoprotein particles to adipose tissue, where they are stored. Serum free fatty acids can bind to serum albumins secreted from the liver and are transported to skeletal muscle or heart, where they are directly metabolized.

Overall, the liver represents an allocation center distributing metabolites as diverse as glucose, cholesterol, ketone bodies and triglycerides between different tissues to meet the energy demands of the organism. Impaired liver function severely deteriorates whole body energy balance.

1.1.1 Regulation of Liver Metabolism

The fast and direct response of the liver to nutritional signals is accomplished by an ingenious and complex system of endocrine signals generated in the pancreas and the adrenal glands. After ingestion, the pancreatic β -cell hormone insulin triggers fast glucose uptake into peripheral tissues such as adipose tissue and skeletal muscle by stimulating translocation of glucose transporter GLUT4 to the cell membrane (14). Glucose enters the liver via a different glucose transporter – GLUT2 – that is not translocated to the cell membrane in an insulin-dependent manner (15). However, insulin inhibits hepatic gluconeogenesis and glycogen breakdown, thereby decreasing hepatic glucose output. At the same time, glycogen synthesis and *de novo*

triglyceride synthesis (lipogenesis) are stimulated. Thus, insulin maintains blood glucose concentrations in a range between 4 and 7 mM (16). Taken together, insulin signals a state of energy abundance and activates storage of fat and glycogen.

Under fasting conditions the peptide-hormone glucagon (secreted from pancreatic α -cells), catecholamines (e.g. epinephrin) and the steroid hormones glucocorticoids (derived from adrenal glands) are released into the serum. Glucagon mainly stimulates hepatic glycogen breakdown within the first 24h of fasting. Once the glycogen stores are exhausted hepatic gluconeogenesis synergistically triggered by glucagon and glucocorticoids becomes the major source of glucose. To conserve blood glucose levels, glucocorticoids suppress glucose uptake in muscle and adipose tissue.

Glucagon, epinephrin and glucocorticoids furthermore enhance lipolysis in adipocytes and liver (17-21) to augment substrate availability for β -oxidation.

1.2 Transcription factors in metabolic control

1.2.1 Molecular mechanisms of metabolic control

Metabolic regulation in complex organisms consists of three main types of control. The first relies on the allosteric control of the activity of a key metabolic enzyme achieved by binding of an activator or inhibitor, which often is the enzyme substrate itself (22). Secondly, equilibrium of an enzyme between its active and inactive state can be adjusted by posttranslational modifications (e.g. phosphorylation, glycosylation, sumoylation etc.) or by proteolytic cleavage. These chemical alterations may also affect protein stability. The third mechanism is transcriptional regulation through which the expression level of key enzymes is adjusted (22). Most metabolic regulations are clearly realized by a coordinated action of all three mechanisms. However, in the following sections the focus will be on the role of transcriptional regulation in metabolic control.

Transcriptional control requires specific signals to be transduced to the nucleus of the cell where subsequently defined sets of genes are targeted. The process can be subdivided into three successive steps that are 1) the transduction of the signal through the cell until it reaches the nucleus (upstream of transcriptional activity), 2) the molecular mechanism by which transcription factors will act and 3) effects that follow downstream of transcriptional activity and that are determined by the target genes ultimately leading to homeostasis.

1.2.1.1 General mechanism of transcriptional regulation

Eukaryotic DNA exists in the compacted form of chromatin, where the DNA is wound around histone proteins in a complex called nucleosome (23). The nucleosome is composed of ~146bp DNA associated with an octamer of two molecules each of core histone proteins (H2A, H2B, H3 and H4) (24). Through DNA histone interaction the DNA is not accessible for the enzyme RNA polymerase II, which catalyses the synthesis of mRNA. This conformation of chromatin is described as closed and is associated with suppression of gene expression (25). It may also be noted here, that further compaction is achieved by interactions between nucleosomes and histones such as H1. Histone H1 has been implicated in prevention of transcription factor binding and thus its removal is a prerequisite for making nucleosomal DNA accessible to transcription factor binding (26).

Transcription factors are proteins that are characterized by an affinity to specific DNA sequences (response elements) to which they can directly bind via a DNA binding domain. They control gene transcription by recruiting co-factors to specific DNA regions that in turn covalently modify histone proteins (e.g. phosphorylation, acetylation, methylation). As a consequence the tightly wound DNA is released allowing the recruitment of large protein complexes which stabilise RNA polymerase II binding. The most frequent observed modification of histone proteins is acetylation by histone acetylases (HATs). Several important co-factors such as p300/CBP have intrinsic HAT activity (27). Increased gene transcription is associated with a concomitant increase in histone acetylation followed by decompaction whereas hypoacetylation is correlated with reduced transcription or gene silencing (25, 28).

Repression of genes is achieved via histone deacetylation a process controlled by histone deacetylases (HDACs) (29). Subsequently, the winding of DNA is increased resulting in a dense chromatin structure and reduced access of transcription factors to their binding sites.

Importantly, transcription factors react on external stimuli and therefore represent proteins that transform signals into transcription or repression of genes that are controlled by them. The fact that aberrant transcriptional activity is frequently observed in metabolic diseases has drawn much attention on the identification of transcription factors involved in the onset of metabolic diseases (16).

1.3 Transcriptional regulation of liver metabolism

In hepatocytes, insulin, glucagon and glucocorticoids are the major signals controlling the transcriptional activity of enzymes involved in carbohydrate-, lipid and protein metabolism by a

wide variety of transcription factors. The major effects on transcriptional regulation of these hormones on liver metabolism are summarized below.

1.3.1 Transcriptional control mediated by glucagon

The peptide hormone glucagon helps maintaining the level of glucose in the blood by binding to glucagon receptors on hepatocytes, causing the liver to release glucose - stored in the form of glycogen - through glycogenolysis. Binding of the hormone to its G-protein coupled receptor leads to dissociation of the heterotrimeric G protein into its α and β,γ -subunits and subsequent translocation of the α -subunit to adenylyl cyclase. Activated adenylyl cyclase generates cyclic adenosine 3',5'-monophosphate (cAMP) – a second messenger, thereby amplifying the incoming signal (Figure 1.1). Increased intracellular cAMP inhibits activity of the transcription factor sterol-regulatory binding protein 1c (SREBP-1c) (30), a factor that is stimulated in an insulin-dependent manner and that activates lipogenic programs (31, 32). Key enzymes controlled by SREBP-1c are e.g. acetyl CoA carboxylase 1 (ACC1), fatty acid synthase (FAS) and stearoyl CoA desaturase 1 (SCD-1) (33). The mechanism however has not been determined yet.

Three main targets of cAMP have been identified: protein kinase A (PKA), GTP-exchange protein EPAC and cyclic-nucleotide-gated ion channels. PKA is activated by the binding of cAMP to the two regulatory R subunits, upon which their dissociation from the catalytic C subunits is initiated. A large number of proteins have been identified as substrates for PKA. The enzyme activates phosphorylase B kinase which in turn phosphorylates phosphorylase B. Phosphorylase B is the enzyme responsible for the release of glucose-1-phosphate from glycogen.

Regulation of transcription by PKA is mainly achieved by direct phosphorylation of the transcription factors CREB, CREM and ATF1 that belong to the bZIP family of transcription factors. Phosphorylation of CREB, CREM or ATF1 is a crucial event, because it facilitates interaction with the transcriptional co-activators CBP and p300. CBP/p300 possess HAT activity and change chromatin structure into an open form by modification of histones so that transcription can occur (see Section 1.2.1.1). Importantly, the phosphorylation sites of CREB, CREM and ATF1 (Ser-133 in CREB, Ser-117 in CREM and Ser-63 in ATF1) are also targeted by a variety of other kinases, supporting the notion that members of the CREB family play an important role in the nuclear response to a variety of external stimuli.

Glucagon signaling is terminated by rapid degradation of cAMP by cyclic nucleotide phosphodiesterase (PDE), by inhibiting PKA activity with the protein kinase inhibitors α , β and

γ (PKIs or dephosphorylation of CREB family members by protein phosphatase 1 and 2a (PP1 and PP2A)).

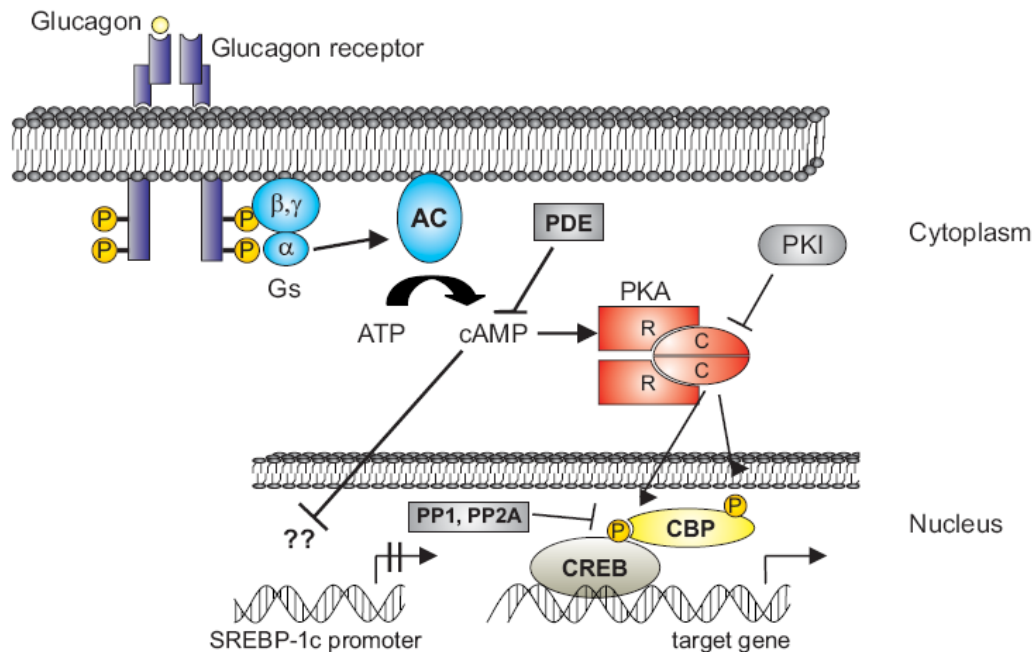


Figure 1.1: Glucagon signaling and transcriptional activation of target genes. Binding of glucagon to its receptor (purple) and its autophosphorylation lead to dissociation of associated G protein (Gs). The α -subunit translocates to adenylyl cyclase (AC) which generates cAMP. cAMP binds to regulatory subunits of PKA (R, red) releasing the catalytic subunits (C, red). C translocates into nucleus, where it phosphorylates transcription factors of the CREB family (CREB, grey). Signal is terminated by phosphodiesterase (PDE), protein kinase inhibitors (PKI) and protein phosphatases (PP1, PP2A).

Transcriptional activation of the key-gluconeogenic enzymes phosphoenolpyruvate dehydrogenase (PEPCK) and glucose-6-phosphatase (G6Pase) expression via glucagons/ cAMP increases hepatic glucose output and at the same time glucagon counteracts lipogenesis by inhibition of SREBP-1c (30).

1.3.2 Glucocorticoids and the glucocorticoid receptor

On the molecular level, glucocorticoids mainly exert their actions via binding to the glucocorticoid receptor and to a minor extend via binding to the mineralocorticoid receptor (34). The glucocorticoid receptor belongs to a specific class of transcription factors – the so-called nuclear hormone receptors. The nuclear hormone receptor superfamily includes receptors for thyroid and steroid hormones, retinoids and vitamin D as well as different “orphan” receptors of unknown ligand (35). Nuclear receptors act as ligand-inducible transcription factors and undergo conformational change upon ligand binding. As all transcription factors they bind to specific recognition sites on the DNA and control gene transcription through recruitment of co-regulators. However, their ligand-binding domain (LBD) distinguishes them from other

transcription factors because their activity can be directly modulated by small molecules making them very attractive targets for pharmacological intervention in diseases (22).

The glucocorticoid receptor is encoded by the gene NR3C1 and the murine protein has a size of 86 kDa. Two isoforms have been identified termed GR- α and GR- β (36). While GR- α is expressed in almost all tissues, GR- β expression is characterized by limited tissue distribution, where it acts as a dominant-negative inhibitor of GR- α (37, 38).

In the absence of its ligand, the GR is localized in the cytosol complexed with a variety of proteins including heat shock proteins 70 and 90 and FKBP52 (FK506 binding protein 52) (39). The endogenous glucocorticoid hormone cortison diffuses through the cell membrane. In the cytoplasm it is converted into the active cortisol (40). It subsequently binds to its receptor releasing in turn heat shock proteins from the inactivation complex. The hormone-bound GR translocates into the nucleus (40) where it binds DNA sequences called Glucocorticoid Response Elements (GREs) (41) via homo- or heterodimerization. However, GR confers its action not only via direct DNA binding but also via protein protein interaction (42, 43).

Targeted knockout experiments in mice demonstrated that ubiquitous deletion of GR is lethal shortly after birth emphasising the pivotal role of the GR for survival (44). In contrast, transgenic mice bearing a mutation in the the GR dimerization motif (GR_{dim} mice), thus unable to bind to GREs, are viable as impressively demonstrated by Reichardt et al. (45). Therefore, many of GR's functions are exerted via protein protein interactions and not through DNA-mediated control of target gene expression.

In the liver, the ligand-bound GR acts as a regulator of gluconeogenesis by enhancing the expression of PEPCK in cooperation with CREB (46-49) and as an inhibitor of glycolysis through increased expression of 6-phosphofructo-2-kinase (50). To provide glucose, the rate of proteolysis is increased in response to GC/GR and coincident with the conversion of carbon skeletons of the amino acids into glucose, the ammonia resulting from deamination of the α -amino group of amino acids is detoxified by the urea cycle. In this respect, GR controls hepatic up-regulation of the pace maker enzyme carbamoylphosphate synthetase (51).

1.3.3 Insulin signaling and transcriptional control

Insulin action is initiated upon binding of the hormone to and activation of its cell-surface receptor. The receptor consists of two extracellular α -subunits and two intracellular β -subunits composing a $\alpha_2\beta_2$ tetrameric complex. Via conformational change of the receptor α -subunits ligand binding leads to induction of tyrosine kinase activity located on the β -subunit and subsequent intramolecular transphosphorylation. Each β -subunit phosphorylates its adjacent

partner (52). Subsequently, numerous proximal substrates are tyrosine phosphorylated including the members of the insulin receptor substrate family (IRS 1 to 4), Shc adapter protein isoforms, Cbl and others (53-56).

Tyrosine phosphorylation of IRS proteins in turn creates recognition sites for additional effector proteins containing Src homology 2 (SH2) domains, e.g type 1A phosphatidylinositol 3-kinase (PI 3-kinase) (57-59). Activated PI 3-kinase generates the lipid phosphatidylinositol 3,4,5 trisphosphate (PIP₃), which triggers a protein kinase cascade by first stimulating phosphoinositide-dependent kinase 1 (PDK1) (60). Finally, PDK phosphorylates two classes of serine/threonine kinases, namely Akt (also known as protein kinase B) and the atypical protein kinase C ζ and λ (PKC ζ / λ). Both kinases have been reported to lead to translocation of glucose transporter GLUT4 (16) (see Figure 1.2) yet this action is independent of transcriptional regulation.

The diversity of mechanisms of insulin-mediated transcriptional regulation is extremely wide, as reflected by the various promoter sequence that harbour so-called insulin response elements (IRS/IRE) (61). Whereas not all factors are known that can bind to these sequences SREBP-1c has been shown to be a major mediator of insulin-dependent transcriptional regulation. The helix-loop-helix protein SREBP-1c stimulates the expression of glycolytic and lipogenic genes in the liver (e.g. liver acetyl CoA carboxylase, fatty acid synthase) (31).

On the other hand, insulin also negatively regulated transcription, in particular of gluconeogenic genes (e.g. PEPCK) (62). Insulin-dependent activation of AKT leads to phosphorylation of FOXO (forkhead family) transcription factors. Phosphorylated FOXOs are transported out of the nucleus resulting in a decreased transcriptional activity of their respective target genes (63-65). This mechanism represents the most common mechanism through which insulin can mediate repressive effects. Decreased gene expression of fructose-1,6-bisphosphatase and glucose-6-phosphatase (gluconeogenesis) have also been associated with forkhead family members (66).

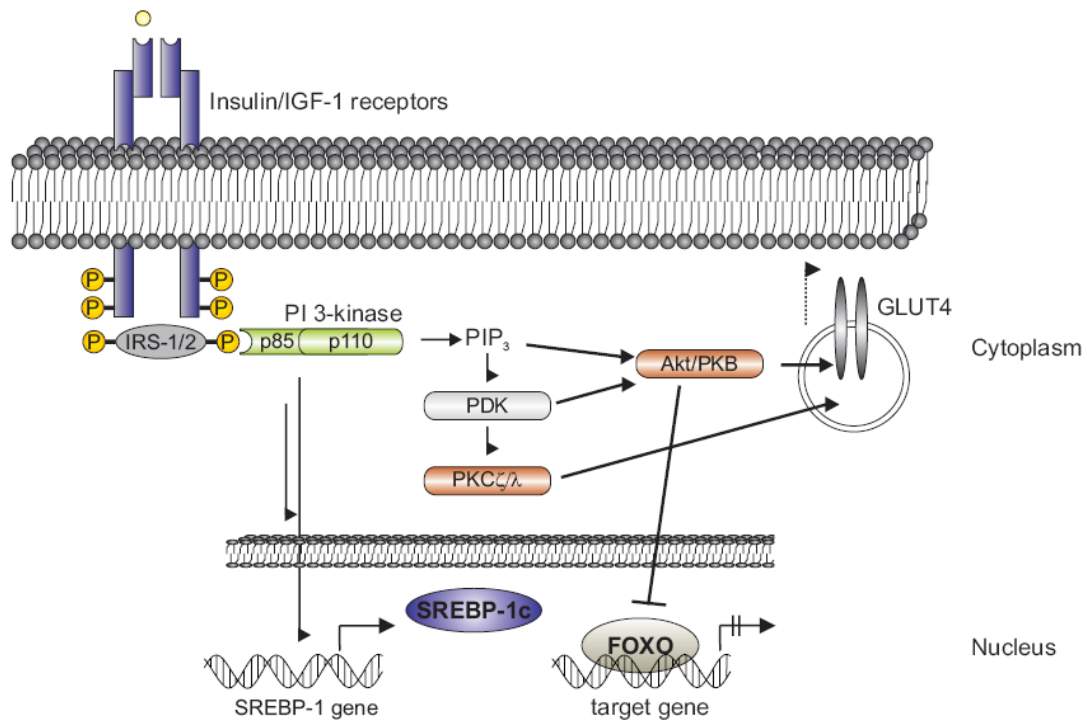


Figure 1.2: **Signal transduction in insulin action.** Upon binding of insulin to its receptor, autophosphorylation of the insulin/IGF-1 receptor and tyrosine phosphorylation of IRS proteins activate a protein kinase cascade that finally leads to the translocation of glucose transporter to the cell membrane. SREBP-1c expression is activated in response to PI-3-K and FOXO-mediated transcription blocked in an Akt/PKB-dependent manner.

1.4 Obesity – a risk factor for metabolic disease

The delicate control of energy balance within an organism strongly depends on the functional integrity of all signaling pathways controlled by hormones. Obesity is often accompanied by a desensitization of metabolic tissues against hormonal signals, especially insulin accompanied by a concomitant hyperactivation of counter-regulatory hormones. Attenuated insulin sensitivity in adipose tissue limits the capacity of the tissue to store excess nutrients as fat. As a result, dyslipidemia by means of increased serum free fatty acids (FFA) concentration promotes fat accumulation in non-adipose tissue. Function and viability of nonadipocytes are compromised when their triglyceride content rises above normal.

Generally, fatty acid delivery to non-adipose tissues is tightly coupled to the tissue-specific need for fuel. Serum FFA levels rise during exercise and fasting to be metabolized in the process of β -oxidation thereby generating energy. In hyperlipidemic situations, however, FFAs that are not needed for oxidative consumption can enter nonoxidative pathways such as ceramide synthesis. Increased ceramide synthesis has been implicated in the induction of β -cell apoptosis in pancreatic islets from obese *fa/fa* ZDF rats (67). Furthermore, long-chain fatty acids increase

intracellular nitric oxide (NO) production (68) thereby stimulating mainly cytotoxic actions of NO probably via greater production of toxic hydroxyl ions from peroxonitrite (69). Altered fatty acid uptake/utilization in heart can stimulate species lipid-induced programmed cell death via accumulation of cardiotoxic lipids (70, 71). These effects together are discussed as lipotoxic effects of FFAs on tissues.

Inflammation has been tightly linked to insulin resistance. Hotamisligil showed that proinflammatory TNF- α was able to deteriorate insulin resistance in adipocytes, macrophages and hepatocytes (72, 73) by activating IKK β /NF κ B and JNK pathways. As a consequence, IRS were Ser/Thr phosphorylated which inhibited tyrosine phosphorylation by the insulin receptor. Therefore, insulin mediated signaling was blunted.

Recently, FFAs were also shown to be strong signaling molecules stimulating the very same inflammatory pathways that have been implicated in manifestations of the Metabolic Syndrome: the IKK/NF κ B pathway (74), the c-Jun amino-terminal kinase (JNK) pathway (75, 76) and the Toll-like receptor 4 pathway (77). Thus, free fatty acids themselves are able to decrease insulin sensitivity.

In summary, dyslipidemia by means of increased serum FFA concentration perturbs all major tissues involved in regulation of metabolic homeostasis and therefore facilitates the manifestation of insulin resistance, a hallmark of the Metabolic Syndrome. The fact that function and viability of nonadipocytes is compromised when their triglyceride content rises above normal implies that normal homeostasis of their intracellular fatty acids is critical for prevention of complications of obesity.

1.4.1 Non-alcoholic fatty liver disease

Fat accumulation in the liver impairs its function as key-switch in metabolic control. Importantly, the amount of triglycerides stored in the liver inversely correlates with the responsiveness of the organ to insulin. Under pathophysiological conditions signal transduction via the insulin signaling cascade is attenuated or blunted. This condition is referred to as hepatic insulin resistance.

The term non-alcoholic fatty liver (NAFLD) describes the accumulation of mainly triglycerides in the hepatocytes so that fat mass exceeds 5% of the organ weight (78). It is a benign and

reversible condition *per se*, but it can progress to more severe liver diseases such as non-alcoholic steatohepatitis (NASH), a form of hepatitis and eventually cirrhosis and liver failure.

In NAFLD, mild to moderate elevations of serum aminotransferases are the most common detected serum abnormalities found in affected individuals (78). Imaging studies such as computer tomography (CT) and magnetic resonance (MR) are sensitive in detecting abnormal retention of lipids within liver cells called steatosis. The grade and stage of the disease can only be determined with a liver biopsy. Using proton MR spectroscopy, the Dallas Heart Study reported that one in three adult Americans has liver steatosis (79). This implies that approximately 70 million adult Americans suffer from NAFLD. Central obesity, Type II Diabetes, dyslipidemia and hypertension are risk factors for the disease. NAFLD can also precede the development of these comorbidities, so it is unclear whether fatty liver causes these complications or *vice versa* (80). Additionally, NAFLD can also be induced by numerous drugs such as estrogens and tamoxifen, by glucocorticoids or toxins (petrochemicals, such as tetrachlorocarbon, phosphorus poisoning, *Amanita phalloides*).

By a pilot study in humans, Marchesini et al. (81) showed a strong correlation between NAFLD and insulin resistance. NAFLD patients had basal hyperinsulinemia under fasting conditions and insulin infusion did not suppress hepatic glucose production. This clearly demonstrated that the liver itself was resistant against the hormone treatment. Furthermore, hypertriglyceridemia together with increased FFA levels was observed in serum in the same patient cohort. FFAs are responsible for reduced insulin clearance – thus the observed hyperinsulinemia. A lower-than-normal decrease of serum FFA levels after insulin infusion suggested a decreased insulin-mediated suppression of lipolysis. The study clearly demonstrated that Non-Alcoholic Fatty Liver Disease represents the hepatic manifestation of the Metabolic Syndrome (81).

The extremely high prevalence of NAFLD together with its implications in the Metabolic Syndrome underline the necessity to understand the molecular basis of the disease and factors causing its development.

1.4.2 Metabolic disease and transcription factors

As described in Section 1.2 and 1.3 transcriptional regulation in energy homeostasis relies on the activity of transcription factors that control expression of distinct gene sets. Metabolic diseases on the other hand are often associated with aberrant expression or activation of transcription factors leading to altered gene expression patterns.

Pharmacological targeting of transcription factors that are known to be differentially regulated in metabolic diseases therefore represents a major aim of biomedical research (22). Modulation of transcription factor activity is difficult to accomplish as they mostly do not possess a ligand binding domain. However, nuclear receptors – a subclass of transcription factors – are characterized by a ligand binding domain to which their endogenous ligands bind. Signaling molecules that can activate hormone receptors include lipophilic substances e.g. estradiol, testosterone, vitamin A or cortisol. The glucocorticoid receptor represents a member of the nuclear receptor family and plays a role in the emergence of NAFLD.

1.4.3 The implication of glucocorticoids in fatty liver development

Increased circulating GC levels have been detected in insulin-resistant patients promoting pathophysiological characteristics such as hyperglycemia, dyslipidemia and fatty liver. In various animal models of obesity, dyslipidemia and hepatic steatosis, circulating GC concentrations are drastically elevated (82, 83). Furthermore, the GR itself has been found to be over-expressed in hepatocytes of rodent diabetes models, in particular in its nuclear fraction (84, 85). Long-term treatment of Wistar rats with low doses of a synthetic glucocorticoid analogon resulted in increased hepatic triglyceride synthesis and decreased fatty acid oxidation promoting hepatic fat accumulation (86). Although chronically elevated GC levels have not been observed in obese subjects, local action of these hormones can still be increased. The enzyme 11- β -hydroxysteroid-dehydrogenase (11 β HSD), that converts the inactive cortison form into the active cortisol, has been demonstrated to increase local tissue GC levels (87). 11 β HSD-deficient mice are protected against diet-induced obesity and are characterized by lower circulating triglyceride levels and enhanced fatty acid oxidation (88). Liver-specific 11 β HSD overexpression resembles many phenotypic features of the Metabolic Syndrome such as abdominal obesity, hypertriglyceridemia and diminished glucose uptake rate by peripheral tissues (89) (glucose intolerance) suggesting an active role of GCs in the emergence of these complications.

Although glucocorticoids are widely considered as a major player causing fatty liver development, little is known about the molecular targets leading to this phenotype. Glucocorticoids have been demonstrated to inhibit the soluble mitochondrial matrix acyl-CoA dehydrogenases and thereby diminish β -oxidation (90). Some authors suggested that GCs decrease the mRNA levels of the enzymes (91), however these results could not be confirmed by others (90).

It has become increasingly clear that visceral fat deposition, which is common in severe obesity, is associated with triglyceride accumulation in the liver. Glucocorticoids are the driving force for visceral fat formation (92) and thus indirectly contribute to the fatty liver phenotype. Visceral adipose tissue has greater lipolytic potential than subcutaneous adipose tissue and the release of FFA from visceral fat directly into the portal circulation creates a “first pass” effect (78). The increased flux of fatty acids to the liver leads to hepatic lipid accumulation, increased hepatic glucose production (93, 94) and decreased hepatic insulin clearance, which in turn leads to insulin resistance and hyperinsulinemia. Furthermore, portal FFAs are known to drive hepatic production and secretion of lipoprotein particles (95) thereby altering the serum lipid profile.

Whether the rather indirect effect of glucocorticoids by elevating circulating FFAs is the major cause of GC-dependent hepatic steatosis is debated, however direct molecular mechanisms of GC-induced steatosis have not been determined.

2 Aim of the Study

Non Alcoholic Fatty Liver Disease nowadays represents the most common form of chronic liver disease in western countries. Due to the often accompanied hepatic insulin resistance, the liver is no longer capable to maintain various functions crucial for whole body energy homeostasis. Hyperactivation of hepatic GC/GR axis clearly promotes the transformation process of the liver towards the pathophysiological NAFLD state, yet the molecular mechanisms underlying these phenotypical effects are largely unknown.

The approach taken in this thesis aims for the characterization of the role of hepatic GR/GC function in the context of fatty liver development and progression. A special focus lays on the identification of transcriptionally regulated metabolic pathways that eventually promote hepatic fat accumulation and target genes that are differentially expressed in correspondence to GC/GR signaling. This work will have new implications for the development of treatment strategies against NAFLD, a research area which has been given rising attention during the past years.

3 Results

It is widely accepted that glucocorticoids contribute to fatty liver development. However, while the correlation between high glucocorticoid levels and hepatic fat accumulation is undoubted molecular rationales for hepatic fat increase remain largely unknown (96). To examine the role of the glucocorticoid receptor (GR) in fatty liver development targeting the GR specifically in the liver would be advantageous. Genetic models of liver-specific targeted knockout for the GR exist (97, 98), but are available only on a mixed genetic background (C57 BL/6J, 129SvEv, FVB/N). To study hepatic GR function in the context of a fatty liver, generation of liver-specific GR knockout mice on fatty liver-prone mouse strains would be necessary. However, this method does not allow the investigation of acute effects during the different stages of fatty liver manifestation. One way to circumvent these drawbacks is to employ transient knock-down techniques by taking advantage of adenoviral gene delivery technology.

3.1 Generation of adenoviruses encoding for shRNAs against murine GR

To investigate the role of the GC/GR axis during fatty liver development adenoviruses encoding for shRNAs targeting the murine GR were generated.

Thus, shRNA sequences targeting the murine glucocorticoid receptor were selected using sequence data derived from Danielsen et al. (99) (accession number: X04435, see Section 5.5.1). One shRNA sequence was kindly provided by Daniel Habermehl from the Department of “Molecular Biology of the Cell I” (Prof. G. Schütz, DKFZ).

Sequences were first adapted to the BLOCK-iT™ U6 RNAi Entry Vector Kit by adding a 5'-overhang of 4 nucleotides and a loop sequence (TTCAAGAGA) and then cloned into the pENTR/U6 vector to obtain a knockdown cassette composed of the U6 promoter driving shRNA expression followed by a Pol III termination signal flanked by two recombination sites. The U6 RNAi cassette was subsequently included into a vector encoding for the human adenovirus serotype 5 (pAd/BLOCK-IT™-DEST) by recombination. The virus is replication-incompetent as the E1 and E3 gene are both deleted from the viral genome. A schematic view of the adenoviral vector construct including the knockdown cassette is shown in Figure 3.1 A. *In vivo* transcription of the oligonucleotide leads to the formation of a stem-loop structure of the shRNA as shown in Figure 3.1 B for one chosen oligonucleotide. This structure facilitates processing by the RNAi machinery leading to the removal of the loop structure by RNase III Dicer. One strand of the derived dsRNA molecule is incorporated into a large protein complex

(with RNase activity) named RNA-induced silencing complex (RISC), that guides the targeted RNA to degradation (100, 101).

Adenoviruses were generated by transfecting the adenoviral vector into human embryonic kidney cells (HEK 293A) that complement for E1 and E3. After virus amplification and purification (see Section 5.5.3 to 5.5.5) the knockdown efficiency of the adenovirus was determined by infecting mouse hepatoma cells (Hepa 1C1 wt cells) with different multiplicities of infection (MOI). As control an adenovirus encoding for a nontargeting shRNA was generated, the sequence of which was tested *in silico* against the mouse genome. No significant sequence homologies were obtained with this sequence. Investigation of the GR levels in cell lysates from infected hepatoma cells via western blot 48h after infection revealed that the vector encoding for the GR shRNA1 proved to be efficient in a dose-dependent manner (Figure 3.1 C). Also GR shRNA2 and 3 were able to diminish GR, however less effectively. Thus for subsequent experiments GR shRNA1 was used.

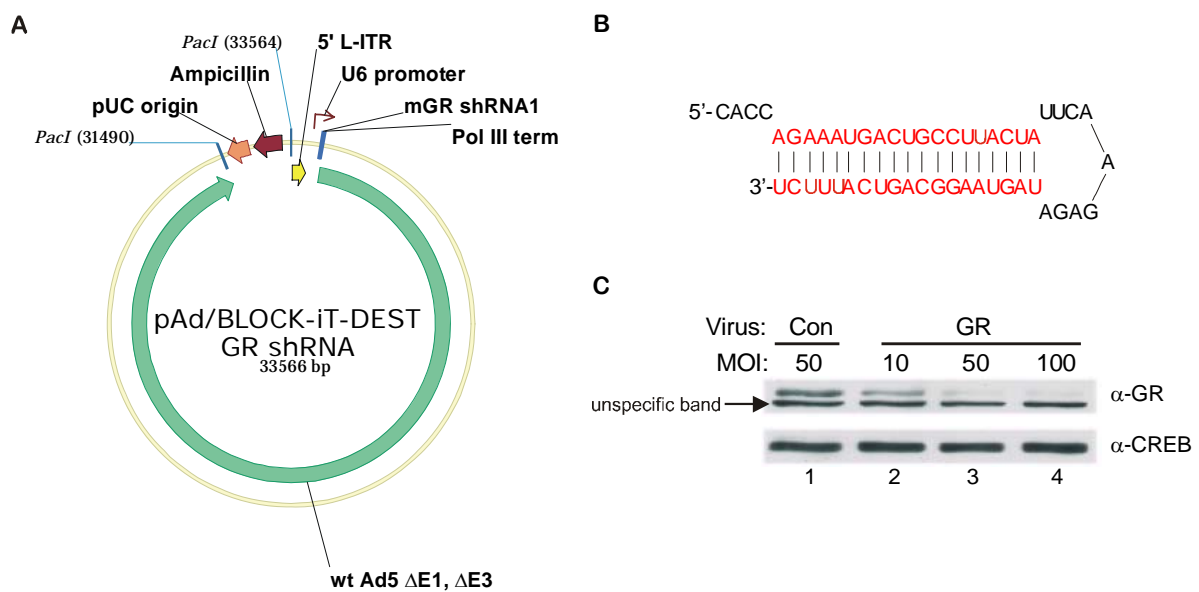


Figure 3.1: Generation of an adenovirus constitutively expressing an shRNA sequence targeting the murine GR. A) Vector map of the pAd/BLOCK-iTTM-DEST GR shRNA consisting of 33566 bp with the viral genome starting at the 5' L-ITR indicated in yellow up to the end of the 3'-ITR (not shown). The knockdown cassette composed of the U6 promoter (indicated with small brown arrow), an oligonucleotide encoding for the shRNA sequence (blue) and a Pol III termination signal adjacent to it. The adenoviral genome sequence shown in lightgreen contains deletions of the early genes E1 and E3. The vector carries the AmpR resistance gene (dark red). B) Schematic view of the shRNA sequence derived from the oligonucleotide sequence included in the vector. In vivo it forms a hairpin structure as shown. Highlighted in red are the 19 nt specifically targeting exon 8 of the murine GR. C) Evaluation of knock-down efficiency of the adenovirus. Cell lysates of mouse hepatoma cells were obtained after infection with different multiplicities of infection as indicated using either a virus encoding for a non-targeting shRNA (Con) or targeting the mGR (GR). Specific antibody against GR was used, the lower band represents an unspecific band observed in hepatoma cells. CREB served as loading control.

3.2 Transient knock-down of hepatic GR in two fatty liver mouse models

Adenoviruses can be injected at any time during the induction of the fatty liver and into any mouse model making it a very flexible tool. The persistence of the virus varies with the transgene included in the viral genome, but typically within one week after injection viruses can still be detected. Administration of the virus via the tail vein leads to an exclusive infection of the liver while other tissues remain unaffected.

To take advantage of these characteristics as a research tool in an initial screening experiment two different fatty liver mouse models were chosen – an acute and a chronic model.

Prolonged fasting periods lead to lipolysis in peripheral tissues(102, 103) e.g. adipose tissue and a subsequent fat transport towards the liver promoting intra-hepatic triglyceride accumulation (104, 105). Increased fat content in the liver deteriorates hepatic insulin sensitivity(78, 81, 106) but fatty liver induction in wildtype mice is easily reversible by feeding the mice *ad libitum* after starvation periods. Therefore, this simple model represents an early step of fatty liver development. To induce a fatty liver, thus wildtype C57 BL/6J mice were starved for 24 hours to acutely induce hepatic fat accumulation.

As a chronic model of fatty liver diabetic db/db mice were chosen. These mice possess a mutation in the leptin receptor gene (long form Ob-Rb) leading to a loss of central nervous food intake control (107, 108). They display a metabolic phenotype characterized by severe obesity, insulin resistance and fat accumulation in the liver (109). Since the fatty liver is not easily reversible they represent a more advanced stage of fatty liver manifestation.

Initially, seven mice per group were injected with adenoviruses encoding for either a non-targeting shRNA or the GR shRNA1. Wildtype C57 BL/6J mice were given a dose of 1×10^9 ifu/mouse, while db/db mice received a dose of 3×10^9 ifu/mouse taking the higher average weight of db/db mice into account (wildtype mice average weight 22.3 ± 0.4 g, db/db mice 47.4 ± 0.7 g). Mice were maintained for 6 days on a chow diet and free access to water. 24h prior to sacrifice food was withdrawn from the wildtype mice. The following day, all experimental groups were sacrificed and biopsies from liver, epididymal fat and muscle (Gastrocnemius) were taken together with serum samples for biochemical analysis.

3.2.1 shRNA-induced knockdown of GR

The shRNA-induced knockdown of the GR in the liver was investigated on the mRNA as well as on the protein level. RNA was isolated from livers of all mice. The obtained mRNA was

reversely transcribed into cDNA and subjected to quantitative RT-PCR using Taqman® probes against the murine GR. The obtained values were normalized against TATA box binding protein (TBP). As shown in Figure 3.2 A, knockdown of the GR in wildtype mice was 1.9-fold ($p \leq 0.001$) and 1.7-fold in db/db mice ($p \leq 0.01$) on mRNA level. Since the knockdown observed at the mRNA level was not very prominent, hepatic protein levels were investigated as well. Liver protein lysates from three animals per experimental group were prepared. Lysates were separated on 10% SDS polyacrylamide gels and investigated by immunoblotting using specific antibodies against GR (Santa Cruz) and Valosin containing protein VCP (Abcam). VCP served in this experiment as marker for unspecific effects observed after viral infection and remained unchanged in all experimental groups. Remarkably, knockdown of hepatic GR was more pronounced on the protein level than on the mRNA level (Figure 3.2 B, compare lanes 1-3 vs. 4-6 in wildtype mice and 7-9 vs. 10-12 in db/db mice). In db/db mice GR was barely detectable despite the fact that on the mRNA level down-regulation of GR mRNA was less pronounced than in control mice.

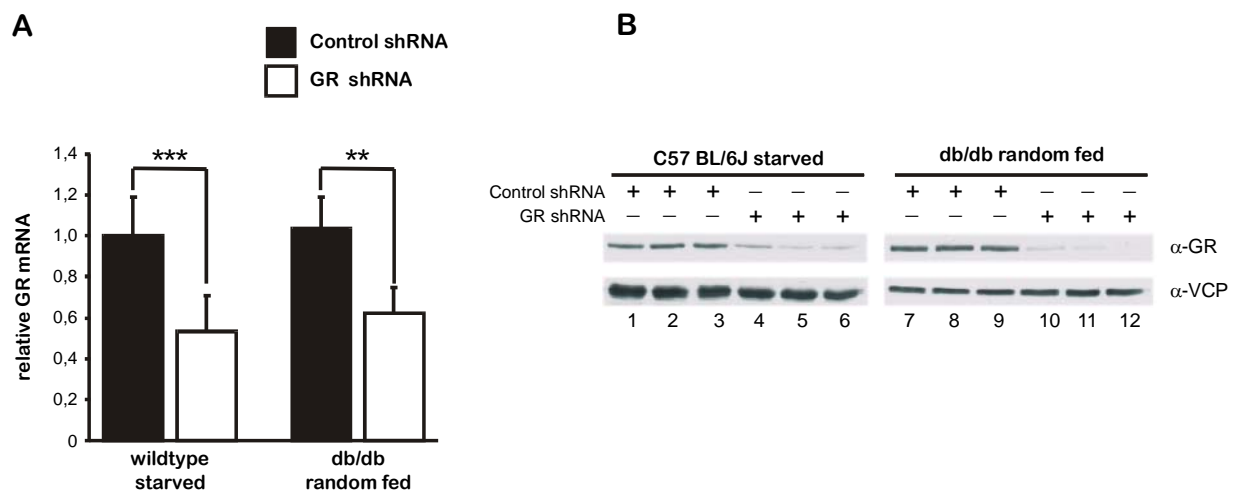


Figure 3.2: Analysis of shRNA-induced GR depletion in the murine liver. Mice were injected with adenoviruses (AV) encoding for non-targeting shRNAs (Control shRNA) or encoding for GR-targeting shRNAs (GR shRNA) as indicated. **A** Quantitative RT-PCR of RNA isolated from livers of all virus-treated mice using a specific Taqman® probe against murine GR. Results were normalized against TBP. Data shown are means and s.e.m. N=7, ** $p \leq 0.01$; *** $p \leq 0.001$ **B** Western Blot analysis of liver lysates prepared from three representative animals per experimental group. 20µg protein were used for SDS-PAGE. Immunoblotting was done using specific antibodies against GR (M-20, Santa Cruz) and VCP (Abcam). Individual lane represents one animal.

Knockdown of hepatic GR to almost undetectable levels alleviated the fatty liver phenotype in db/db mice where hepatic triglyceride levels were reduced (control 492 ± 45 vs. GR shRNA 376 ± 81 µmol/g liver). In the acute model hepatic triglyceride content was not diminished by GR shRNA adenovirus administration probably due to lower viral dosage.

Overall, the data reveal that the adenovirus developed against murine GR is able to deplete the protein *in vivo* with high efficiencies.

3.2.2 Target gene analysis after GR knockdown

3.2.2.1 Examination of pathways regulating hepatic fat content

Next, target genes involved in liver fat metabolism were investigated. Principally, liver fat content can increase due to *de novo* fat synthesis (lipogenesis) or due to decreased oxidative consumption of fatty acids (β -oxidation). Altered influx or efflux of triglycerides also represents a possible explanation. Rate-determining enzymes and/or transporters were chosen to investigate the respective pathways.

Figure 3.3 represents the results obtained after target gene analysis in wt mice after starvation. To evaluate the effects of hepatic GR knockdown, expression of gluconeogenic genes was investigated as positive control. During extended fasting periods serum glucocorticoid levels rise, activating the GR(110). In the liver, activated GR stimulates gene expression of gluconeogenic genes – namely phosphoenolpyruvate carboxykinase (PEPCK) to maintain blood sugar levels within a narrow range(46, 47, 49). Depletion of hepatic GR, therefore should lead to attenuated activation of PEPCK expression compared to starved wildtype mice. As shown in Figure 3.3, GR depletion led to an only 25% reduction (relative mRNA levels control virus: 1 vs. GR shRNA: 0,76) of PEPCK expression under starvation conditions. These results suggest that hepatic activation of GR in control mice might have been only moderate under the experimental conditions. This might explain why the overall effects on target genes investigated were mild. However, GR knockdown led to a highly significant increase in β -oxidation as shown by the increase in the expression of carnitine palmitoyl transferase 1a (CPT1 α), a transporter limiting fatty acid transport through the mitochondrial membrane, thereby representing the rate-determining step in β -oxidation. Most interestingly, gene expression of a key-regulator of lipogenic and fat transport programs – peroxisome proliferation activation receptor gamma (PPAR γ) – was diminished highly significant. Interestingly, lipogenic gene expression was not affected instead slight activation of acyl-CoA carboxylase 1 (ACC1) was observed. However, this activation was not significant. No major changes were observed in fat transport or serum fat regulation (Figure 3.3).

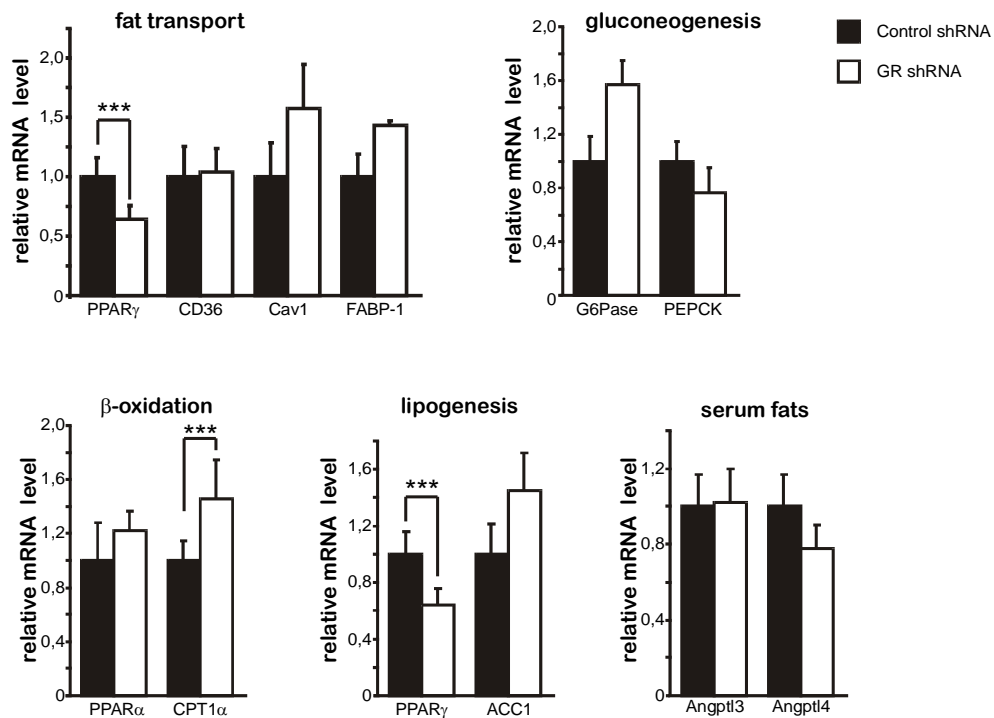
C57BL/6J starved

Figure 3.3: Target gene analysis in wildtype mice after GR depletion. Animals were starved for 24h prior sacrifice. RNA was isolated from livers of all animals, transcribed into cDNA and subjected to quantitative qPCR evaluation using specific Taqman® probes against the target genes as indicated. ACC1 - acyl-CoA carboxylase, Angptl3 – angiopoietin-like 3, Angptl4 – angiopoietin like 4, Cav1-caveolin1, CPT1 α – carnitine palmitoyl-transferase 1 α , FABP-1- liver fatty acid binding protein, G6Pase- glucose-6-phosphatase, PEPCK – phosphoenolpyruvate carboxykinase, PPAR α – peroxisome proliferation activating receptor α , PPAR γ - peroxisome proliferation activating receptor γ (depicted twice to show involvement in different pathways). Data shown are means and s.e.m. N=7 per group *** $p \leq 0.001$.

The same investigations were undertaken in db/db mice. Also in this experiment, the effect of GR depletion on PEPCK expression was investigated as a positive control. As shown in Figure 3.4, transient knockdown of hepatic GR caused a 40% reduction of PEPCK expression, the effect of which was statistically significant.

Again, a highly significant reduction of PPAR γ expression was seen accompanied by downregulation of distinct target genes of PPAR γ , namely fat transporters CD36 ($46\% \pm 15\%$) and Cav1 ($51\% \pm 15\%$, $p \leq 0.05$). Interestingly, classical lipogenic genes such as ACC1 were not affected suggesting a specific down-regulation of fat import into liver under these conditions. Furthermore, enhanced CPT1 α indicated accelerated β -oxidation, consistent with observations made in wildtype mice after starvation.

Finally, in db/db mice GR depletion affected regulation of serum fats as indicated by the changed expression of liver-specific angiopoietin-like 3 (Angptl3, $43\% \pm 7\%$, $p \leq 0.05$) and

Angptl4 ($57 \pm 8\%$). Angptl3 and 4 are proteins secreted into the serum. They act as inhibitors of lipoprotein lipase (LPL) (111), which is localized on the surface of adipocytes. Reduced expression of these factors might indicate an increased activity of LPL leading to faster fat clearance because of accelerated triglyceride uptake into fat cells. However, in the experiments undertaken serum triglyceride levels were increased in GR shRNA injected mice (control vs GR shRNA $3.0 \pm 0.9 \mu\text{mol/ml}$ vs. $8.6 \pm 2 \mu\text{mol/ml}$). It is unclear whether decreased liver fat uptake contributes to the elevated serum levels and it remains to be determined whether LPL activity on adipocytes was increased as a consequence of decreased Angptl3 levels in these mice.

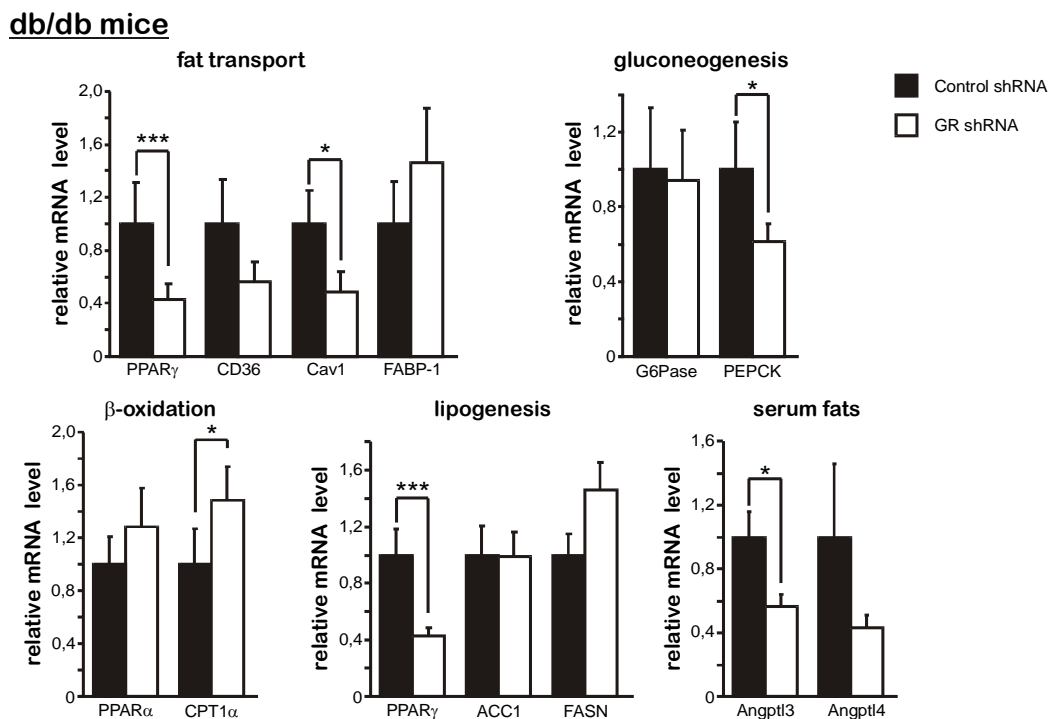


Figure 3.4: Target gene analysis in db/db mice after GR depletion. Animals were injected one week prior sacrifice and maintained on standard chow diet until sacrifice. RNA was isolated from livers of all animals, transcribed into cDNA and subjected to quantitative qPCR evaluation using specific Taqman probes against the target genes as indicated. ACC1 - acyl-CoA carboxylase, Angptl3 – angiopoietin-like 3, Angptl4 – angiopoietin like 4, Cav1- caveolin1, CPT1 α – carnitine palmitoyl-transferase 1 α , FABP-1- liver fatty acid binding protein, G6Pase- glucose-6-phosphatase, PEPCK – phosphoenolpyruvate carboxykinase, PPAR α – peroxisome proliferation activating receptor α , PPAR γ - peroxisome proliferation activating receptor γ . Data shown are means and s.e.m. N=7 per group * $p \leq 0.05$ *** $p \leq 0.001$.

In summary, effects of transient GR knockdown were more pronounced in db/db mice as suggested by suppression of PEPCK expression. These observations correlate with the initial viral doses used in the individual experiments (1×10^9 ifu/mouse in wildtype mice vs. 3×10^9 ifu/mouse in db/db mice).

Analysis of potential target genes of GR revealed that PPAR γ and CPT1 α were two genes consistently regulated in both mouse experiments. In contrast, no significant changes in lipogenesis were observed.

In db/db mice GR knockdown furthermore led to suppression of fat transporters Cav1 and CD36 as well as Angptl3 and 4, which represent secreted inhibitors of LPL.

3.2.2.2 Hes-1 – a transcription factor differentially regulated after hepatic GR knockdown

When investigating genes differentially regulated after hepatic GR knockdown, the transcriptional repressor Hairy and Enhancer of Split 1 (Hes-1) was found to be increased after GR depletion in wildtype mice (1.3 fold, $p \leq 0.05$) and more dramatically in db/db mice (2,6-fold, $p \leq 0.001$) on the mRNA level. These changes were also reflected in the protein levels of Hes-1 as shown in Figure 3.5. While no dramatic effects were detectable in C57 BL/6J mice (Figure B compare lanes 1-3 vs. 4-6), a marked up-regulation of Hes-1 was present in db/db mice injected with GR (Figure C compare lines 1-3 vs. 4-6).

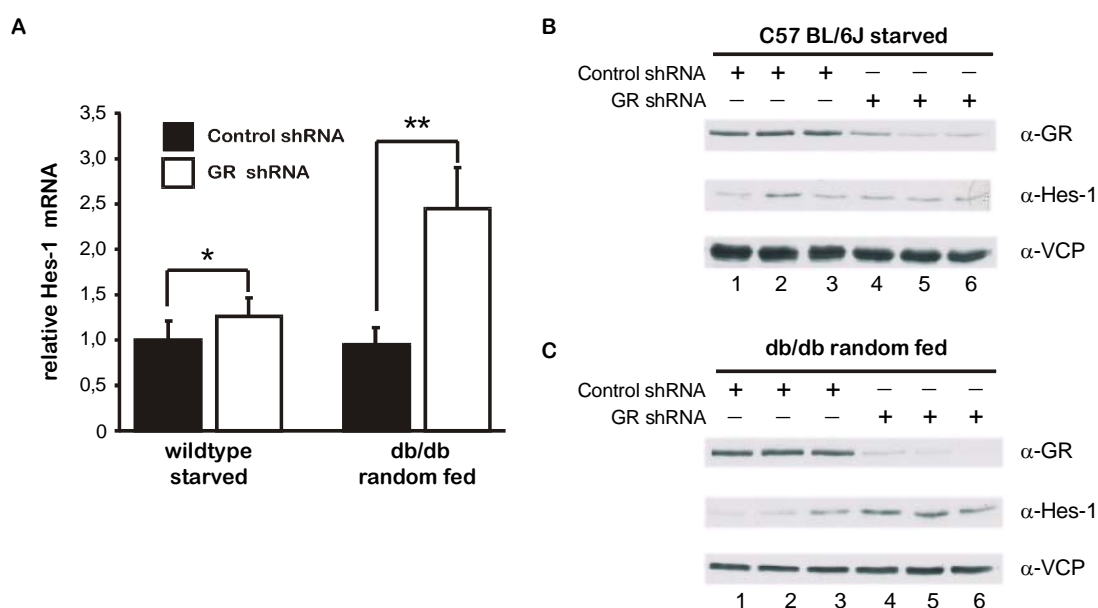


Figure 3.5: Hes-1 expression is up-regulated after GR knockdown. C57 BL/6J mice were injected with adenoviruses encoding for either non-targeting shRNA (control shRNA) or GR shRNA (109ifu/mouse) and starved 24h before sacrifice. Db/db mice were injected with 3×10^9 ifu/mouse of the same viruses as indicated. A) Quantitative RT-PCR from hepatic RNA isolated from these mice using specific Taqman® probes against Hes-1. TBP was used for normalization. Data shown are means and s.e.m. N=7 per group * $p \leq 0.05$, ** $p \leq 0.01$. B) Western Blots from hepatic protein extracts isolated from the same animals as under A) and probed with specific antibodies as indicated. Individual lane represents one mouse. VCP served as loading control.

These findings were very interesting since recently, Hes-1 has been identified as a novel regulatory switch and key determinant in hepatic lipid homeostasis under fasting conditions

(one simple model of fatty liver). Remarkably, Hes-1 was shown by Herzig et al. to inhibit the expression of nuclear hormone receptor peroxisome-proliferator-activated receptor γ (PPAR γ), a key regulator of insulin-dependent lipogenesis in hepatic tissue (112).

Intriguingly, as shown in Figure 3.5 knockdown of the GR led to an up-regulation of Hes-1 in two models of fatty liver development and the increased Hes-1 levels correlated with inhibition of PPAR γ consistent with literature data. However, the functional role of Hes-1 in fatty liver development was completely unclear.

3.3 Investigation of Hes-1 levels in different fatty liver mouse models

To investigate the hypothesis that differentially expressed Hes-1 represents a characteristic of fatty liver development and a downstream target of the GR pathway, Hes-1 expression patterns in several fatty liver mouse models were examined.

3.3.1 Starvation-induced fatty liver

In an initial test experiment Hes-1 levels in starved and refed mice were measured. Male 9 week old C57 BL/6J mice were starved for 6 hours, 24h and 48h with free access to water. Control mice were starved for the same time but subsequently refed for another 24h before sacrifice. Liver biopsies and serum samples were taken from all mice for biochemical analysis.

To monitor the amount of fat stored in the liver during treatment liver lipids were isolated (see Section 5.3.8) and triglyceride content was measured (see Section 5.3.10.1). After 24h food deprivation hepatic triglycerides were elevated 7.6-fold compared to the control group (Figure 3.6 A compare bar 1 vs. bar 3,). Two days of starvation led to a 13-fold accumulation of TGs in the liver.

Hes-1 expression was determined using qPCR analysis. Thus, mRNA was isolated from liver samples of fasted and refed animals and transcribed into cDNA. Interestingly, Hes-1 expression was down-regulated on the mRNA level 3.4-fold after 24h of starvation, the level of which did not further decrease during longer starvation periods (Figure 3.6 B 2.8-fold after 48h starvation). Hes-1 protein level was also diminished compared to control mice (Figure 3.6 C, compare lane 1-3 vs. 4-6). Control mice did not differ in their Hes-1 values irrespective of the duration of starvation before the 24h refed period (data not shown).

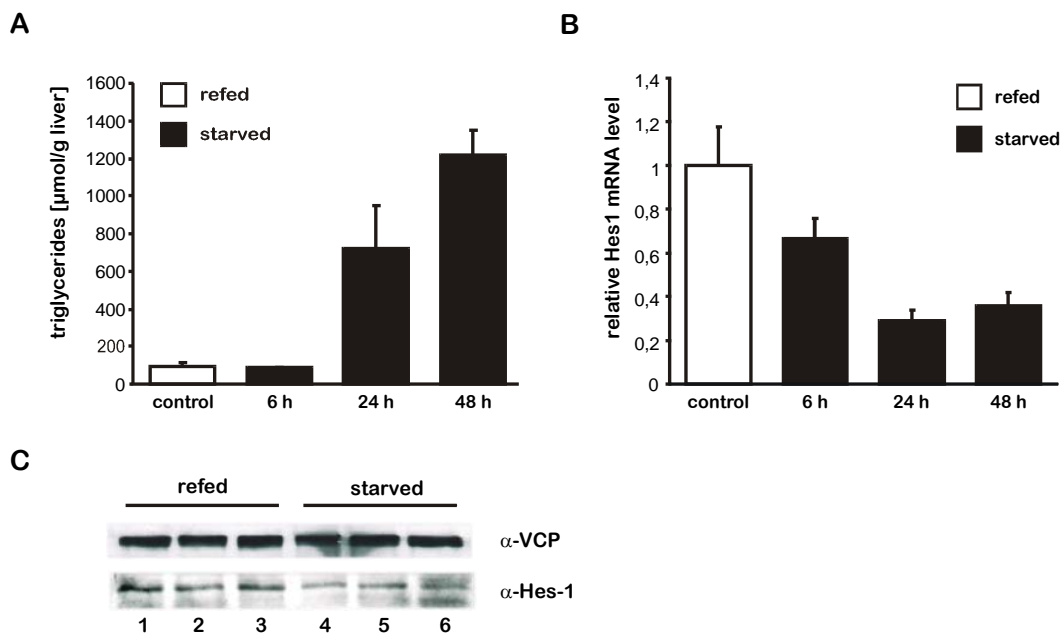


Figure 3.6: Starvation-induced fatty liver and hepatic Hes-1 expression. A) Triglyceride content in liver extracts from C57 BL/6J mice. Time of starvation as indicated. Data shown are mean values and s.e.m. N=3. B) Quantitative RT-PCR analysis from RNA isolated from the same animals as under A) using Hes-1 specific primers. mRNA expression normalized to TBP values. Data are shown as mean values and s.e.m. N=3. C) Western Blot analysis of hepatic Hes-1 expression of mice starved for 48h (lane 4 to 6) or starved for 48h and then refed for 24h (lane 1-3). VCP serves as loading control.

Down-regulation of Hes-1 under fasting conditions inversely correlated with increased liver triglycerides. However, while triglyceride levels still increased after 48h of starvation, Hes-1 levels did not further decline indicating that minimum expression is already reached after 24h food deprivation.

3.3.2 Chronic fatty liver models

Db/db mice: Next, db/db (C57 BLKS/J *Lepr*^{-/-}) animals were examined as an example of a chronic fatty liver model. Since a marked Hes-1 down-regulation in C57 BL/6J mice was already observed after 24 h starvation, db/db mice and wildtype controls with the same genetic background (C57 BLKS) were starved for 24 h or starved and subsequently refed for 24h. Surprisingly, in hepatic protein extracts of starved animals, no differences in Hes-1 protein levels were detected. However, in the refed group Hes-1 protein levels were significantly inhibited in db/db animals (Figure 3.7). Since it was observed before (Figure 3.6), that starvation itself diminishes Hes-1 protein levels, the comparable low protein amounts of Hes-1 seen in db/db and wildtype mice might be associated with a starvation-induced Hes-1 inhibitory factor/ signal.

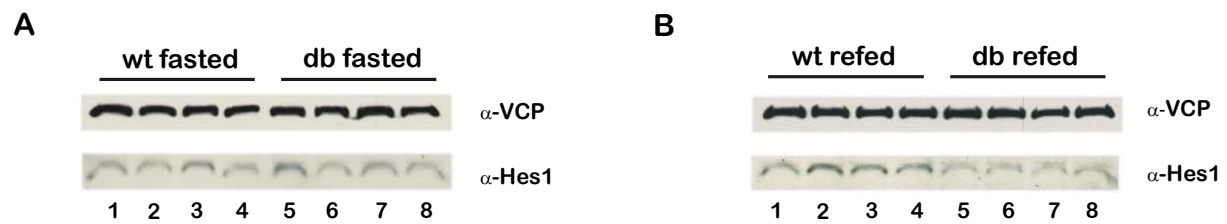


Figure 3.7: Hes-1 expression in db/db mice – a standard model of fatty liver. A) Western Blot analysis of liver protein extracts from db/db mice or wt controls after 24 h starvation. B) Western Blot analysis of liver protein extracts from db/db mice or wildtype controls after 24h starvation and 24h refeeding period. VCP served as loading control.

Polygenic NZO mice: Db/db mice are excellent models of monogenic obesity and useful for researching type 2 diabetes, however they do only partially reflect the more common human obesity-induced diabetes (diabesity) syndromes and their dramatic phenotype is less characteristic for the metabolic syndrome (113, 114). Common human diabesity syndromes are polygenic, not monogenic, and therefore a polygenic mouse model of severe obesity and impaired glucose tolerance was chosen in addition to db/db mice. New Zealand Obese (NZO/HIJ) mice are in this respect the most useful mouse strain for investigations. These mice exhibit high birth weights and develop severe obesity even when maintained on a standard diet containing 4,5% fat (113, 115). Both sexes are characterized by impaired glucose tolerance, but subsequent type II diabetes maturity onset is limited to males with a phenotype penetrance of less than 50%. Therefore, these mice allow observation of Hes-1 levels in a complex model of the so called metabolic syndrome that is mainly characterized by alterations in fat metabolism.

To explore whether Hes-1 downregulation is a feature of fatty liver in New Zealand Obese mice, male 10 weeks old mice were starved for 24h and sacrificed or refeed after the starvation period for 24h and then sacrificed. As wildtype control served New Zealand Black mice (NZB). As shown in Figure 3.3, there is a tendency towards attenuated hepatic Hes-1 protein levels in NZO mice after re-feeding compared to NZB litters (Figure 3.8 compare lane 1-3 vs. 4-6). .

NZB mice display a number of autoimmune abnormalities and during the course of the experiment NZB mice from the starvation group had to be sacrificed because of wounds and impaired wound healing most likely caused by autoimmune reactions. Hence, the number of mice investigated after starvation was decreased drastically.

Hepatic Hes-1 protein levels of an unaffected NZB mouse were compared to a starved NZO mouse and a marked reduction in the New Zealand Obese mouse was observed. However, this tendency needs to be confirmed under starvation conditions by a representative group of animals.

In summary, NZO mice exhibit a tendency towards lowered hepatic Hes-1 levels while at the same time have higher hepatic fat content (116).

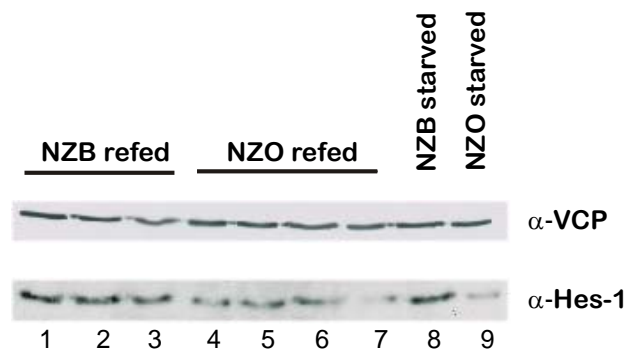


Figure 3.8: Hepatic Hes-1 expression in New Zealand Obese mice – a polygenic model of obesity and diabetes. Western Blot analysis of wildtype new zealand black mice (NZB) or new zealand obese mice (NZO) after starvation for 24h (fasted) or after starvation for 24h and subsequent refeeding for another 24h (refed).

3.3.3 Model of diet-induced obesity (DOI)

Finally, the influence of dietary components on hepatic Hes-1 expression was probed. In cooperation with the group of Sander Kersten from the University of Wageningen C57BL/6J mice were maintained either on a chow diet containing 10% fat or on a high fat diet with 45% fat. This high fat diet has been demonstrated in the past to lead to hepatic fat accumulation and to promote the development of a fatty liver (117) (109).

C57BL/6J mice were maintained on the either chow diet or high fat diet for 2 weeks or 16 weeks and then sacrificed in the random fed state. Protein extracts from liver were made and Hes-1 levels were investigated by immunoblotting.

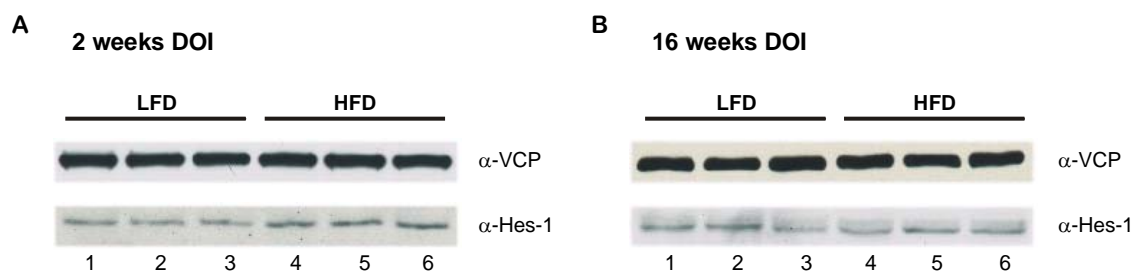


Figure 3.9: Hepatic Hes-1 levels diet-induced obesity. A) Western Blot analysis of hepatic Hes-1 expression with Hes-1 specific antibody in mice maintained for 2 weeks on a diet as indicated. LFD – 10% low fat diet; HFD – 45% high fat diet. VCP served as loading control. B) Western Blot analysis of hepatic Hes-1 expression with Hes-1 specific antibody in mice maintained for 16 weeks on a diet as indicated. LFD – 10% low fat diet; HFD – 45% high fat diet. VCP served as loading control.

Unexpectedly, high-fat feeding of C57BL/6J mice for two weeks led to a slight induction of Hes-1 expression (Figure 3.9). Elevated Hes-1 protein levels, however, were not observed after 16 weeks treatment. These data suggest, that excess fats causing a fatty liver are not responsible for diminished Hes-1 levels. Furthermore, they indicate that the inhibition of Hes-1 distinguishes different models of fatty liver development induced by different signals.

Taken together, Hes-1 expression is diminished in starvation-induced fatty liver and chronic monogenic and polygenic mouse models of fatty liver disease. Hence, Hes-1 expression in fact is down-regulated in a variety of models. In contrast, Hes-1 levels remained largely unaffected in fatty livers that develop upon diet-induced obesity.

3.3.4 Determination of serum glucocorticoids in fatty liver mouse models

In the GR knockdown experiment Hes-1 expression was initially found to be activated. Thus, it was tempting to speculate that decreased Hes-1 levels would likely be caused by activation of hepatic GR in the investigated models. Using a radioimmuno-assay serum glucocorticoid levels were determined after starvation, in db/db mice and in NZO mice.

As shown in Figure 3.10, serum glucocorticoids are increased in db/db mice when compared to their respective controls (388 ± 69 ng/ml vs. 113 ± 5 ng/ml, $p \leq 0.01$). As explained earlier, fasting is accompanied by enhanced GC levels and therefore mice fasted for 24h have significantly higher serum GC levels (356 ± 95 vs. 52 ± 6 ng/ml). Unexpectedly, hypercorticoism was not observed in refed NZO mice when compared to their control background (NZB mice). However, as shown in Figure 3.8, most dramatic effects on Hes-1 levels in NZB were measured under fasting conditions. Limited sample numbers did not allow examination of serum GC levels, so more studies are necessary to determine whether GC levels differ between NZB and NZO mice after fasting.

Serum samples for high fat diet fed mice were not available, but several researchers already proved that 16 weeks of HFD have no influence on serum GC parameters (118-119).

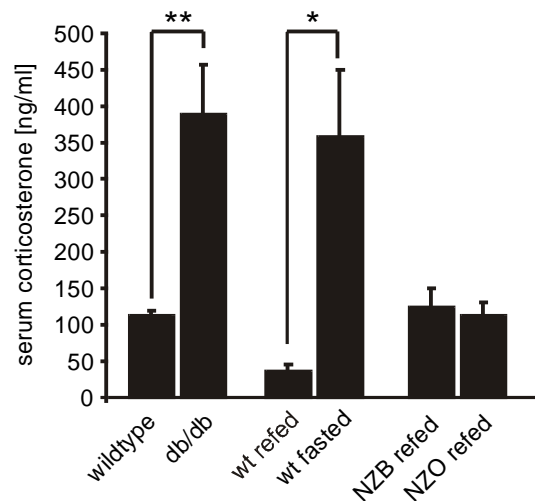


Figure 3.10: Serum glucocorticoid levels in different mouse models. Radioimmunoassay was used for determination of GC levels. Probed were db/db mice vs. control mice (bar 1 vs. bar 2), C57BL/6J fasted for 24h (wt fasted) or fasted and then refed for 24h (wt refed, bar 3 vs. bar 4) and refed NZO vs. refed NZB mice as indicated. Data shown are means and s.e.m. N=4 per group, * $p \leq 0.05$ ** $p \leq 0.01$.

3.4 The physiological signal causing decreased Hes-1 expression

Observing the strong correlation between serum glucocorticoid levels and decreased Hes-1 levels, it was important to investigate the functional relevance of an activated GC/GR axis in the regulation of hepatic Hes-1 protein levels.

3.4.1 Glucocorticoid treatment of C57BL/6J mice and the consequences on hepatic Hes-1 expression

To test the hypothesis that GCs can trigger Hes-1 down-regulation *in vivo*, 10 weeks old male C57 BL/6J mice were injected with 1.2 mg/kg dexamethasone (dex) or 0.9% sodium chloride (saline) daily intraperitoneally over a period of 3 weeks (120-121). Mice were housed individually and injections were performed at 8 am at the beginning of the 12h light phase. The weight development of each individual animal was assessed daily and is shown in Figure 3.11 A. In the experimental period, dex-treated animals lost $10\% \pm 3\%$ body weight while the weight of the control group was constant ($100 \pm 0.9\%$ of initial body weight). The dramatic body weight change measured at day 17 was caused by overnight starvation of the mice because on day 17 a glucose tolerance test was performed (indicated with an arrow, Figure 3.11 A). Food consumption of all animals was monitored and did not differ between the two experimental groups (data not shown), although GCs have been described to stimulate appetite (122, 123). Hence, the weight loss in the dex-treated group is not due to altered food intake but most likely because of the catabolic action of glucocorticoids (102).

13 days after start of dex injections, blood samples were withdrawn from the mice and serum lipid parameters were measured. Surprisingly, serum triglycerides were decreased significantly in the dex-treated animals (Table 1) compared to the control group, while non-esterified fatty acid (NEFA) levels were indistinguishable between the two groups. Interestingly, the amount of cholesterol was increased in the group receiving dexamethasone.

Table 1: Serum lipid parameters 13 days after Dexamethasone injection

	Saline	Dexamethasone	p-value
Triglycerides	17.6 ± 2.7 μ mol/ml	12.2 ± 0.5 μ mol/ml	0.0077
Cholesterol	97.4 ± 6.9 mg/dl	134.8 ± 9.0 mg/dl	0.006
NEFA	14.4 ± 3.3 mg/dl	16.2 ± 6.2 mg/dl	0.583

After 17 days, the influence of glucocorticoids on the systemic glucose sensitivity was assessed. For this purpose, a glucose tolerance test was performed on day 17 of dexamethasone injection. Overnight-fasted animals received an intraperitoneal injection of glucose (see Section 5.4.1) and declining blood glucose levels were monitored over 2h. As shown in Figure 3.11 B, both groups were equally glucose sensitive despite altered serum cholesterol levels. The area under the curve ($AUC_{\text{control}} = 29880 \text{ min} \times \text{mg/dl}$, $AUC_{\text{dex}} = 32089 \text{ min} \times \text{mg/dl}$) did not differ significantly.

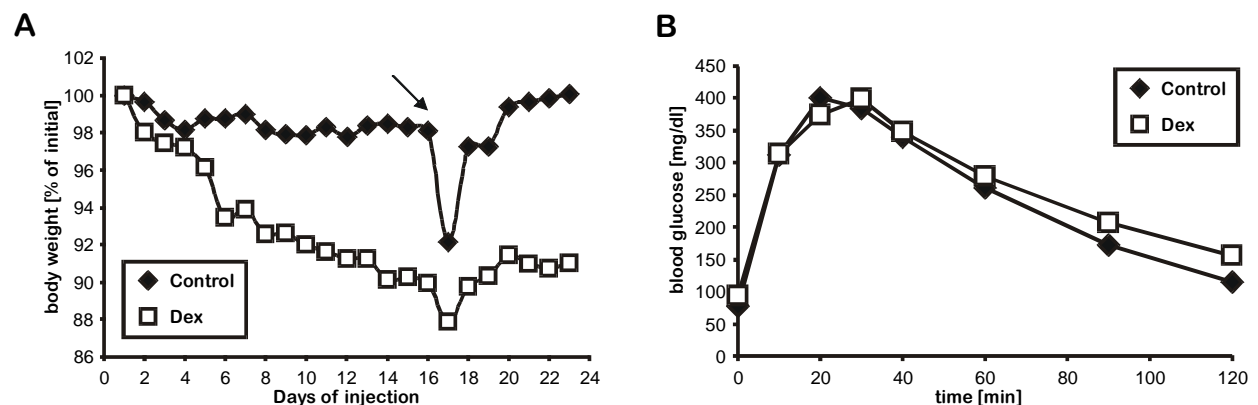


Figure 3.11 Glucocorticoid treatment leads to weight loss. A) Weight development of C57 BL/6J mice injected with 1.2 mg/ kg dex or saline (control) i.p. daily. Arrow indicates overnight starvation during course of experiment. N=4. B) Glucose tolerance test of C57 BL/6J mice after 17 days of daily injections. Mice were starved overnight and were injected with 10 μ l of a 20% w/v glucose solution per g body weight. N=4.

Bernal-Mizrachi et al. described that a 3-week dex injection into C57 BL/6J mice impair glucose tolerance and systemic insulin sensitivity (120). They also observed changes in fat metabolism contributing to the reported phenotype. To reproduce these observations, animals

were sacrificed 23 days after injection and important tissues of energy homeostasis were isolated and weighed. In Table 2 results of different organ weights after dissection are summarized.

Table 2: Organ weight parameters and blood glucose in dexamethasone injected C57BL/6J mice

	control	Dex	p-value
Body weight [g]	24.9 ± 0.82	22.5 ± 0.4	0.0019
Blood glucose [mg/dl]	160.5 ± 17.9	119 ± 14.1	0.011
Liver weight [g]	1.29 ± 0.09	1.06 ± 0.03	0.004
Epidydymal fat [mg]	149.5 ± 28.2	132 ± 22.3	-
Gastrocnemius + Soleus [mg]	151 ± 5.7	135.8 ± 7.5	0.0004
Tibialis anterior [mg]	50.8 ± 2.7	44.6 ± 3.4	0.001
Heart [mg]	161.5 ± 12.4	159.5 ± 9.7	-

Clearly, muscle mass of peripheral muscles (gastrocnemius + soleus 10% weight loss and tibialis anterior 12% weight loss) was reduced, while no influence of dexamethasone on heart muscle mass was observed. The amount of epidydymal fat, the main visceral fat depot of the mouse remained unaffected by chronic GC treatment arguing against the hypothesis that GC treatment generally increases visceral fat depots (124, 125).

The absolute liver weight of the dex-treated animals was 18% less than in control mice but relatively to the body weight the liver weight was comparable (5.2% of body weight in control mice, 4.7% in dex-treated mice, Table 2).

To investigate the effects of glucocorticoid treatment on hepatic lipid homeostasis, liver fats were isolated and measured. Hepatic triglycerides were 3-fold increased in dexamethasone-treated mice and the TG accumulation was highly significant ($p \leq 0.01$, Table 3). Furthermore, the rise in triglycerides was specific as hepatic NEFA and cholesterol content remained unchanged after dex injection. The experiment clearly demonstrated that chronically elevated glucocorticoid levels augment liver triglyceride content and therefore promote fatty liver development.

Interestingly, accumulation of hepatic triglycerides did not coincide with elevated serum triglyceride levels. Compared to the levels after 13 days of injection serum triglycerides declined approximately 2-fold in both experimental groups on day 23, but there were no

differences between dex-treated and saline-treated animals at the day of sacrifice (Table 3). Again, serum cholesterol – a prognostic marker for the development of the Metabolic Syndrome – was increased highly significant. Free fatty acid levels in liver and serum were indistinguishable between the experimental groups.

Table 3: Lipid parameters at day of sacrifice.

	Control	Dex	p-value
<i>Liver</i>			
Triglycerides [$\mu\text{mol/g liver}$]	60.9 \pm 52.2	183.51 \pm 40.1	0.0098
Cholesterol [mg/g liver]	264.3 \pm 78.9	192.2 \pm 22.2	0.129
NEFA [mg/g liver]	66.5 \pm 31.1	49.7 \pm 14.6	0.365
<i>Serum</i>			
Triglycerides [$\mu\text{mol/ml}$]	8.29 \pm 2.2	4.41 \pm 2.1*	0.064
Cholesterol [mg/ml]	96.4 \pm 4.5	121.3 \pm 9.6*	0.0056
NEFA [mg/ml]	28.3 \pm 10.5	35.3 \pm 6.1*	0.359

Data are shown as mean \pm standard deviation. Per experimental group N=4, *Mean values are from three animals only. Serum samples were not available for one animal.

Finally, Hes-1 expression was investigated on the mRNA and on the protein level. The dex-induced fatty liver correlated with diminished Hes-1 levels on the mRNA level (4.5-fold decrease, $p < 0.001$, see Figure 3.12 A) as well as on the protein level (Figure 3.12 B). At the same time, liver fat accumulation was observed. Other members of the Hes-1 family that are usually not expressed in hepatocytes namely Hes-3 and Hes-5 (126) were investigated for compensatory up-regulation. However, levels of Hes-3 and Hes-5 were not detectable in liver after GC stimulation.

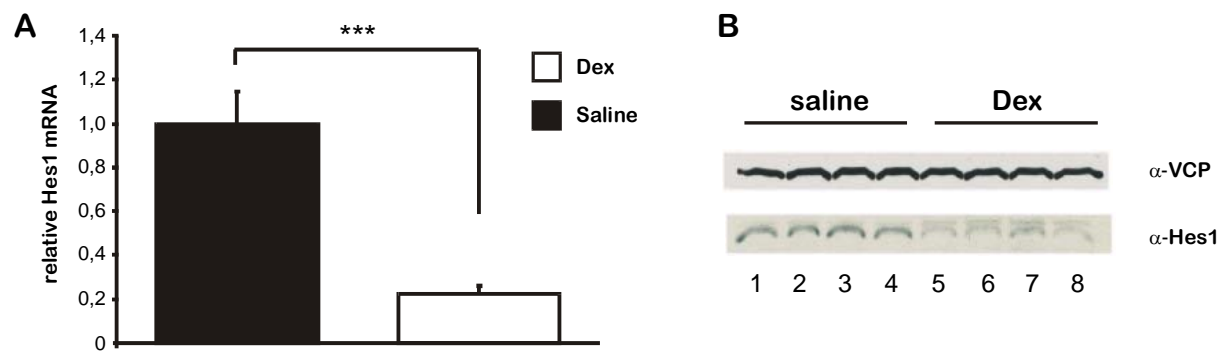


Figure 3.12: Chronically elevated glucocorticoid levels inhibit hepatic Hes-1 expression. A) Quantitative RT-PCR analysis of RNA isolated from livers of C57 BL/6J mice treated for 3 weeks with 1,2 mg/kg dexamethasone using Hes-1 specific primers. Normalisation against TBP. Shown are mean values and s.e.m. N=4. B) Western Blot Analysis of hepatic protein lysates from the same animals as under A). VCP serves as loading control.

The experimental results underline the concept that *in vivo* glucocorticoids are the signal causing decreased Hes-1 expression. The data are consistent with the observation, that Hes-1 expression is attenuated in fatty liver mouse models and that Hes-1 expression increased in GR loss-of-function models.

3.4.2 Starvation experiment in mice with a hepatic glucocorticoid receptor knock-out

Glucocorticoids exert their action via the glucocorticoid receptor and to a lesser extend through the mineralocorticoid receptor. The synthetic glucocorticoid analogue dexamethasone, however, almost exclusively binds to the GR. Therefore, effects seen after dex treatment are attributed to the GR. In earlier experiments a correlative relationship between elevated glucocorticoid levels and diminished hepatic Hes-1 expression has been established.

To ultimately prove a causal link between the GC/GR axis and the regulation of Hes-1 expression *in vivo*, mice bearing a targeted genetic disruption of the glucocorticoid receptor in the liver (L-GRKO) were used. The mice were kindly provided by M. Kirilov and G. Schütz (DKFZ). Generation of the L-GRKO mice has been described previously (97, 98).

Three mice per experimental group were available, however control mice were 4 months old while L-GRKO mice were 6 months old. To test the regulation of hepatic Hes-1 expression depending on a functional GR, control mice and L-GRKO mice were starved for 48h to increase serum GC levels and to induce triglyceride accumulation in the liver. Control refed groups for both genotypes were starved for 48h and subsequently refed for 24h. At the day of sacrifice body weight and blood glucose was determined. As shown in Table 4, L-GRKO mice were in average heavier than controls. No apparent differences in blood glucose values were measured,

although in L-GRKO mice blood glucose values in response to fasting had been reported to be decreased because of limited activation of gluconeogenic programs (98).

Table 4: Body weight and blood glucose parameters of L-GRKO mice

	control starved	L-GRKO starved	control refed	L-GRKO refed
body weight [g]	28.3 ± 0.7	32.9 ± 7.8	32.6 ± 5	36.9 ± 5.3
blood glucose [mg/dl]	79 ± 22	75 ± 13	148 ± 16	162 ± 11

As shown in Figure 3.13, a 2.5-fold induction of hepatic TG content was measured in wildtype mice after 48h starvation. In contrast, starvation of L-GRKO mice for 48h led only to a mild rise in liver triglyceride levels (1.4-fold induction). Moreover, in starved L-GRKO mice Hes-1 mRNA levels were maintained on refed niveau while in the wildtype mice a 2.3-fold decrease was observed following starvation. Despite the limited number of animals per group the data suggested, that a functional GR is necessary to conduct the glucocorticoid-mediated suppression of hepatic Hes-1.

Most notably, L-GRKO mice are protected against the GC/GR-dependent fatty liver induction. Therefore, the results clearly established a direct causal link between the GR activation and Hes-1 suppression.

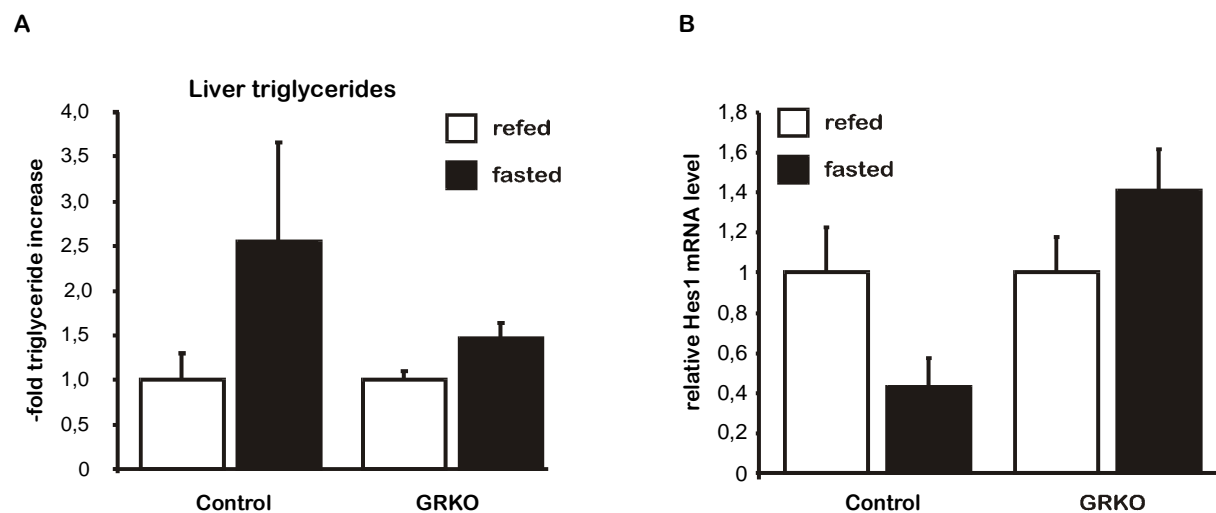


Figure 3.13: The Glucocorticoid receptor is necessary for starvation induced Hes-1 down-regulation. A) Induction of triglycerides in hepatic lipid extracts from wt or liver glucocorticoid receptor knock out (GRKO) mice after 48h starvation (fasted) or 48h starvation and 24h refed period. Shown are mean values and s.e.m. N=3 per group. B) Quantitative RT-PCR from RNA isolated from the same animals as under A) with Hes-1 specific probes. Normalization against TBP. Shown are mean values and s.e.m. N=3 per group.

3.5 Rescue of Hes-1 levels during starvation and in a pathophysiological mouse model

3.5.1 Hepatic Hes-1 overexpression in wt C57BL/6J mice

The inhibition of Hes-1 expression in fatty liver mouse models (see Section 3.3) prompted us to restore the protein levels transiently. Adenoviruses containing either a rat Hes-1 transgene or the GFP protein were used. Transgene expression was under the control of the constitutively active CMV promoter (Figure 3.25). 1×10^9 ifu were injected via the tail vein into C57BL/6J mice.

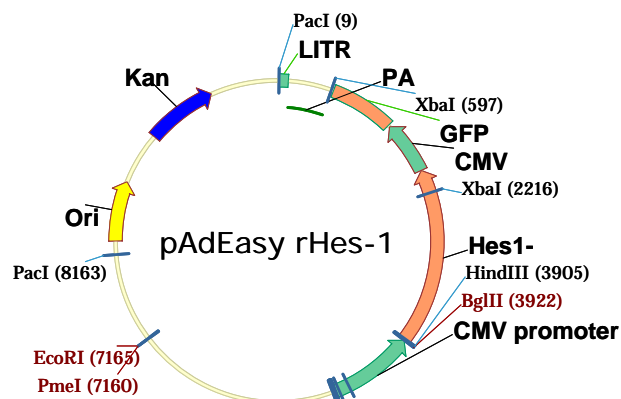


Figure 3.14: Adenoviral vector encoding rat Hes-1. Expression of the transgene Hes-1 (orange) is driven by CMV promoter (light green). To monitor virus localization GFP as second transgene (light green) is included. Vector carries a Kan^R resistance gene and the adenoviral genome of serotype 5. E1 and E3 are deleted (not shown).

First, the effect of transient Hes-1 expression in liver was investigated in male 8 weeks old C57 BL/6J mice treated with either GFP expression virus or Hes-1 expression virus. Initially, each experimental group consisted of five mice. On the day of injection no statistically significant differences in weight or blood glucose levels between the four groups were determined (Table 3.1). After injection, mice were maintained for six days on a chow diet. On day 6, the animals were starved for 48h (starvation group) to induce fat accumulation in the liver (see Section 3.3.1). Control mice were refed after the starvation period for 24h before sacrifice. On the day of sacrifice again no differences in body weight or blood glucose levels were measured (Table 5).

Table 5: Body weight and blood glucose at start and end of experiment

		GFP starved	Hes-1 starved	GFP refed	Hes-1 refed
day 0	body weight [g]	17.94 ± 1.6	18 ± 1.3	17.42 ± 1.9	19.2 ± 1
	blood glucose [mg/dl]	145 ± 12	168 ± 18	150 ± 13	161 ± 16
day of sacrifice	body weight [g]	15.43 ± 1.3	16.5 ± 1.2 [*]	16.7 ± 1.5	17.5 ± 0.6 ^{**}
	blood glucose [mg/dl]	39 ± 5	43 ± 9 [*]	126 ± 34	125 ± 15 ^{**}

^{*}one mouse died in this experimental group during course of experiment, ^{**} two mice died during experiment

Notably, injection of Hes-1 expression virus led to an increased mortality of C57 BL/6J mice (3 of 10 animals died within 8 days after injection). The molecular rationale, however, is unclear. Starvation of C57BL/6J mice led in the control virus group to a 4-fold induction of hepatic triglycerides (814 $\mu\text{mol/g}$ liver fasted vs. 211 $\mu\text{mol/g}$ liver refed). Animals injected with Hes-1 virus responded with a mixed phenotype. In two animals a marked reduction in hepatic triglyceride levels after starvation was observed (197 and 231 $\mu\text{mol/g}$ liver), while the two other animals had equally high triglycerides (1078 and 874 $\mu\text{mol/g}$ liver) compared to mice injected with control virus. Within the refed groups, a tendency towards lower liver triglycerides in the Hes-1 group was observed (mean of 89 $\mu\text{mol/g}$ liver vs. 211 $\mu\text{mol/g}$ liver in the control group, Figure 3.15 A). However, this effect was not statistically significant.

Hes-1 had been implicated in hepatic lipid metabolism, though it was unknown whether Hes-1 would affect systemic insulin resistance when over-expressed in liver. To test this, an insulin tolerance test was performed 5 days after virus-injection. Animals received an insulin dose of 1.5 U/ kg body weight and the blood glucose decline was monitored for 2h. The test was performed before a fatty liver was induced by starvation. Therefore, the impact of Hes-1 overexpression under otherwise physiological conditions was investigated. Hepatic Hes-1 expression in wildtype C57BL/6J mice did not have any beneficial or negative effects on systemic insulin sensitivity (Figure 3.15 B). It remains speculative, however, whether insulin sensitivity in healthy mice is maintained at an optimum, or whether it could be still increased by manipulations such as hepatic overexpression of Hes-1.

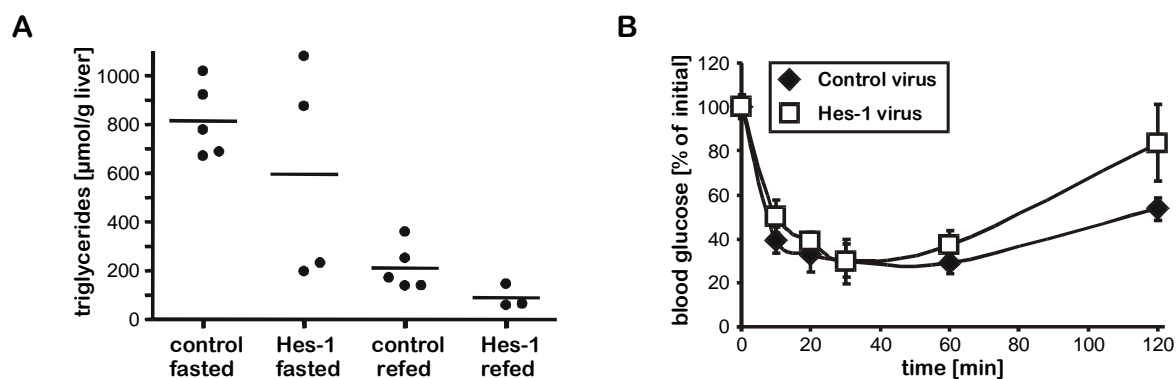


Figure 3.15: Transient Hes-1 expression in C57BL/6J mice. A) Triglyceride content in liver extracts of starved or refeed C57BL/6J mice injected with 1×10^9 ifu GFP control or Hes-1 adenovirus. Dots represent individual animal. B) Insulin tolerance test in C57BL/6J mice after adenoviral injection. Animals were injected at 0 min with insulin (1,5U/kg bodyweight) and the blood glucose levels were measured at the timepoints indicated. Shown are mean values and s.e.m. N=5.

3.5.2 Hepatic Hes-1 overexpression in db/db mice

Db/db mice are characterized by dyslipidemia and develop a fatty liver when fed *ad libitum*. In refed db/db mice, a marked down-regulation of Hes-1 protein has been demonstrated in previous experiments (see Section 3.3.2). Therefore, hepatic Hes-1 levels were restored in a mouse model with chronically perturbed liver lipid metabolism to evaluate the protein's function in this setting and to investigate the impact of hepatic Hes-1 expression on systemic insulin sensitivity.

Male, 13 weeks old db/db mice were injected with 1×10^9 ifu of either Hes-1-expressing adenovirus or GFP control adenovirus. Animals were sacrificed 7 days (starvation groups) or 8 days (refed groups) after adenoviral injection. On day 0 no significant differences in body weight or blood glucose were determined (Table 7). During the experiment, Hes-1 injected mice had a tendency towards lower total body weight as they lost more of their initial weight (Figure 3.16 A). The trend was at no time point statistically significant, however, on day 5, weight differences were most considerable ($p=0.058$). The Hes-1 specific effects on body weight on the days of sacrifice for starved or refed animals, respectively, might be masked by the influence of starvation and refeeding on total body weight. As shown in Table 6 the absolute body weight values of starved GFP mice were higher than starved Hes-1 mice, although animals lost the same percentage of initial body weight after 7 days in both groups (Figure 3.16 A). Also in the refed group no differences in the percental body weight loss was observed after 8 days.

Blood glucose decrease in starved mice was equal in both groups (70 mg/dl after starvation), after refeeding, however, a trend towards normalized blood glucose levels was detected in Hes-1 expressing mice (Hes-1: 163 mg/dl vs. 352 in GFP mice, Table 6) strengthening the notion that these mice had improved glucose control.

Table 6: Body weight and blood glucose parameters at day of sacrifice

		GFP starved	Hes-1 starved	GFP refed	Hes-1 refed
day 0	body weight [g]	54.6 ± 1.5	51.3 ± 3.1	51.4 ± 2.6	48.6 ± 3.2
	blood glucose [mg/dl]	442 ± 41	332 ± 65	360 ± 38	352 ± 96
day of sacrifice	body weight [g]	50.4 ± 1.6	46.6 ± 2.2	49.6 ± 2.6	45.8 ± 1.6
	blood glucose [mg/dl]	70 ± 21	70 ± 19	237 ± 150	163 ± 38

On day 5, an insulin tolerance test in mice fed *ad libitum* was conducted. Intriguingly, systemic insulin sensitivity was markedly improved as shown in Figure 3.16 C. Blood glucose levels in Hes-1 mice declined faster, reaching statistical significance 60 min and 120 min after insulin injection. Hes-1-injected mice exhibited a stronger response to insulin characterized by the 53% decrease of blood glucose levels compared to a 32% decrease in GFP-treated mice. Integration of the curve revealed differences in the area under curve (AUC) value of 20% ($AUC_{GFP}=8395 \text{ min} \times \text{mg/dl}$ vs. $AUC_{Hes-1}= 6697 \text{ min} \times \text{mg/dl}$).

Hepatic triglycerides in db/db animals are moderately elevated (127). Therefore, liver fat content was stimulated additionally by starvation for 48h before sacrifice. To examine the impact of Hes-1 on hepatic lipids, liver fat was extracted and triglyceride and cholesterol levels were determined colorimetrically.

Remarkably, restored hepatic Hes-1 expression prevented hepatic triglyceride accumulation during starvation (Figure 3.16 D, Hes-1 virus 215 ± 84 vs. GFP virus $631 \pm 148 \mu\text{mol/g}$ liver, $p=0,016$). Consistently, total triglycerides in refed mice were also 3,4-fold lower in Hes-1 expressing mice (Hes-1 virus 99 ± 28.6 vs. GFP virus $334 \pm 98 \mu\text{mol/g}$ liver, $p=0.04$).

Furthermore, the effect was highly specific for triglycerides since hepatic cholesterol levels remained unaffected (Figure 3.16 F). Liver cholesterol levels did not change in response to starvation and re-feeding in liver and injection of Hes-1 virus also did not influence the liver cholesterol levels.

To investigate whether the effects of Hes-1 on hepatic TG levels have an impact on VLDL secretion or blood lipid parameters in general serum triglycerides were measured. Generally, the serum TGs ranged between 8 and 25 $\mu\text{mol/ml}$ (3.16 E). These values underline the severe hypertriglyceridemia, since mice fed a high fat diet have serum triglycerides around 2 $\mu\text{mol/ml}$ (128). However, despite reduced liver TGs, serum TGs were indistinguishable between the experimental groups. Furthermore, within the experimental groups the variation between individual animals was very high, indicating that the extend of hypertriglyceridemia was diverse.

In summary, Hes-1 re-expression in livers of db/db mice, a chronic fatty liver model, generally improves the diabetic phenotype by reducing hepatic triglyceride storage and improving systemic insulin sensitivity. Trends towards normalized blood glucose levels in refed animals remain to be confirmed by further experiments.

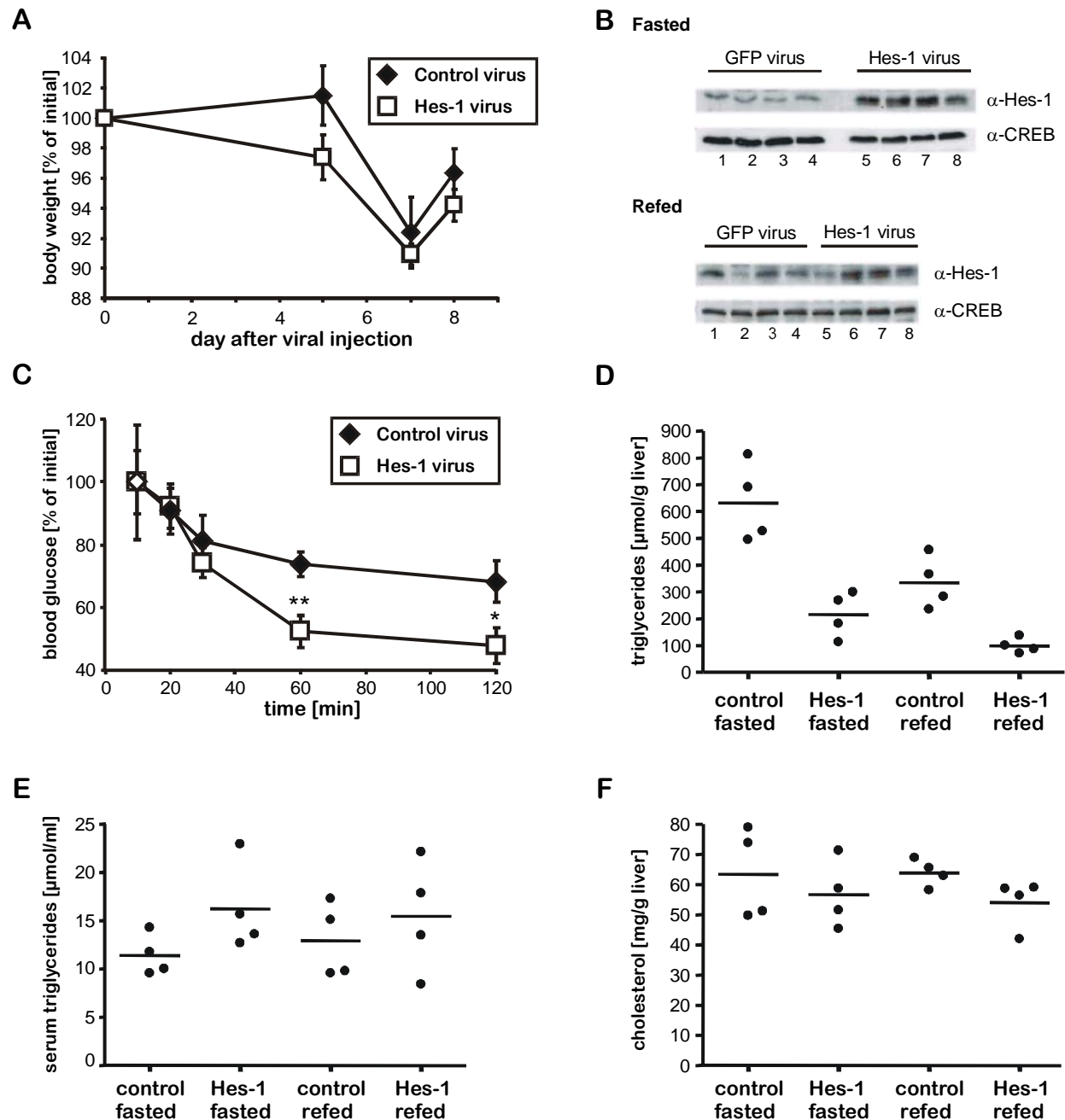


Figure 3.16: Transient Hes-1 expression in db/db mice improves the metabolic phenotype. A) Body weight development of C57 BL/6J mice injected with 10^9 ifu GFP control virus or rat-Hes-1 virus during the course of experiment. *** $p \leq 0.001$, * $p \leq 0.05$ $N=8$, at day 8 $N=4$ B) Western Blot analysis of Hes-1 overexpression in virus treated animals using Hes-1 specific antibody. CREB served as loading control. C) Insulin tolerance test in db/db mice after adenoviral injection. Animals were injected at 0 min with insulin (1,5U/kg bodyweight) and the blood glucose levels were measured at the timepoints indicated. Shown are mean values and s.e.m. $N=5$. D) Triglyceride content in liver extracts of starved or refed db/db mice injected with 1×10^9 ifu GFP control or Hes-1 adenovirus. Same mice as under A) $N=4$. Dots represent individual animal E) Serum triglyceride levels of the same animals. $N=4$. F) Cholesterol content in liver extracts of the same animals as under B) $N=4$.

3.5.3 Phenotype analysis of Hes-1 overexpression in db/db mice

Hes-1 is a transcription factor regulating gene expression, therefore the phenotype in db/db mice observed after adenoviral injection of Hes-1 was investigated on the molecular level using RT-PCR techniques.

Biochemical pathways known to either regulate or have an impact on lipid metabolism were probed by investigating expression levels of rate-determining enzymes/ transporters within these pathways. The results of this analysis are listed in Table 7.

Table 7: Gene expression data from db/db mice treated with Hes-1 virus or control

Gene	GFP refed	GFP starved	Hes-1 refed	Hes-1 starved
<i>De-novo triglyceride synthesis</i>				
PPAR γ	1	0.74	0.78	0.75
FAS	1	0.1	1.51	0.13
ACC1	1	0.25	1.15	0.18
SCD1	1	0.15	0.98	0.16
<i>β-oxidation</i>				
PPAR α	1	0.71	0.9	0.74
CPT1 α	1	1.37	1.05	1.92
<i>Fat transport</i>				
FABP-1	1	0.71	0.59	0.79
Caveolin	1	0.62	0.66	0.61
CD36	1	1.14	0.77	1.21
ApoB	1	1.08	1.31	1.6
MTTP	1	1.05	1.11	0.97
<i>Gluconeogenesis</i>				
GK	1	0.54	0.78	0.44
PEPCK	1	0.67	1.39	1.18
G6Pase	1	0.44	1.04	0.85
<i>Glycogen and Pentose Shunt</i>				
PDK4	1	2.94	0.59	2.01
PP1s3c	1	1.12	0.67	1.47
PGDH	1	0.21	0.46	0.18

First, the influence of Hes-1 on *de novo* triglyceride synthesis was investigated. Synthesis of triglycerides is under control of the enzymes acyl-CoA carboxylase 1 (ACC1), fatty acid synthase (FAS) and stearoyl-CoA desaturase (SCD1), whose expression is mainly regulated on the transcriptional level (129, 130). Since PPAR γ has been described as a Hes-1 target, its expression was determined in correspondence to Hes-1 overexpression. A mild effect of Hes-1 overexpression on PPAR γ expression was observed (GFP refed 1 vs Hes-1 refed 0.78 and GFP starved 0.74 vs. Hes-1 starved 0.75 relative units).

During starvation, lipogenic processes are dramatically downregulated reflected by decreased expression of FAS (10-fold less), ACC1 (4-fold less) and SCD1 (6.7-fold less) in starved GFP animals compared to the refed GFP group. As shown in Table 8, hepatic Hes-1 expression did not alter this regulation. Only in the Hes-1 refed group was a 50% increase in FAS expression observed, though this effect did not reach statistical significance.

Interestingly, fat transport seems to be differentially regulated in Hes-1 expressing mice under refed conditions. Liver-specific fatty acid binding protein (FABP-1), CD36, and caveolin 1 are transporters for free fatty acids which are esterified upon incorporation into the cell as triglycerides. Therefore, fat transporters control substrate availability of FFAs and limit the rate of esterification. Interestingly, expression of FABP-1, caveolin and CD36 is decreased in refed animals injected with Hes-1 virus point towards an attenuated uptake rate of free fatty acids by the liver. This suggests that decreased influx of FFAs is responsible for the diminished triglyceride levels observed in mice treated with Hes-1 adenoviruses. Remarkably, these results resembled the observations obtained in mice after hepatic GR knockdown, underlining the importance of Hes-1 as downstream target of GR.

To investigate whether triglyceride efflux is also influenced by viral Hes-1 expression, the key-determinants of VLDL production were examined. However, hepatic VLDL production was not altered as demonstrated by the unchanged expression of microsomal triglyceride transport protein (MTTP). On the other hand, a 1,3-fold induction of low density lipoprotein ApoB-100 is produced. Hes-1 injected mice were not characterized by elevated serum triglyceride levels (see Figure 3.27 E), consistent with the result that MTTP expression remained unchanged.

The data implies, that triglyceride and/or free fatty acid disposal in the liver is decreased. This effect was not, however, reflected in serum triglyceride parameters that remained unaffected by hepatic Hes-1 re-expression.

Hes-1 expression in the liver also affected genes implicated in the regulation of glucose homeostasis and glycogen storage. Glycogen storage and hepatic fat storage inversely correlate and a shift towards higher lipid accumulation has been demonstrated to promote hepatic insulin resistance (131, 132). Pyruvate dehydrogenase kinase 4, an inhibitory kinase of the pyruvate dehydrogenase complex (PDC), was 1.7-fold downregulated in Hes-1 expressing refed mice indicating an activated PDC. The oxidative consumption of pyruvate by PDC limits availability of pyruvate for gluconeogenesis thereby decreasing hepatic glucose output. Consistent with activated PDC, blood glucose levels in Hes-1 expressing mice were lower under refed conditions compared to control mice as shown in Table 7.

Furthermore, phosphoglucanate dehydrogenase activity was 2.2-fold reduced in Hes-1 expressing mice (refed). Phosphoglucanate dehydrogenase is one of only three enzyme producing NADPH, which is used in a wide variety of anabolic cellular processes e.g. fatty acid synthesis from C2-precursors. Reduced NADPH levels could therefore imply diminished fatty acid synthesis and subsequently, less fat accumulation in the liver.

The expression data point out that Hes-1 indeed affects hepatic lipid homeostasis. In this respect, mainly limited FFA influx seems to contribute to the observed phenotype.

3.5.4 Reconstitution of diminished Hes-1 in dexamethasone-treated mice

Finally, effects of Hes-1 reconstitution in dexamethasone-induced fatty liver models were investigated. Mice were treated with dex as described in Section 3.4.1 to induce hepatic fat accumulation and deplete hepatic Hes-1 levels. One week prior to sacrifice, mice were injected with adenoviruses encoding GFP or ratHes-1. Mice were sacrificed and liver biopsies were taken for biochemical analysis.

Liver protein extracts of all mice were immunoblotted using Hes-1 specific antibody. Dexamethasone treatment diminished Hes-1 protein levels significantly as shown in Figure 3.17 (compare 1.X vs 2.X where X indicates the individual animal number). Injection of ratHes-1 expression virus (10^9 ifu/ mouse) yielded moderate overexpression of Hes-1 in the liver (compare 1.X vs 3.X and 4.X)

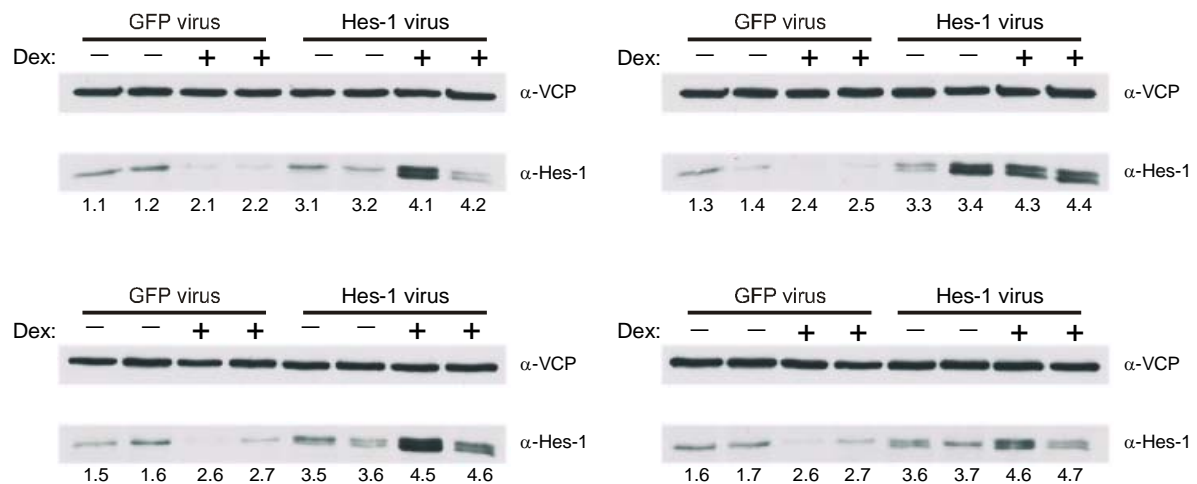


Figure 3.17: Evaluation of Hes-1 expression in C57BL/6J mice after three weeks dexamethasone treatment. Liver protein extracts of all animals were immunoblotted and probed with Hes-1 specific antibody. Individual lane represents one animal. VCP served as loading control.

Effects of dexamethasone injection on hepatic lipid content were evaluated. Three weeks injection caused 1.5-fold triglyceride accumulation in liver in mice injected with GFP expressing virus (Figure 3.18 A, compare bar 1 vs. bar 2). in mice receiving Hes-1 virus, triglyceride enrichment in liver was prevented (compare bar 2 vs. bar 4), ultimately proving that restored Hes-1 levels are protective against GC/GR induced fatty liver development. Hes-1 target gene identification confirmed fat transport genes caveolin1 and CD36 (Figure 3.18 B) and key-regulators of β -oxidation (PPAR α , and CPT1 α) that had been identified in GR knockdown studies (Section 3.2) as potential Hes-1 targets in db/db mice (Section 3.5.3).

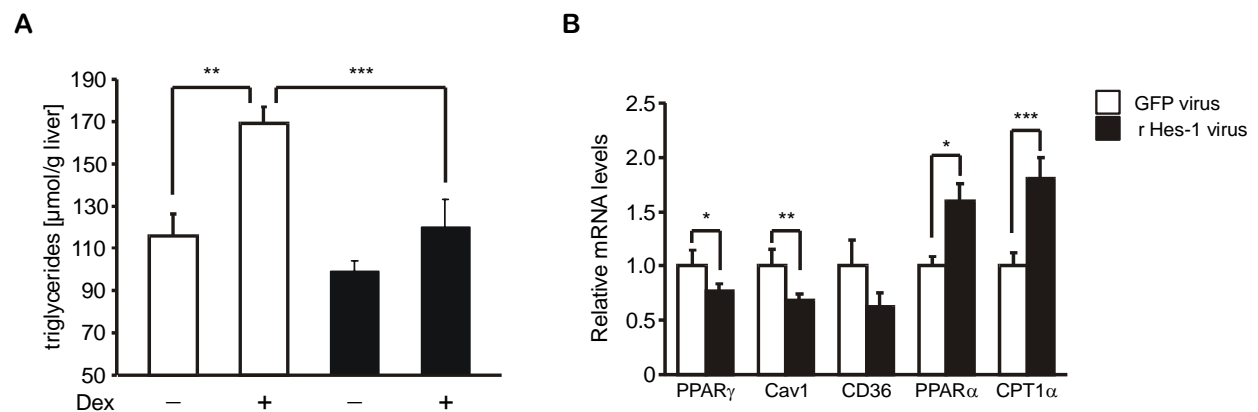


Figure 3.18: Rescue of hepatic Hes-1 after glucocorticoid treatment prevents fat accumulation in the liver. A) Triglyceride measurement in liver lipid extracts from C57BL/6J mice treated for three weeks with 1.2 mg/kg dex or saline and injected with adenoviruses expressing GFP (white bars) or rHes-1 (black bars) Data shown are means and s.e.m. N=5, B) Quantitative RT-PCR of mRNA isolated from the same animals as under A using specific Taqman® probes for Cav1, CD36, CPT1 α , PPAR α and PPAR γ . N=7 * $p \leq 0.05$, ** $p \leq 0.01$, *** $p \leq 0.001$.

3.5.5 Generation of Hes-1 RNAi Adenoviruses

Overexpression of Hes-1 promoted changes in lipid homeostasis. To confirm direct target genes of Hes-1, a loss of function approach was chosen. For this purpose, Hes-1 shRNA constructs were designed and tested for knock-down efficiency *in vitro* and *in vivo*. Oligonucleotides comprising the shRNA sequence were selected employing the BLOCK-iT™ RNAi Designer from Invitrogen (<https://rnaidesigner.invitrogen.com/rnaiexpress>, for details see Section 5.5). The Hes-1 target sequence with accession number NM_008235 was used and 7 shRNA oligonucleotides recognizing sequences within the open reading frame, the 5' UTR and the 3' UTR were tested. Virus was generated as described (see Section 5.5). To test knock-down efficiencies, mouse hepatoma cells (Hepa 1C1 wt) were infected with multiplicities of infection ranging from 1 to 100. The cells were incubated for two days with virus and mRNA as well as protein lysates were analyzed for the respective target protein knock-down. An adenovirus containing an unspecific shRNA sequence was used as control.

From all viruses tested, pAD BLOCK-iT/DEST mHes1 RNAi4 showed best knock-down efficiency in Hepa 1C1 wt cells. A 4-fold reduction of Hes-1 mRNA was observed at MOIs of 10 and 100 (Figure 3.19 A), while the Hes-1 mRNA in the control groups remained unchanged. Western blot analysis confirmed a dose-dependent down-regulation of Hes-1 protein levels. However, treatment of Hepa 1C1 wt cells with control RNAi virus also decreased Hes-1 protein levels (Figure 3.19 B). At all virus doses tested, Hes-1 RNAi virus exceeded the knockdown effect observed with the control virus. The mechanism causing Hes-1 depletion after treatment with control virus remained unclear.

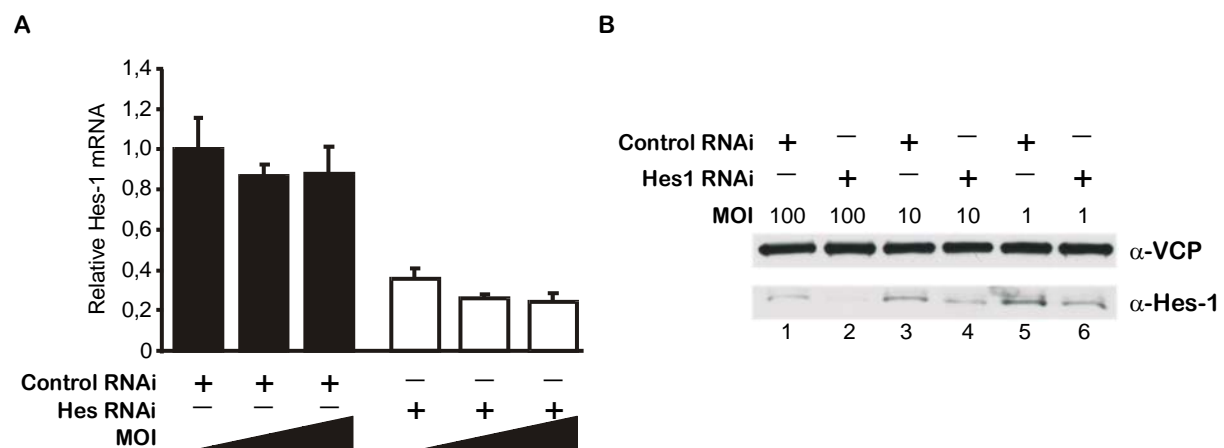


Figure 3.19: Transient Hes-1 knock down using adenoviruses. A) Quantitative RT-PCR from mRNA extracted from Hepa 1C1 wt cells treated for 48h with adenoviruses containing either a shRNA against murine Hes-1 or an unspecific shRNA. MOI as indicated. Data were normalized to TBP. Data are means and standard deviation. N=2 B) Western Blot analysis from protein extracts of Hepa 1C1 wt cells treated for 48h with the same viruses as under A). Immunoblot with specific antibodies. VCP serves as loading control.

To test whether the unspecific effects on Hes-1 expression seen after control virus treatment would affect starvation-induced down-regulation of Hes-1 *in vivo* control measurements were undertaken. mRNA samples from C57BL/6J mice injected with 10^9 ifu of a random shRNA expressing adenovirus and starved overnight (5 mice) and control mice refed for 6h (5 mice) were kindly provided by M. Berriel-Diaz. In a qPCR experiment no difference in the regulation of Hes-1 levels depending on food access was observed in these samples, strengthening the notion that viral injection interferes with Hes-1 regulation (Figure 3.20 A). These results were confirmed by examination of a second mouse experiment. Samples of two mice per group were obtained from E.Chichelnitskiy. Mice had been starved for 24h or starved and subsequently refed for 24h. As shown in Figure 3.20 B after starvation Hes-1 expression was not reduced approximately 2-fold (compare to Figure 3.6) but remained unchanged. Mechanistically, it is elusive, how adenoviruses compromise Hes-1 regulation under fasting conditions *in vivo*.

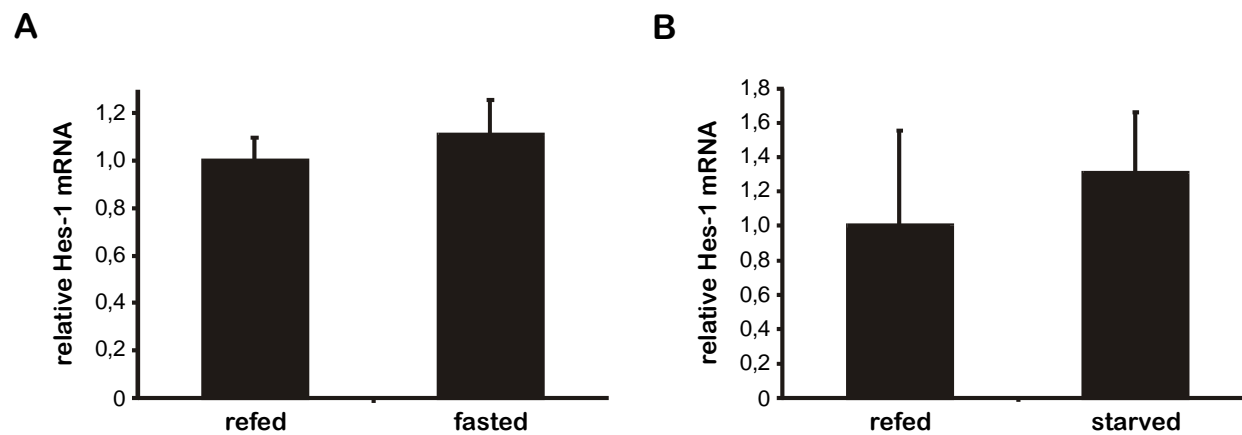


Figure 3.20: De-regulation of Hes-1 expression in response to adenoviral injection. A) C57BL/6J mice were injected with 10^9 ifu of an adenovirus expressing an unspecific shRNA construct. 7 days after injection mice were fasted overnight or fasted and then refed for 6h. mRNA from livers was isolated and the relative Hes-1 expression was examined in qPCR experiments. Normalization against TBP. Data shown are means and s.e.m. N=5 B) C57BL/6J mice were injected with 10^9 ifu of an adenovirus expressing an unspecific shRNA construct. 7 days after injection mice were fasted for 24h or fasted and then refed for 24h. mRNA from livers was isolated and the relative Hes-1 expression was examined in qPCR experiments. Normalization against TBP. Data shown are means and standard deviation. N=2

3.5.6 RNAi experiment in primary hepatocytes

Since unspecific virus effects were observed in mice, effects of hepatic Hes-1 depletion were investigated in primary hepatocytes kindly provided by S. Bohl and P.Nickel from the Department of Systems Biology of Signal Transduction (Prof.Dr. U. Klingmüller, DKFZ).

Cells were treated with a MOI of 100 for 48h. A virus encoding for a non-targeting shRNA was used as negative control as well as non-virus treated cells, to investigate non-specific viral effects. One hour prior harvest, cells Hes-1 expression was stimulated with 10 μ M forskolin. Hes-1 knockdown was evaluated in protein lysates and on the mRNA level. Figure 3.21 depicts the results obtained on the protein level. In uninfected cells and after treatment with non-

targeting virus (sh Con) no significant changes in cellular Hes-1 protein levels are seen. Forskolin treatment induced Hes-1 expression in all controls (compare lane 1 vs. 2 and lane 3 vs. 4). Hes-1 levels were diminished after infection with Hes-1 targeting shRNA virus (compare lane 1 vs 5). Forskolin treatment failed under these conditions to increase cellular Hes-1 levels.

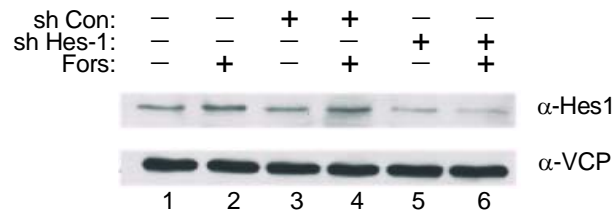


Figure 3.21: Hes-1 is depleted in primary hepatocytes. Primary hepatocytes were treated with adenoviruses encoding for a non-targeting shRNA sequence (control shRNA) or Hes-1 targeting shRNA (Hes-1 shRNA) at a MOI of 100 or PBS only (no virus). Forskolin (10 μ M) was used to stimulate Hes-1 expression 1h prior harvest. 48h after infection protein lysates were prepared and evaluated via Western Blot using specific antibodies. VCP served as loading control.

Selected target genes identified in gain-of function experiments were investigated after Hes-1 knockdown. Special emphasis was put onto genes regulating fat transport, such as caveolin 1 and CD36. As shown in Figure 3.22, Hes-1 depletion resulted in increased PPAR γ (3-fold compared to untreated cells, 1.8-fold compared to control-virus treated cells) levels as well as activation of caveolin1 expression (2-fold). Evaluation of effects caused by Hes-1 on CD36 and FABP-1 were not conclusive due to unspecific effects the adenovirus itself caused. In Figure 3.22, dramatic induction of CD36 expression (22-fold) after infection with control virus was observed (compare bar 1 vs. bar 2 CD36), FABP-1 was induced 11-fold in control-virus treated cells. The remarkable unspecific effects of the adenovirus however, where not a general feature but limited to a few genes.

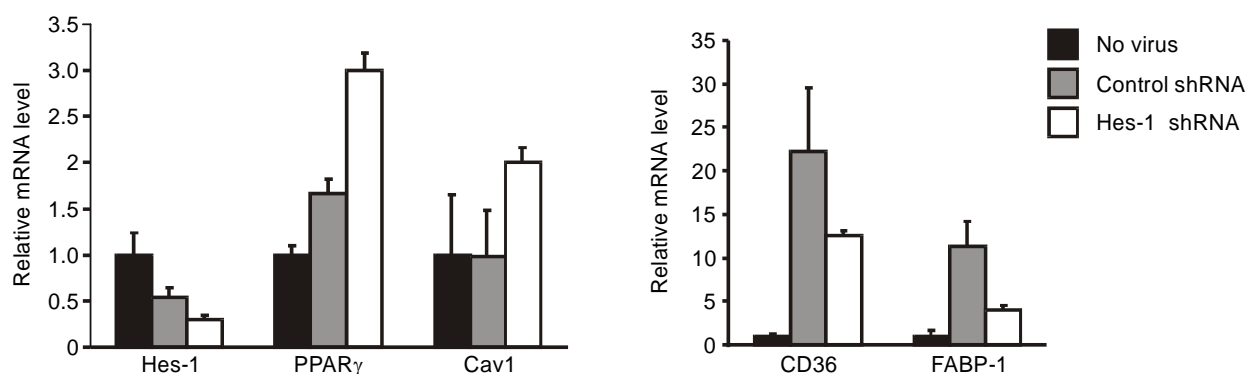


Figure 3.22: PPAR γ and Cav1 are up-regulated after Hes-1 depletion in primary hepatocytes. Primary hepatocytes were treated with adenoviruses encoding for a non-targeting shRNA sequence (control shRNA) or Hes-1 targeting shRNA (Hes-1 shRNA) at a MOI of 100 or PBS only (no virus). After 48h RNA was isolated, transcribed into cDNA and analysed by qPCR using specific Taqman $^{\circledR}$ probes. Data shown are means and standard deviation. N=2

The loss of function analysis in primary hepatocytes, therefore, confirmed target genes of Hes-1 namely PPAR γ and caveolin1.

3.5.7 Promoter analysis of new target genes for N-Box elements

Hes-1 is a transcriptional repressor and associates to well-known response elements on the DNA – N-box elements (CACNAG) and C sites (CACGNG) (133). In studies with the human PPAR γ promoter N-Box elements to which Hes-1 associated were already identified (211). To test whether CD36 and Cav1 represent direct inhibitory targets of Hes-1 the 5'-UTR between -1000bp and -1bp were searched for putative N-Box elements using Tessmaster *in silico* analysis. The sequences were derived from accession number NT_165760 in case of CD36 and from NT_039340.7 for Cav1, respectively. Two putative N-Box elements were identified in the investigated 5'-UTR of CD36, namely CACGAG (-5bp/-10bp) and CACAAG (-951bp/-956bp). No obvious binding sites were retrieved from analysis of the 5'-UTR of caveolin 1. Absence of classical binding sites on the caveolin promoter might indicate a different mechanism of inhibition.

3.6 Mechanism of GC/GR mediated Hes-1 repression

3.6.1 Glucocorticoids regulate Hes-1 expression on the transcriptional level

Cellular Hes-1 levels are affected by a wide variety of signals including hormones regulating energy homeostasis. Previous studies demonstrated that the fasting hormone glucagon stimulated Hes-1 expression in a cAMP/CREB dependent manner (112). Glucagon activates an intracellular cascade of reactions finally leading to phosphorylation of the transcription factor cAMP responsive element binding protein CREB (see Section 1.3.1).

The observation that other fasting hormones – namely glucocorticoids - diminished Hes-1 on mRNA and protein level thus was surprising. Therefore, the mechanism of GC-induced Hes-1 depletion was investigated.

To this end, rat hepatocytes (H4IIE cells) were stimulated with dexamethasone, forskolin (an activator of CREB (134)) or combinations of both to mimick the effects of fasting hormones in cell culture. Exposure of cultured hepatocytes to 10 nM dexamethasone for 3 hours significantly decreased Hes-1 expression (Figure 3.23 A, lane 2 compared to lane 1). *In vitro* activation of the GC/GR axis therefore reversed the effects seen in the loss of function model of hepatic GR (see Section 3.2.2.2).

In contrast to GCs, forskolin treatment (10 μ M for 1h) stimulated Hes-1 expression (Figure 3.23 A lane 3 compared to lane 1). Co-treatment with both stimuli (lane 4) abolished forskolin-stimulated Hes-1 expression indicating opposing effects of forskolin and dexamethasone.

Glucagon-regulated stimulation of Hes-1 expression is controlled by a proximal promoter element containing a cAMP response element (CRE) between -217 and -211 bp, where CREB is constitutively bound. Phosphorylation of CREB on Ser-133 activates Hes-1 expression. The co-treatment studies in H4IIE hepatocytes indicated that glucocorticoids surprisingly counter-acted glucagons action. Consequently, the effect of glucocorticoids on CREB phosphorylation was investigated. Notably, the amount of P-CREB in the cell was attenuated after stimulation with 10 nM dexamethasone as shown in Figure 3.23 A (compare lane 1 vs. lane 2). Forskolin, in contrast, stimulated serine-phosphorylation of CREB.

Glucocorticoids mainly mediate their actions through binding to the glucocorticoid receptor (GR), a nuclear receptor and transcriptional regulator. Altered CREB phosphorylation pointed towards interference with transcriptional activation of the Hes-1 promoter and not e.g. towards accelerated degradation of Hes-1 protein.

In transient transfection assays, the transcriptional activity of the Hes-1 promoter in presence and absence of GCs was assessed. Transcriptional activation was studied in human hepatoma cells (HepG2) using the reporter gene vector pGVB Hes-1 prom (-467/+160). The reporter gene vector contained the murine proximal Hes-1 promoter region (-467/+160) controlling the expression of the luciferase reporter-gene. Promoter activity was stimulated by co-transfection of a vector encoding protein kinase A (PKA wt), a down-stream target of the cAMP signalling pathway, which phosphorylates CREB. As a negative control a kinase deficient PKA (PKA mut) construct was co-transfected.

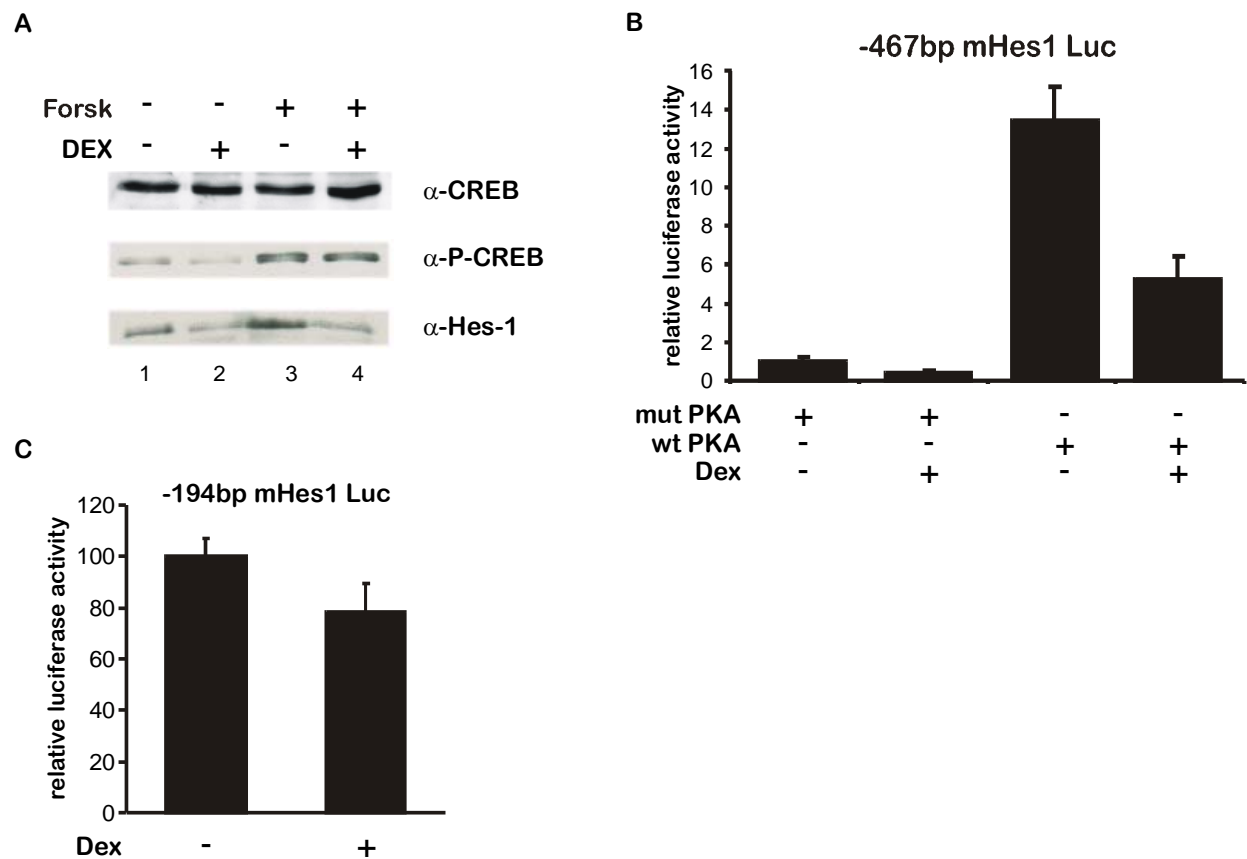


Figure 3.23: Glucocorticoids inhibit Hes-1 expression in vitro by dephosphorylation of CREB. A) Western Blot analysis of H4IIE rat hepatocytes treated for 3 h with 10 nM dexamethasone and 1h prior to harvest with forskolin (10 μ M). B) Transient transfection of HepG2 hepatocytes with the proximal Hes-1 promoter (-467bp to 60bp) and co-transfection with expression vectors for PKA or kinase-deficient PKA (PKA mut). 24h after transfection stimulation with 10 μ M dexamethasone for 24h. C) Transient transfection with proximal mHes-1 promoter (-194bp to 60bp) into HepG2. Stimulation as in B. Data shown are means and s.e.m. N=9

Co-transfection of 50 ng PKA expressing vector to 100ng reporter gene vector caused 13, 4-fold increase in promoter activity as shown in Figure 3.23 B. Dexamethasone treatment attenuated basal promoter activity approximately 2,5-fold (compare bar 1 and 2). Furthermore, GCs also diminished PKA-dependent up-regulation of promoter activity 2,6-fold (compare bar 3 and 4). Hence, diminished Hes-1 levels after GC treatment are caused by transcriptional regulation of its expression.

Glucocorticoid stimulation of a shorter Hes-1 promoter construct comprising the sequence between -194bp and +60 bp (pGL2 mHes1 -194bp) had no significant effects on transcriptional activity (Figure 3.14 C) narrowing down the GR responsive region to -467bp to -194bp.

3.6.2 Direct interference of GR on the Hes-1 promoter

3.6.2.1 *In silico* analysis of the proximal Hes-1 promoter

Glucocorticoids regulate Hes-1 expression on the transcriptional level (see Section 3.6.1). Thus, the proximal promoter region was searched for consensus glucocorticoid response elements (GREs) and other transcription factors that might mediate GC/GR effects.

In silico analysis of the murine proximal Hes-1 promoter sequence (-440bp to -4bp) using the Transcription Element Search System from Pennstate University (<http://www.cbil.upenn.edu/cgi-bin/tess/tess?RQ=SEA-FR-Query>) revealed several putative binding sites for transcription factors. Figure 3.24 shows a comprehensive overview of factors that were found via Tessmaster search and that likely bind to recognition elements on the Hes-1 promoter together with transcription factors that have already been published.

```

-440 ATCCTCTTTA CCTTGTTC TCCTTTTTTC AATCACTAAA TTTTGTCTTG
-390 GCCTATATCT GTTCAAAATA TTTTTCAAAT GAACTTATTA TACAAAGTAG
-340 TTATATTGCA TGCAGCAAGA ACAATAAAAA CCAAAGGCCT GGCCACAAAA
-290 GAAATAGACT AGACTAAAAC TAAGCAAAGC CCAGAGGAAA GAGTTAGCAA
-240 AGGGTTAAAA TCCTTTTGAT TGACGTTGTA GCCTCCGGTG CCCCAGGCTC
-190 AGGCGCGCGC CATTGGCCGC CAGACCTTGT GCGTAGCGGC CAATGGGGGG
-140 GCGCAGTCCA CGAGCGGTGC CGCGTGTCTC TTCCTCCCAT TGGCTGAAAG
-90  TTA CTGTGGG AAAGAAAGT T TGGGAAGTTT CACACGAGCC GTTCGCGTGC
-40  AGTCCCAGAT ATATATAGAG GCCGCCAGGG CCTGCG

```

Figure 3.24: Promoter Analysis of proximal Hes-1 promoter region (-440bp to -4bp). Binding sites were identified using bioinformatic search of known responsive elements (Tessmaster analysis) and literature data. Putative binding sites of transcription factors are indicated color coded. red: Hes-1 N-Box elements, grey: CREB, blue: C/EBP- α , green background: GR, yellow background: RBP-J κ , magenta background: c-FOS, underlined AP-1 site.

The analysis revealed three N-Box elements in this region (-53 to -58bp, -127bp to -132bp and -160 bp to 165bp), where Hes-1 itself associates in an autoregulatory manner to repress its own expression (135). The most proximal Hes-1 binding site (-53bp to -58bp) overlaps with a binding site for RBP-J κ (-56bp to -62bp). In total three binding sites are published for RBP-J κ on the Hes-1 promoter (136), however they were not found by Tessmaster search. A putative NFkappaB site (5'-GGGAAGTTTC-3') was identified between -60 bp and -69 bp, partially overlapping with RBP-J κ sites. Additionally, the very same region also revealed a positive hit

for AP-1 from -59 to -65bp (5'-AGTTTCA-3') as well as a putative binding site for C/EBP α (-61bp to -71bp).

Most interestingly, the *in silico* study recognized four putative binding sites for the GR between -427bp and -422bp, -350bp and -361bp, -318 bp and -323bp and between -158bp and -163bp. The consensus sequence of a glucocorticoid response element (GRE) is 5'-AGAACCnnnTGTACC-3' (137). But half site AGAACA as well as TGTGCC, which is related to the right half site of the 15 bp consensus, have both been shown to bind the glucocorticoid receptor (138) (139) (140). Exactly these two half sites have been identified on the Hes-1 promoter. Also the half site TGTTCC has been reported to be contacted by the GR (141). The putative site 5'-TGAACCTATTAT-3' is somewhat less characteristic as four mismatches indicate a decreased likelihood for GR binding when comparing to another consensus model 5'-AGAACAnTGTTCT-3'.

3.6.3 The GR binds to the proximal Hes-1 promoter region

Since the *in silico* analysis clearly suggested association of the GR to the proximal Hes-1 promoter, it was tested, whether the GR binds *in vivo*. To address this question chromatin immunoprecipitation (ChIP) experiments from liver extracts of mice starved for 48h or mice that were refed for 24h after the starvation period were performed. Samples from starved mice were investigated since upon ligand binding GR shuttles to the nucleus, where it exerts its action. ChIP experiments do not allow the mapping of distinct response elements, but of promoter regions around 1000 bp size (see Section 5.3.11). Thus, the individual elements identified in the Tessmaster analysis cannot be mapped with this assay. Rather an overall binding of the GR in the proximal promoter region can be assessed.

As shown in Figure 3.25, using a GR-specific antibody the proximal Hes-1-promoter region was pulled-down confirming that GR is present in this DNA region. However, the amount of GR detected was variable between the mice (compare lanes 1-4, GR antibody). In one starved mouse (Figure 3.25, lane 1) no GR could be detected on the Hes-1 promoter despite three technical replicates of the experiment, although enhanced GR binding was predicted after fasting. *In vivo*, however, the results were less definite. Despite higher glucocorticoid levels, increased binding of GR to the proximal promoter in starved animals could not be demonstrated.

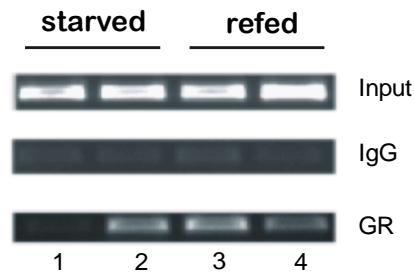


Figure 3.25: The glucocorticoid associates *in vivo* with the Hes-1 promoter. Chromatin immunoprecipitation from crosslinked liver protein/DNA extracts from C57BL/6J mice starved for 48h (starved) or refed after starvation for 24h (refed) using a GR-specific antibody or unspecific IgGs. After de-crosslinking, PCR of DNA with primers specific for the proximal Hes-1 promoter region was performed. Shown is a representative result of three experiments.

3.6.4 The GR binds to two elements on the Hes-1 promoter

To verify the *in silico* identified GREs Avidin-Biotin-Conjugated DNA binding Assays (ABCD- Assay) were performed. Biotin-labeled oligonucleotides covering adjacent regions of the Hes-1-promoter, a consensus GRE element as positive control and a random DNA sequence as negative control were probed against protein extracts from H4IIE rat hepatocytes (see Section 5.3.10). Oligonucleotides were designed as such that predicted GREs were intact. Proteins bound to the respective oligonucleotides were eluted and identified in western blots.

Figure 3.26 shows the result of the ABCD assay. A weak GR binding to the oligonucleotide comprising the region from -392 to -345bp was measured (compare lane 1 to lane 6). This sequence was also predicted to harbour a GRE (-361/-350bp). Association of GR to the -440bp to -393bp region, however, was even stronger, while no GRE was identified using bioinformatics tools (lane 2 vs. lane 6). Compared to a random oligonucleotide no increased binding of GR was observed between -296bp and -210bp (lane 3, 4 and 5 vs. 6).

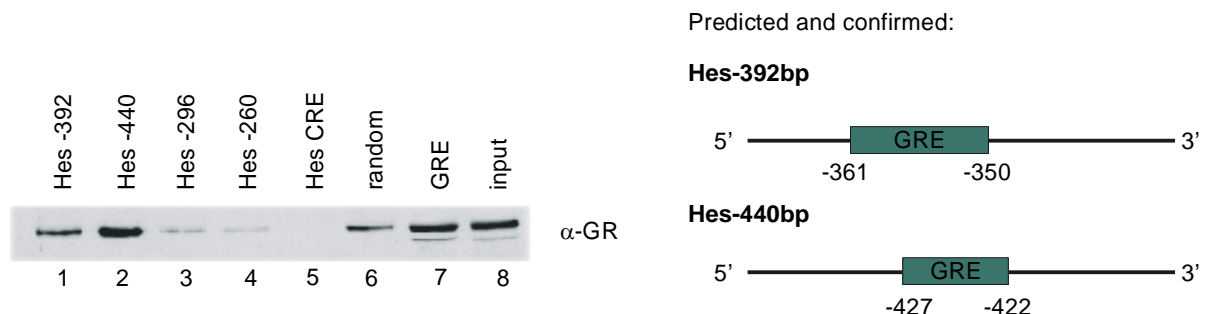


Figure 3.26: The GR occupies to binding sites on the Hes-1 promoter. ABCD-Assay with oligonucleotides spanning the proximal promoter region of the Hes-1 promoter. Hes-392 (-392bp/-345bp), Hes-440 (-440bp/-393bp), Hes-296 (-296bp/-261bp), Hes-260 (-260bp/-225bp), Hes CRE (-226/-196). Western Blot analysis of bound proteins using specific antibodies against GR (Santa Cruz, M-20). Input represents 10% of the protein lysates used for the ABCD Assay. Shown on the right site is a schematic view of oligonucleotides comprising GREs (green).

To characterize the GREs as repressive or activating elements, further studies need to be done requiring transfection assays with *Hes-1* promoter constructs comprising mutated versions of the identified GREs. These experiments are currently undertaken and are beyond the scope of this thesis.

3.7 GR-mediated dephosphorylation of CREB

In transient transfection experiments GCs interfered with *Hes-1* gene expression directly on the transcriptional level (see Section 3.6.1). On the protein level glucocorticoids inhibited the activation of cAMP-responsive element binding protein (CREB), a key-regulator of *Hes-1* gene expression, by decreasing its phosphorylation at Ser-133.

Attenuated P-CREB levels provide a second rationale for decreased *Hes-1* promoter activity, yet the mechanism of dephosphorylation induced by glucocorticoids was uncertain.

3.7.1 Dexamethasone treatment of MKP-1^{-/-} mice

GCs are generally capable of altering cellular phosphorylation status e.g. by activation of phosphatases. The activation of a CREB phosphatase by GCs was one possible explanation for the observed dephosphorylation. Depending on the cell type and physiological context, different CREB phosphatases such as PP1 (142), PP2A (143) and mitogen-activated protein kinase phosphatase-1 (MKP-1, also termed Dual-specific phosphatase 1, DUSP-1) (144) inactivate CREB. Among them, only MKP-1 has been described to be activated by glucocorticoids, therefore its function in a metabolic context was further investigated.

MKP-1 has been implicated in GC-induced insulin resistance as a potent inhibitor of insulin-triggered glucose uptake (145). Interestingly, MKP-1^{-/-} mice display a metabolic phenotype. They are lean due to reduced body adiposity and have a decreased liver weight, apparently because of reduced hepatic triglyceride levels (146). Furthermore, in isolated MKP-1-deficient mouse embryonic fibroblasts (MEFs), cAMP-induced CREB phosphorylation is markedly increased and sustained compared to wildtype MEFs (144). Based on the available published data, we speculated that glucocorticoid-stimulated expression of MKP-1 leads to inactivation of CREB by dephosphorylation. Subsequently, anti-lipogenic *Hes-1* expression might be inhibited and fat storage programs could no longer be suppressed.

To test this hypothesis, 3 and 4 months old male MKP-1-deficient C57 BL/6J mice (MKP-1^{-/-}) and controls (MKP-1^{+/+}) were treated with 1,2 mg/kg dexamethasone for three weeks

intraperitoneally to induce MKP-1 expression in wildtype animals and fat accumulation in the liver. Determination of body weight on day 0 revealed that MKP-1 $-/-$ mice generally had lower initial body weights than wildtype control mice (26.6 ± 3.9 g vs. 30.24 ± 3.8 g, $p = 0.041$) confirming published data (146).

After two weeks of injection, a glucose tolerance test was performed. Saline-injected MKP-1 $+/+$ mice were sensitive to glucose (Figure 3.27). MKP-1 $+/+$ mice treated with synthetic glucocorticoids showed a tendency towards glucose intolerance. The area under the curve (AUC)-value shows a 14% total increase ($AUC_{wt}=27584$ min·mg/dl vs. $AUC_{wt+Dex}=31550$ min·mg/dl) for the dex-treated MKP-1 $+/+$ group. MKP-1 $-/-$ mice injected with saline cleared glucose from the periphery with a slightly increased efficiency compared to wildtype mice ($AUC_{MKP-1 -/-}=24061$ min mg/dl). In contrast to dexamethasone-treated MKP-1 $+/+$ mice, the MKP-1 $-/-$ mice were protected against glucocorticoid-induced glucose intolerance ($AUC_{MKP-1 -/- + Dex}=23021$ min mg/dl, Figure 3.27) and this effect was found to be statistically significant.

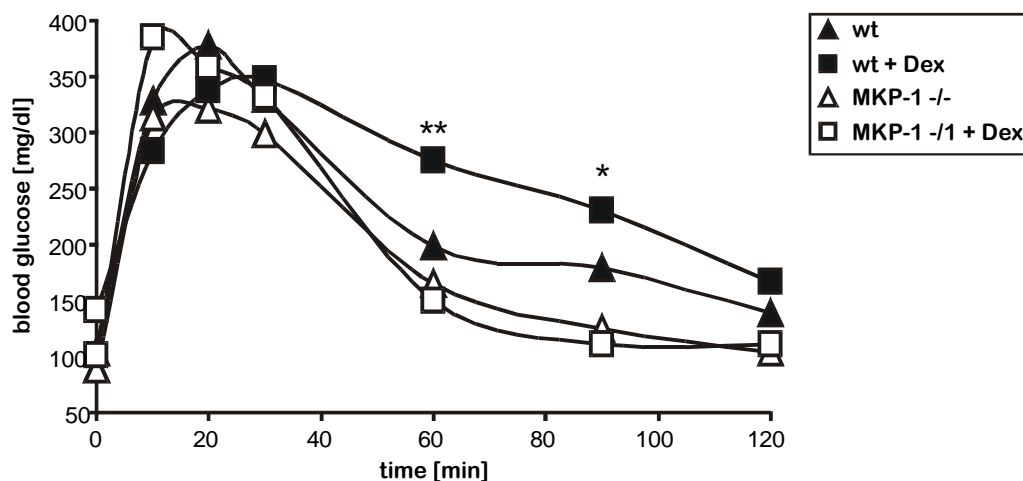


Figure 3.27: MKP-1 mice are protected against GC-induced glucose intolerance. Glucose tolerance test in wildtype and MKP-1 $-/-$ mice after 16 days of treatment with saline or 1,2 mg/kg dexamethasone. N=4, except wildtype + Dex: N=3. Data shown are means, Student's t-test compared wt mice vs. MKP-1 $-/-$ mice after dex treatment of both. * $p \leq 0.05$, ** $p \leq 0.01$.

The observed differences in glucose sensitivity between wildtype and MKP-1 $-/-$ mice implied a different body fat content. Therefore, body fat parameters were examined. Mice were sacrificed 3 weeks after the start of injection and the total body weight and epididymal fat pads were weighed. As shown in Table 8, a significant body weight reduction after GC-treatment was observed in the MKP-1 $+/+$ mice compared to saline-treated wildtype controls (20% less after dex-treatment, $p=0.035$). The weight loss is attributed to muscle atrophy (20% less gastrocnemius after dex-treatment) and the loss of visceral fat mass (32% less after dex),

respectively. In MKP-1 $-/-$ mice the GC-induced weight loss was less pronounced (8,5%) and, in addition, also less visceral fat was degraded (17%). Notably the muscle mass remained almost unchanged (6% less gastrocnemius after dex-treatment) despite the high dose of a catabolic stimulus.

Table 8: Weight parameters at day of sacrifice

	wildtype	wildtype + dex	MKP-1 $-/-$	MKP-1 $-/-$ + dex
body weight [g]	31.1 ± 4.3	25 ± 1.3	26.1 ± 3.2	23.9 ± 3.3
blood glucose [mg/dl]	130 ± 14	139 ± 32	115 ± 24	103 ± 9
liver weight [g]	1.64 ± 0.35	1.03 ± 0.14	1.16 ± 0.21	1.01 ± 0.13
epididymal fat [mg]	208 ± 61	141 ± 95	141 ± 58	117 ± 46
gastrocnemius* [mg]	176 ± 20	141 ± 11	155 ± 19	146 ± 19
tibialis anterior [mg]	58 ± 11	45 ± 8	52 ± 7	43 ± 6

*gastrocnemius and soleus were dissected and weighed together

Upon dexamethasone treatment hepatic MKP-1 increased dramatically (Figure 3.28 A, compare lane 1-2 vs. 3-4), while in control treated mice hepatic MKP-1 was barely undetectable.

To correlate the observed glucose sensitivities of the GTT (Figure 3.27) with hepatic triglyceride content, liver lipid extracts were investigated. As shown in Figure 3.28 B in MPK-1 $+/+$ mice dex treatment did not result in hepatic triglyceride accumulation (control: 96 ± 11 vs. MKP-1 $-/-$ 125 ± 32 $\mu\text{mol/g}$ liver). Total triglyceride levels did not differ between any of the groups. Therefore, the different glucose sensitivities might not be explained by an altered hepatic lipid profile, but might indicate different effects of GCs on muscle of MKP-1 $-/-$ mice. The sustained muscle mass after dexamethasone treatment in MKP-1 $-/-$ represents one possible explanation, since it indicates higher glucose disposal capacity in peripheral tissues compared to mice with muscle atrophy.

Finally, protein levels of the GR, P-CREB and Hes-1 were assessed in western blots. In both genotypes investigated, GR was down-regulated on the protein level after chronic GC treatment for 3 weeks. However, downstream effects of the GC/GR axis were still functioning as represented by diminished CREB phosphorylation (Figure 3.28 C).

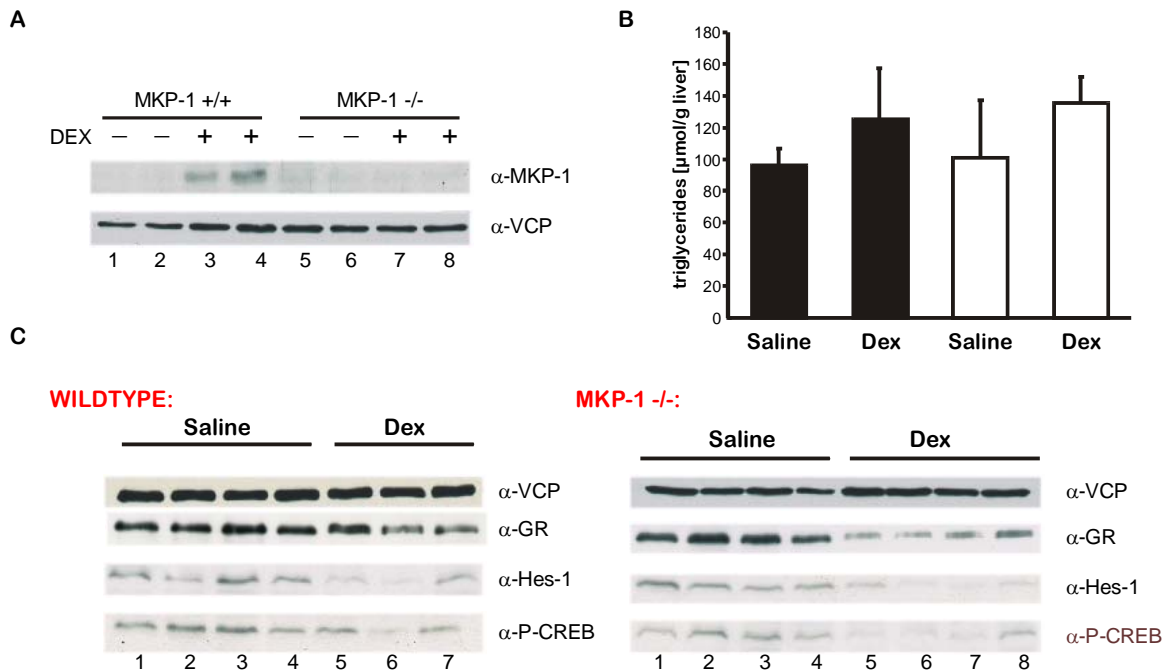


Figure 3.28: In MKP-1 ^{-/-} mice improved glucose tolerance does not depend on Hes-1. A) Western Blot analysis of hepatic protein extracts obtained from MKP-1 ^{+/+} mice or MKP-1 ^{-/-} mice. Animals were injected for 3 weeks with 1.2mg/kg dexamethasone or saline. Lysates of 2 mice per group were analysed for MKP-1 expression. VCP served as loading control. B) Triglyceride content in hepatic lipid extracts of wildtype or MKP-1 ^{-/-} mice after 3 weeks treatment. N=4, except wildtype + Dex: N=3. Data shown are mean values and s.e.m. C) Western Blot analysis of hepatic protein extracts from the same mice as under A) with specific antibodies. Treatment as indicated. VCP served as loading control.

Attenuated CREB phosphorylation in MKP-1 ^{+/+} mice and MKP-1 ^{-/-} mice argues against the notion that MKP-1 might be the GC-dependent CREB phosphatase. Finally, inhibition of Hes-1 expression was observed in all groups after dexamethasone treatment, irrespective of the absence of MKP-1 (Figure 3.28 C). Although MKP-1 ^{-/-} mice were protected against GC-induced glucose intolerance this effect is not caused by sustained P-CREB and Hes-1 levels. It was therefore concluded under these experimental conditions MKP-1 was not the glucocorticoid-induced CREB phosphatase.

3.7.2 Protein-protein interactions

Transcriptional activation of a CREB phosphatase by GC/GR would not necessitate GR to directly interact with CREB. In contrast, recruiting such a phosphatase specifically to CREB might implicate binding of GR to the transcription complex formed around CREB.

To form a transcription initiation complex CREB is phosphorylated at Ser133 by PKA (see Section 1.3.1) the phosphorylation of which being a prerequisite of interaction with the histone acetyltransferase p300. CREB contacts via its kinase-inducible domain KID the KIX domain of p300 (147-149), thereby stabilising the interaction. Subsequently, p300 alters the local chromatin structure by acetylating histones. These processes facilitate effective transcription (150)(see Section 1.2.1).

In Figure 3.29 the domain structures of p300 and CREB are summarized.

A study of Imai et al. (151) demonstrated that GR can directly associate with CREB *in vitro*. No functional data, however, about the impact of such an interaction on CREB activation status was available. Moreover, GR can principally also associate with the histone acetylase p300 (152). Complex formation between CREB and p300, however, is inevitable for transcriptional activation. By affecting CREB/p300 interaction, GR therefore could diminish transcriptional activation.

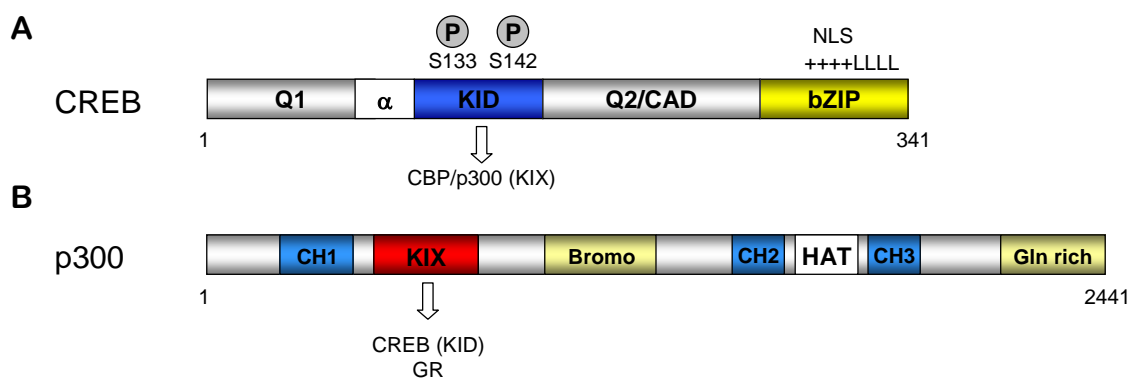


Figure 3.29: Domain structure of CREB and CBP. A) Domain structure of CREB, Q1 and Q2/CAD represent contact elements of basal transcription, bZIP mediates CREB binding to CREs and KID (kinase inducible domain) represents the domain, where CREB is phosphorylated (Ser133 and Ser142). Highlighted is the possible interaction of the KID domain with p300/CBP. B) Domain structure of p300: CH1/ CH2 and CH3 are cysteine/histidine rich domains, KIX – CREB binding domain, Bromo-bromodomain, HAT histone acetyltransferase domain and Gln-rich – Gln rich domain. Highlighted is the possible interaction between the KIX domain and GR (152).

3.7.2.1 The GR preferentially binds to the bZip domain of CREB

To test this hypothesis, full-length CREB, CREB domains KID and bZip, as well as the p300 domain KIX (see Figure 3.29) were mapped for a putative association of GR using a Mammalian-Two-Hybrid approach. A GAL4 GR fusion protein as well as VP16 fusion proteins of the putative interaction partners were employed.

To exclude any unspecific binding effects between VP16 and GAL4 or VP16 and GR, in a control transfection the ability of the VP16 transactivation domain to interact with GAL4GR or GAL4DBD was examined. For this purpose, 600 ng of an artificial GAL4Luc promoter construct (comprising 5 GAL4 binding elements only) were co-transfected with 50ng of a vector encoding for a GAL4GR fusion protein or the GAL4 DNA binding domain (GAL4DBD) and 50 ng of a plasmid encoding for the transactivation domain of VP16 (pCMV VP16).

As shown in Figure 3.30, the VP16 co-transfection with a GAL4GR construct did not result in increased luciferase activity under unstimulated conditions when compared to VP16–GAL4DBD co-transfection (compare bar 1 and bar 3). Stimulation with 10nM dexamethasone did not alter luciferase activity in VP16-GAL4DBD co-treated cells (bar 1 vs. bar 2). After dexamethasone-treatment, however, a 12-fold induction of luciferase activity was observed when VP16-GAL4GR was co-transfected (bar 1 vs. bar 4). The effect, however, was not due to dex-stimulated interaction of VP16 with GAL4GR, but due to binding of glucocorticoids to the GR and its subsequent activation. The activation of GAL4GR after glucocorticoid stimulation could be observed in transfections without VP16 (data not shown).

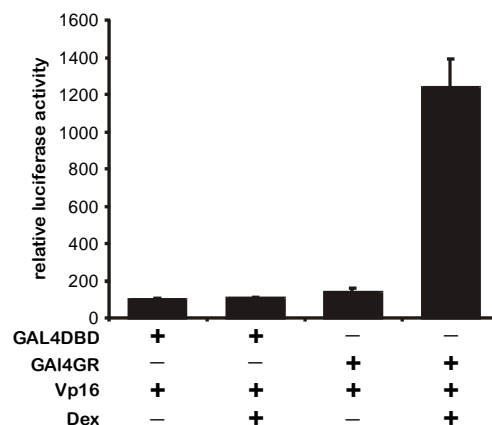


Figure 3.30: The VP16 does not interact with either GAL4DBD or GAL4GR. 5xGAL4Luc promoter was co-transfected with expression vectors for GAL4DBD, GAL4GR and VP16 as indicated. 24h post-transfection the cells were treated with 10nM Dex or control for another 24h. Luciferase activity is shown relative to GAL4DBD (1st bar). Data shown are means and s.e.m. of nine experiments.

Since no relevant background association of VP16 with GAL4GR occurred, a second experiment was conducted in which 600ng GAL4LUC and 50ng GAL4GR were transfected into HEK293 cells. Plasmids encoding for VP16 or fusion proteins between VP16, full length CREB, CREB domains (KID, bZip) or domains for p300 (KID) were co-transfected. The interference of GC/GR with CREB phosphorylation in cells had been observed after dex treatment (see above). The influence of dexamethasone treatment on protein interaction was investigated in the transfection assay to assess this observation. Increased luciferase activity in this assay indicated interaction of two proteins or protein domains, respectively. Figure 3.31 summarizes the obtained results.

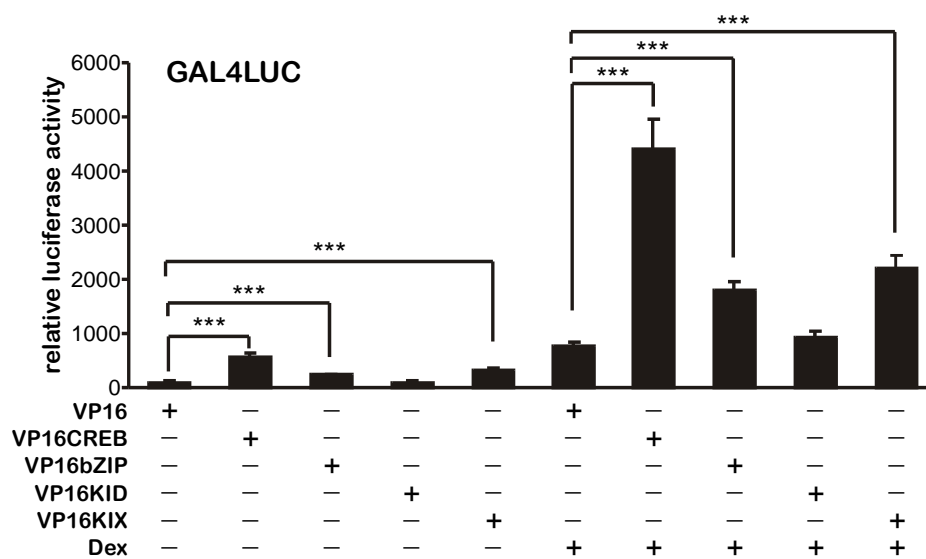


Figure 3.31: GR interacts via the bZIP domain with CREB. HEK293 cells were transiently transfected with 600ng GAL4Luc vector and 50ng GAL4GR vector. Vector constructs (100ng) encoding for VP16 or VP16 fusion proteins were co-transfected as indicated. Transfection was treated 24h after transfection with Dex for 16h. Cells were harvested and luciferase assay was performed to evaluate promoter activity. Data shown are means and s.e.m. N=9. ***p<0.001.

Co-transfection of VP16CREB with GAL4GR and GAL4Luc resulted in a 5.6-fold activation of promoter activity under basal conditions (Figure 3.31 compare bar 1 vs. bar 2), suggesting a protein protein interaction between GR and CREB. The same effect was seen after dex treatment (5,9-fold activation, compare bar 6 vs. 7). However, the absolute luciferase activity was enhanced in all samples treated with dex due to activation of GAL4GR as described above. Unexpectedly, VP16 KID co-transfection did not stimulate transcriptional activation (Figure 3.31 compare bar 1 vs. 4 and bar 6 vs. 9). VP16bZip and GR instead interacted as shown by 2.3-fold enhanced promoter activity (bar 1 vs 3 and bar 6 vs.8).

Interestingly, co-transfection of GAL4GR with VP16KIX led to a 3.3-fold activation of transcriptional activity (compare bar 1 vs bar 5) suggesting that GR and p300 associate transiently under untreated conditions. The interaction was also detectable after dex-treatment (bar 6 vs 10).

The data confirmed that GR associates with CREB and p300. Moreover, the bZip domain of CREB was identified to mediate GR/CREB interaction. Whether the protein-protein interactions are inhibitory or activating cannot be concluded from this explicit Mammalian Two Hybrid experiment.

3.7.2.2 GC/GR can decrease CREB activity in a cell-autonomous system

Given the fact that GR interacts with CREB, it was tested, whether it is a common feature of GC/GR to attenuate CREB activity.

A plasmid containing an artificial promoter sequence comprising 5 GAL4 binding elements that control luciferase reporter gene expression (pGAL4-Luc) was chosen to assure no binding of the ligand-bound GR to DNA. 600ng GAL4-Luc reporter gene vector was co-transfected together with either 20 ng of an expression plasmid encoding for GAL4DBD or GAL4CREB fusion protein into human embryonic kidney (HEK) 293 cells. The GAL4 transactivation domain in the fusion proteins mediates their binding to the artificial promoter sequence comprising only GAL4 response elements. To activate CREB phosphorylation 100 ng of an expression vector encoding wt PKA (control: kinase-deficient PKA) was co-transfected. Endogenous GR was activated by treatment of the cells with 10 nM dex for 16h.

GAL4CREB co-transfection led to a 5.8-fold induction of basal GAL4-Luc promoter activity compared to GAL4DBD/GAL4-Luc (Figure 3.32). This observation might be explained by a basal phosphorylation of GAL4CREB by endogenous protein kinases. Intriguingly, the activating effect of GAL4CREB could be decreased 2.1-fold by dexamethasone and the effect was highly significant ($p < 0.001$).

Phosphorylation of GAL4CREB by co-transfection with wt PKA increased the luciferase activity 59-fold compared to GAL4DBD/GAL4-Luc basal activity. Dexamethasone treatment inhibited PKA-stimulated CREB activation 1,8-fold ($p < 0,05$). Effects of dexamethasone and PKA on GAL4DBD were also tested, but did not yield activation or repression of GAL4-Luc promoter activity (data not shown).

Since the artificial promoter sequence is solely composed of GAL4 response elements, direct GR DNA-binding to the promoter sequence is extremely unlikely. The results sustain the hypothesis that for GC-mediated repression of CREB activity the GR does not need to bind to glucocorticoid response units on the DNA. Consequently, protein-protein interactions are necessary for GC/GR mediated CREB inactivation. Moreover, decrease of CREB activity is likely to be a general mechanism of GR function as observed on the Hes-1 promoter.

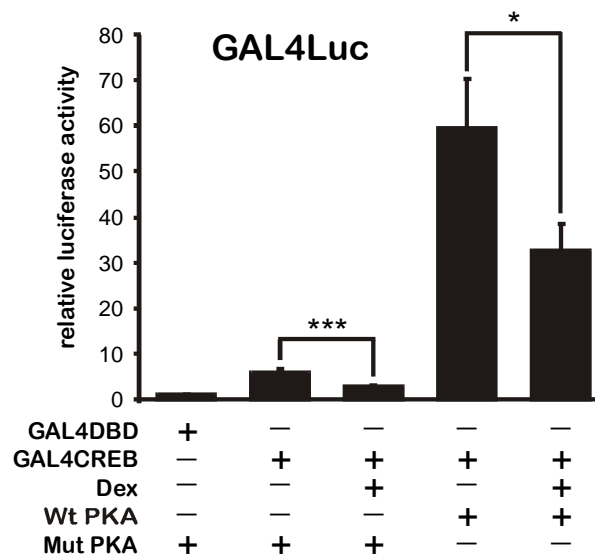


Figure 3.32: Glucocorticoids inhibit CREB activity under basal and activated conditions. A) 5xGAL4Luc promoter was co-transfected with GAL4DBD or GAL4CREB and wildtype or kinase-deficient PKA as indicated. 24h post-transfection the cells were treated with 10nM Dex or control for another 24h. Luciferase activity shown are relative to GAL4DBD (1st bar). Data shown are means and s.e.m. of nine experiments.

3.7.3 p300 can reverse GR/GC-mediated inhibition of CREB

Mechanistically, it remained unclear how GR conferred CREB inhibition. Association of GR to the KIX domain of p300 may limit the amount of available p300 for CREB. In this case, CREB and GR would compete for the same domain - KIX.

In a variation of the Mammalian Two Hybrid assay (see Section 3.7.2), increasing amounts of p300 (10 to 50 ng) were co-transfected with 600 ng GAL4-Luc, 20 ng GAL4CREB and 100 ng PKA into HEK293 cells. To maintain the same transfected DNA amounts cells not receiving p300 were co-transfected with an empty vector (pcDNA3).

Transfected cells were subsequently stimulated for 16h with 10 nM dex. As in earlier tests, dex-treatment decreased PKA-dependend activation of CREB 2.1-fold. With increasing amounts of p300 dex-dependent CREB inhibition could be completely abolished therefore restoring CREB

activity (Figure 3.33). Therefore, p300 can counter-act the effects of activated GR on CREB. The results supported the mechanistic model that GR via binding to the KIX domain of p300 is able to disrupt the transcriptional activation complex formed between CREB and p300. It predicts furthermore that GR possesses a higher affinity for KIX than KID. The observed dephosphorylation of CREB in this model would chronologically follow disruption of KIX-KID interaction.

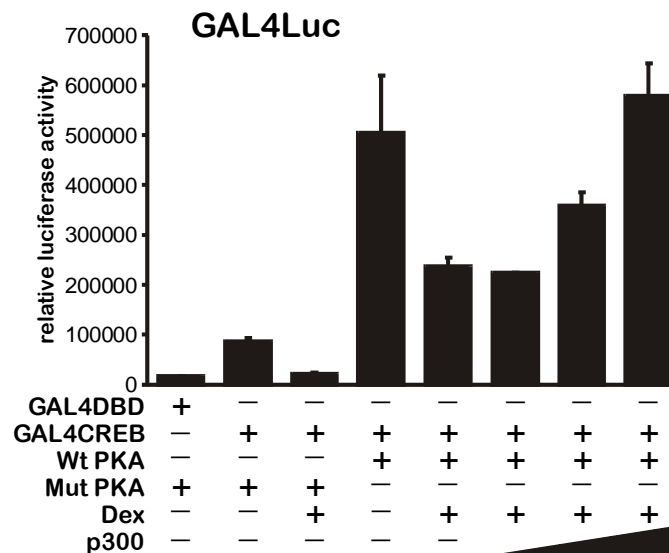


Figure 3.33: p300 abolishes GC-dependent inhibition of CREB activity. 5xGAL4Luc promoter was co-transfected with GAL4DBD or GAL4CREB and wildtype or kinase-deficient PKA as indicated. Increasing amounts of p300 or empty vector were co-transfected. 24h post-transfection the cells were treated with 10nM Dex or control for another 24h. Luciferase activities shown are relative to GAL4DBD (1st bar). Data shown are means and standard deviations of three experiments.

3.7.4 Consequences of CREB dephosphorylation for Hes-1 promoter activation

Finally, the impact of GC treatment on the transactivation machinery (comprised of CREB, p300 and other proteins) on the *Hes-1* promoter was assessed, using chromatin immunoprecipitation experiments in H4IIE rat hepatocytes.

H4IIE cells were stimulated for 3h with 10 nM dex or solvent only, and chromatin immunoprecipitation was accomplished as described in Section 5.3.11 using antibodies against CREB, P-CREB, p300, acetyl-Histon H3 or irrelevant IgGs. As shown in Figure 3.34, dex treatment had no influence on the amount of CREB bound to the proximal Hes-1 promoter region. However, the amount of P-CREB (Ser-133) was minimized after glucocorticoid stimulation (compare lane 1 and 2). Moreover, p300 was released from the transactivation complex after GC-treatment, resulting in diminished levels of acetylated histone H3. These data

clearly indicated that glucocorticoids lead to the disruption of a transactivation complex and subsequently to a condensation of chromatin, thereby shutting down transcription at the *Hes-1* promoter.

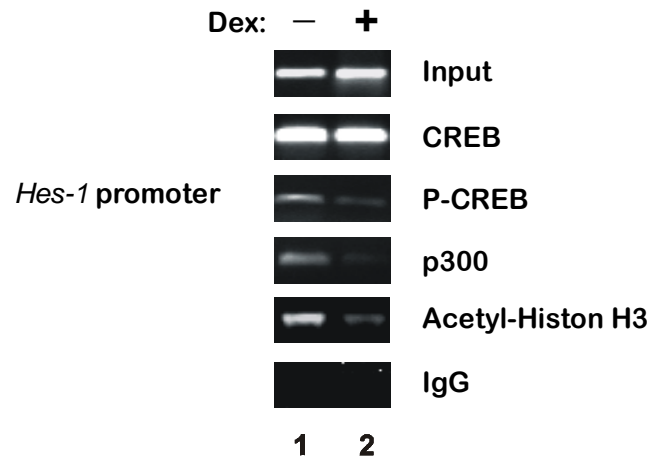


Figure 3.34: Glucocorticoid treatment leads to disruption of P-CREB/p300 transactivation complex on the *Hes-1* promoter. H4IIE rat hepatocytes were stimulated for 3h with 10 nM dexamethasone or remained untreated. Endogenous proteins were cross-linked with DNA using formaldehyde. After sonification of cells immunoprecipitation with 5 μ g of antibodies specific for CREB, P-CREB (Ser-133), p300 and acetyl-Histon H3, respectively was completed. As control for unspecific binding irrelevant IgGs were used. After proteinase K digest, DNA was isolated and probed against PCR primers specific for the proximal *Hes-1* promoter region. For the assay 10% of the chromatin samples were used as input.

4 Discussion

Recent evidence suggests that glucocorticoids promote Non-alcoholic Fatty Liver Disease – a disease strongly associated with other co-morbid conditions such as insulin resistance, dyslipidemia and hypertension.

Paterson et al. showed, that liver specific activation of GC/GR axis is sufficient to resemble main characteristics of the Metabolic Syndrome (fatty liver, insulin resistance, hypertension), even in the absence of elevated circulating glucocorticoid levels (87, 89). We investigated the molecular mechanisms underlying this phenotype by taking advantage of adenovirus-based gene delivery of sequences encoding shRNAs against murine GR. Targeting hepatic GR in the context of fatty liver shed new light on the development and progression of the disease.

4.1 Acute hepatic GR knockdown in fatty liver ameliorates steatosis by decreased fat import and increased fat utilization

In the current work, transient knock-down of hepatic glucocorticoid receptor alleviated the fatty liver phenotype in chronically obese db/db mice by decreasing hepatic triglyceride levels. It indicates the pivotal role the activated hepatic GC/GR-axis plays in the development of Non-Alcoholic Fatty Liver Disease. The effects are mainly attributed to reduced expression of proteins essential for fat import (CD36, Cav1, PPAR γ) and increased oxidative utilization of triglycerides (CPT1 α). Surprisingly, in none of the investigated fatty liver models did ablation of GR and concomitant PPAR γ depletion cause reduced *de novo* triglyceride synthesis as measured by rate-limiting factors such as acyl CoA carboxylase and fatty acid synthase. The results indicate that it is unlikely that glucocorticoids promote fatty liver development by stimulation of lipogenesis.

The work describes that facilitated fat import into the liver causes fatty liver development in response to glucocorticoids. Until now, hepatic fat accumulation in hypercortisolism was mainly attributed to lipolytic abdominal fat depots (153) that secrete FFA into serum, and because of close proximity the FFAs accumulate in the liver (“first pass” effect). Interestingly, the central obesity phenotype (characterized by abdominal fat) is especially highly associated with NAFLD and insulin resistance (153). In contrast, FFA serum concentration and flux in individuals with predominantly lower body obesity tend to be normal regardless of BMI. The mechanism,

referred to as the “first pass” effect, still may profoundly contribute to the observed net fat influx. Increased expression of fat transporters, however, dramatically accelerate this process.

Several murine models of obesity, including ob/ob, A-ZIP, aP2/DTA and KKAy develop fatty livers that express enhanced levels of adipogenic transcription factors (e.g. PPAR γ , sterol-regulatory element binding protein 1 SREBP-1 and FABP4 and 5), while the normal liver lacks such expression (154-155). The unique role of PPAR γ in development and maintenance of steatotic liver is highlighted by numerous studies (156-158), clearly demonstrating lipid accumulation in hepatocytes upon PPAR γ activation (159). In the current work we demonstrate that glucocorticoids seem to promote hepato-specific activation of PPAR γ expression. The results indicate a strong correlation between GR knockdown and PPAR γ depletion in liver, thereby suggesting an activating function of GR on hepatic PPAR γ expression. Since the obese state is often accompanied by hyperactivation of GC/GR either by increased circulating glucocorticoids (160, 161) or by enhanced tissue-specific transformation of precursors (87) the observations provide additional insights into hepatic PPAR γ activation. The obtained data are in agreement with experiments showing that glucocorticoids increase PPAR γ mRNA levels (162, 163). However, PPAR γ regulation by the hormone seems to depend on the celltype. In 3T3 L1 adipocytes GC-treatment was overall reported to decrease PPAR γ levels (164), but when examining individual isoforms PPAR γ 1 and 2, Vidal-Puig et al. showed dex-dependent increase of PPAR γ 1 after exposure to GCs (165).

In contrast to surprisingly unaltered lipogenic programs, fat transport in db/db mice after GR RNAi was decreased as indicated by diminished Cav1 and CD36 expression. Both genes are characterized by similar expression patterns with highest abundance in adipose tissue (166). Cav1 deficiency is accompanied by kinetically delayed serum triglyceride clearance (166), thus implying a role as fat transporter. As a consequence, Cav^{-/-} mice display a lean phenotype with decreased white adipose tissue (167). Liver specific functions of Cav1 have not been studied systematically, but our results suggest that down-regulation of hepatic Cav1 protects against steatotic liver formation.

Transmembrane glycoprotein CD36 represents a transporter of long chain fatty acids with highest expression in macrophages, myocardial and skeletal muscle, and adipose tissue (168-170). Ablation was associated with a large decrease in fatty acid incorporation into triglycerides, which could be accounted for by an accumulation of diacylglycerides (171, 172).

In the employed hepatic GR loss-of-function model, CD36 depletion correlates with attenuated fat accumulation. Cav1 and CD36 transporters are target genes of PPAR γ (173-176) which argue for an indirect effect of GR on their expression via increased activity of PPAR γ . However, direct transcriptional activation of CD36 and Cav1 cannot be excluded from these data.

Results from this work lead to the current working model that hepatic GR activation by means of increased PPAR γ expression promotes fatty liver development by increased net fat influx through fat transporters CD36 and caveolin1.

4.2 Effects of transient hepatic GR knockdown on glucose metabolism

In contrast to its effects on hepatic fat accumulation, the consequences of hepatic GR ablation on hepatic glucose metabolism have been investigated in several studies including genetic (97, 98, 177) and pharmacological approaches (83, 178). Specifically targeting hepatic GR function is favourable due to the fact, that *de novo* glucose synthesis that contributes e.g. to high blood glucose levels in diabetic states is mainly dictated by the liver. Furthermore, systemic inhibition of the GR with pharmacological antagonists of glucocorticoids (RU-486) had, despite remarkable inhibitory effects on gluconeogenesis (178), unfavourable extra-hepatic effects, including activation of the HPA axis (177). Opherk et al. demonstrated that mice bearing a targeted disruption of hepatic GR have very low blood glucose levels after prolonged fasting. In contrast, in the experiments presented here transient knock-down of hepatic GR was not accompanied by lower fasting glucose levels in comparison to controls. However, Opherk observed the effects after 28h of starvation while in our studies wildtype mice were starved for 24h suggesting that GR/GC activation was not completely realized at this time point. Into this direction point also data about the marginal differences of PEPCK activity in GR knockdown mice, which were not prominent. The absent induction of PEPCK in control mice might indicate that hepatic GR was not completely activated after 24h starvation thus explaining the observed phenotype.

4.3 Transcriptional repressor Hes-1 represents an inhibitory GR target in steatotic liver

It is commonly accepted that perturbations in liver metabolism as seen in insulin resistant states largely depend on the aberrant transcriptional activity of genes encoding metabolic key enzymes (16). Therefore, transcription factors putatively regulating the expression of such enzymes were identified. In gene profiling, studies in wt and db/db mice injected with GR shRNA adenovirus

induction of transcriptional repressor Hes-1 was noticed on mRNA and protein level, while expression of family members Hes-3 and Hes-5 remained unchanged upon hepatic GR depletion.

Hes-1 is a well-established down-stream target of the Notch signaling pathway and its expression can be activated by ligands of the Notch receptor, namely Jagged 1 and Delta-like. Hes-1 expression, however, can also be triggered independently of Notch. A wide variety of other stimuli as different as β -estradiol (in epithelial cells), TGF- β (179), VEGF and TNF- α (180) regulate Hes-1 expression, and obviously always the cellular context plays a major role in these processes. The only evidence that Hes-1 is regulated by stimuli that control energy homeostasis comes from Shinozuka et al. who demonstrated that glucocorticoids induce Hes-1 expression in pancreatic HIT-T15 cells (181) and additionally from Herzig who showed glucagon-dependent Hes-1 activation (112).

In the current work, Hes-1 expression in hepatocytes was differentially regulated after GC treatment. Following dexamethasone stimulation, Hes-1 levels were inhibited on the mRNA level and on the protein level *in vitro* and *in vivo* (in several models including long-term dexamethasone treatment of mice) and increased upon hepatic GR depletion. From this we conclude hepatic Hes-1 expression is negatively regulated by glucocorticoids and their respective receptor.

Glucocorticoids have implications in the regulation of biologically diverse processes such as inflammation and energy homeostasis. Hes-1, on the other hand, responds to pro-inflammatory signals such as TNF α (180). In this regard, it does not seem surprising that the *Hes-1* gene promoter activity is attenuated by GCs. Whether Hes-1 regulation plays a role in inflammatory processes is presently unknown.

If Hes-1 is also directly regulated by hormones of energy metabolism such as insulin is currently investigated, however, in hepatocellular carcinoma cells increased expression and activation of IRS-1, IRS-2 and IRS-4 correlated with higher Hes-1 levels in these samples (182). It was shown that *Hes-1* gene expression is stimulated via the MAPK pathway (183). TGF α -stimulated Erk1/Erk2 phosphorylation led to stimulation of RBP-J (CSL) that in turn caused enhanced transcriptional activity of the *Hes-1* gene. Insulin is well known to affect the MAPK pathway, but insulin-controlled Hes-1 regulation remains speculative. Hes-1 levels further depend on nutritional signals such as glucose levels. In neuronal stem cells, Hes-1 is down-regulated when cells are cultured in high glucose medium (184).

4.4 Role of Hes-1 in hepatic lipid metabolism

Hes-1 is expressed in a wide variety of tissues with the highest abundance in lung and the gastrointestinal tract of both adults and embryos (185). Heart, muscle and kidney also produce high levels of Hes-1 in the embryo but at low levels in the adult (185). Hes-1 expression is controlled in a tissue-specific manner.

Targeted disruption of the *Hes-1* gene in mice leads to severe neurulation defects and death during gestation or directly after birth (186). By inhibiting neural bHLH activators Mash-1 and MATH-1, suppression of neural differentiation is induced by forced expression of Hes-1 suggesting a critical role of Hes-1 in embryogenesis (187).

Despite its ubiquitous expression, the function of Hes-1 in the adult organism is only recently emerging. The few studies undertaken in this regard point towards an involvement of Hes-1 in the regulation of hematopoiesis (188-190), osteoblastogenesis (191, 192) and energy metabolism (112, 193). Soukas et al. identified Hes-1 in a global expression profiling screen as a critical factor of pre-adipocyte differentiation (194). Overexpression of Hes-1 in 3T3 L1 cells inhibited differentiation into adipocytes accompanied by a remarkable down-regulation of C/EBP- α and PPAR γ (193), both markers of adipogenesis. Furthermore, in transient transfection assays Hes-1 was able to block promoter activity of fatty acid synthase (195). In hepatocytes, Hes-1 overexpression was demonstrated to directly repress PPAR γ expression in a glucagon/cAMP-dependent manner (112). Taken together, Hes-1 was identified as a negative regulator of mainly lipogenic programs in liver and adipose tissue.

It is shown in the work presented here that reconstitution of hepatic Hes-1 levels in mouse models with elevated GC/GR action (db/db mice and dexamethasone treated mice) ameliorated a concomitant fatty liver phenotype present in these mice. Moreover, this effect is highly specific as no effects on cholesterol metabolism are evident. Most intriguingly, liver-specific restoration of Hes-1 significantly improved systemic insulin sensitivity in db/db mice thereby alleviating the overall diabetic phenotype. Hes-1 exerted a protective action mainly by limiting triglyceride influx into the liver, while no apparent effects on triglyceride synthesis were observed.

After one week of liver-specific Hes-1 expression in a db/db mouse model, animals showed a tendency towards normalized serum blood glucose levels. Further studies need to be carried out to confirm this effect of Hes-1 on glucose metabolism.

The presented data establish Hes-1 as a new target for the treatment of Non-Alcoholic Fatty Liver Disease. Maintenance of hepatic Hes-1 levels critically influences the amount of disposable triglycerides in the liver, and therefore represents a new key regulator in hepatic lipid homeostasis.

4.5 Genes regulated in Hes-1 loss-of function and gain-of-function models

The current research was able to confirm PPAR γ depletion in Hes-1 gain-of-function models *in vivo* (112) and PPAR γ activation after acute Hes-1 knockdown in primary hepatocytes. Effects of Hes-1 on fatty acid synthase expression were not observed in either gain-of function or loss-of function models, despite reports by Ross et al., that Hes-1 inhibits FAS expression (195). However, they claimed that inhibition of FAS expression depends on the ability of Hes-1 to interfere with SREBP-1 (12) by inhibiting association of SREBP-1 to its response unit. In the investigated models absent SREBP-1 activation might provide one rationale that no Hes-1 effects on FAS expression were detectable.

In addition to its recently emerging role in the lipid metabolism, Hes-1 might also affect glucose homeostasis. Hes-1 potentiates JAK/STAT signaling through protein-protein-interaction with STAT3 (196) where it does not exert its action as a transcription factor. The reported interaction is particularly interesting regarding the recently described role of STAT3 in the suppression in hepatic glucose production (197, 198). In the present study, hepatic over-expression of Hes-1 in db/db mice that are characterized by abnormally high hepatic glucose output led to normalized blood glucose parameters. No significant repressive effect on rate-limiting enzymes such as G6Pase and glucokinase were observed in refed animals. Moreover, slight activation of PEPCK and G6Pase was observed under fasting conditions. These data do not support the notion that Hes-1 mediated potentiation of hepatic STAT3 signaling contributes to normalized hepatic glucose production. How Hes-1 overexpression caused decreased serum glucose concentration needs to be further investigated.

Reconstitution of diminished Hes-1 levels in db/db mice and dexamethasone-treated mice by means of adenoviral gene delivery caused repressed expression of PPAR γ , Cav1 and CD36 – intriguingly exactly the genes that had been identified in mice with acute knockdown of hepatic GR. *Vice versa* depletion of Hes-1 results in a marked increase in PPAR γ levels accompanied by a rise in caveolin 1.

Methodological limitations due to unspecific virus effects did not allow conclusions for CD36. Hes-1 overexpression data, however, indicate that indeed Hes-1 targets the *CD36* gene. Due to the fact that PPAR γ activates caveolin1 and CD36 expression, it is tempting to speculate that PPAR γ depletion is the sole mechanism of Hes-1 mediating Cav1 and CD36 promoter repression. While consistent, the observed down-regulation of PPAR γ after Hes-1 overexpression was only moderate in magnitude. Therefore, PPAR γ down-regulation may not fully account for decreased Cav1 and CD36 expression.

Hairy-related proteins repress transcription by binding to specific hexameric sites and are characterized by a WRPW motif through which interaction with the transcriptional co-repressor groucho (or the mammalian homolog of groucho TLE) is mediated. This protein complex is sufficient to inhibit target gene expression (199-201). Hes-1 belongs to the so-called C-class proteins of transcriptional repressors and exerts its action by binding to class C sites (CACGNG) as well as N-box sequences (CACNAG) on the promoter of its target genes. To some degree, Hes-1 also associates to class B sites (CANGTG) (133). In this work, N-Box elements were identified in the 5'-UTR of CD36 suggesting physical presence of Hes-1 in this region. Cav1 was not characterized by N-box motifs or C class binding sites. Hes-1 can inhibit target gene expression, however, via a dominant-negative mechanism by forming non-functional heterodimers with bHLH-type transcriptional activators that bind E box sequences (133). One example for this mechanism is the antagonizing effect of Hes-1 on transcriptional activity of muscle determination factor MyoD thereby inhibiting MyoD-induced myogenesis (185). In future studies on the Cav1 promoter, it might be interesting to search for E box motifs and to search for bHLH-type transcriptional activators.

4.6 GR-mediated regulation of the Hes-1 promoter

GR mediated fatty liver formation via repression of anti-lipogenic Hes-1 includes several mechanisms on the *Hes-1* gene promoter that probably act in concert. Glucocorticoids negatively regulated cAMP-stimulated transcriptional activation. Antagonism between glucocorticoids and cAMP signaling has already been observed on the corticotropin-releasing hormone (CRH) gene promoter (202) and on the surfactant protein A (SP-A) promoter (203). In case of CRH, heterologous promoter approaches allowed identification of the DNA sequence mediating glucocorticoid repression of forskolin activated CRH expression –the cAMP response element (CRE) (202).

In the present work, dephosphorylation of CREB at Ser-133 is observed after glucocorticoid treatment in hepatocytes, an effect known from hippocampal neurons (204). This effect may contribute to the decreased levels of P-CREB found on the proximal *Hes-1* promoter after GC stimulation. Attempts to identify a GR/GC-dependent phosphatase were not successful. Despite observations that P-CREB levels are sustained in mice bearing a targeted disruption of Mitogen activated protein kinase phosphatase 1 (MKP-1), we could not see protection against GC-mediated CREB dephosphorylation in MKP-1 $-/-$ mice. Inhibition of protein synthesis using cycloheximide promotes accumulation of P-CREB within the cells suggesting that continuously a CREB phosphatase is expressed (data not shown). In contrast to these observation, Rosen et al. demonstrated that glucocorticoid repression of endogenous CRH gene expression did not require ongoing protein synthesis (205).

Imai et al. showed in *in vitro* experiments that CREB and GR can associate (151) and we could identify the bZIP domain of CREB as responsible for the interaction. bZIP has been reported before to interact with transcription factor TORC. Secondly, we could also confirm association of GR with the KIX domain of p300. Given the fact that the transcriptional activation complex composed of CREB and p300 is stabilized via interaction between CREB's kinase inducible domain KID and p300's domain KIX, one possibility of GR mediated interruption might be competitive binding of GR and CREB for the same p300 binding domain KIX. In this context, the ability of overexpressed p300 to revert the inhibitory effects of GR on CREB mediated transcriptional activation support this notion. Alternatively, association of GR with the bZIP domain of CREB could lead to structural changes of CREB thereby disrupting the privileged p300/P-CREB interaction complex. In both scenarios released phosphorylated CREB might then in turn be more easily accessible for CREB phosphatases.

While at present the exact mechanistic details remain unclear, the negative effect of the GC/GR axis might represent a more common feature of gene regulation and could reveal new mechanistic insights into how glucocorticoids can negatively regulate target genes. Although beyond the scope of this work, implications of these mechanism for long-term memory adaptation are plausible. Glucocorticoids are for long known to interfere with long-term memory and learning capacity, while activated CREB plays a key-role in these processes.

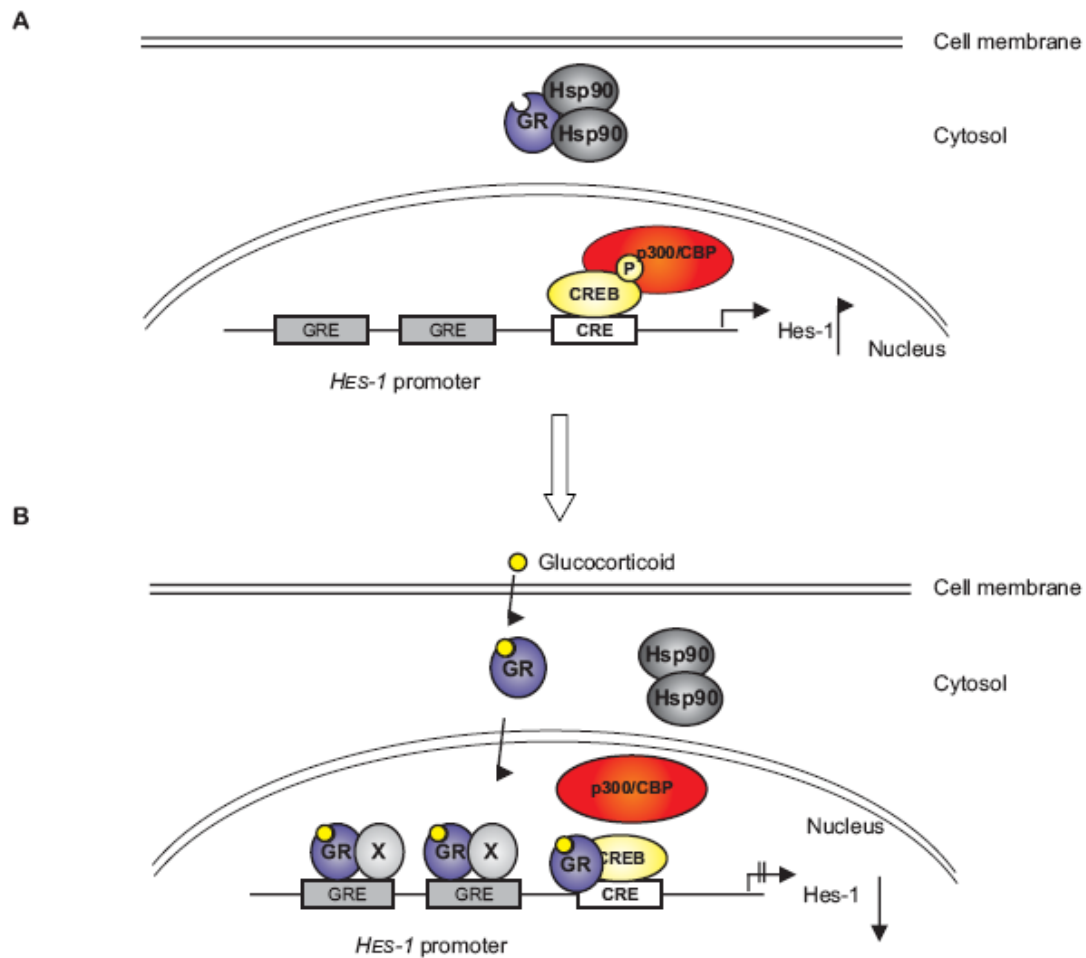


Figure 4.1: Glucocorticoid mediated repression of Hes-1 transcription. A) Transcriptional activation of Hes-1 promoter in response to cAMP signaling. cAMP response element binding protein CREB (yellow) is phosphorylated and interacts with histone acetylase p300. By acetylating local histones chromatin structure is altered and transcription activated (not shown). B) Glucocorticoids cross the cell membrane bind to the glucocorticoid receptor (GR, blue) releasing it from an inactivation complex with heat shock proteins. GR translocates to the nucleus where it binds to GR response elements (GRE, grey) on the Hes-1 promoter and where it associates with the p300/P-CREB complex facilitating its disruption. Release of p300 indicates decreased promoter activity.

In silico studies on the Hes-1 promoter revealed putative binding motifs for GR which were confirmed *in vitro*. In ABCD assays, GR binding was positively matched with the localization GRE half site TGTTC (141, 206) (207). The GRE 5'-TGAACCTATTAT-3' comprised a lower GR affinity and resembles more closely the consensus hormone response element 5'-AGAACA_{nnn}TGTTCT-3' (208) than a canonical GRE (5'-GGTACA_{nnn}TGTTCT-3') (40). The region might therefore also be targeted by nuclear receptors such as the mineralocorticoid receptor or the androgen receptor.

While GR binding to two predicted regions was confirmed, no conclusions about the nature of the response elements – whether activating or repressing – can be drawn. Molecular mechanisms of GR-dependent cis-repression of target genes are largely unsolved. To further

characterize the identified GREs mutation analysis in transfections using proximal Hes-1 promoter constructs is necessary.

4.7 Outlook

Non-Alcoholic Fatty Liver Disease is the most common chronic liver disease and is tightly associated with resistance of the liver against insulin action. The high prevalence of NAFDL necessitates the development of new intervention strategies based on the underlying molecular mechanisms. Glucocorticoids promote the development and progression of the diseases and the study presented here aimed for the identification of metabolic pathways involved in this process. The current study identified the transcriptional repressor Hes-1 as a GC/GR-controlled target gene in liver. Maintenance of hepatic Hes-1 levels have been demonstrated to be critical to limit fat influx into the organ and to preserve hepatic insulin sensitivity. Hes-1 antagonizes GC-triggered transcriptional activation of target genes of fat import and prevents accumulation of fat in the liver. Restoration of hepatic Hes-1 levels represents an attractive target for therapeutical intervention against GC/GR-dependent fatty liver. These findings will have implications for the development of treatment strategies against NAFDL and its associated co-morbidities.

The work presented here furthermore demonstrated an antagonistic action of the fasting hormones glucagon and glucocorticoids on hepatic lipid metabolism as shown by the regulation of anti-lipogenic Hes-1 contrasting their synergistic action on glucose metabolism. The data evidence that the transcription factors activated by the hormones – namely the glucocorticoid receptor and CREB interact with each other. The functional consequences of this interaction will increase the understanding of the synergistic and antagonistic effects mediated by GR and CREB. Further studies that describe the nature of this interaction in detail, however, are needed to unravel its metabolic meaning.

5 Methods and Materials

5.1 Molecular Biology

5.1.1 DNA gel electrophoresis

For routine applications (fragments from 200 bp) normal agarose (Roth, Cat No. 12656) was dissolved in standard 1x Tris-borate-EDTA (TBE) buffer. Agarose was melted, cooled down, and 1 µl of ethidium bromide (10 mg/ml) were added per 100 ml of agarose solution. Depending on the gel size and concentration, gels were run at a voltage between 60 and 120 V with constant current.

5.1.2 Extraction of DNA fragments from agarose gels

DNA fragments were excised from agarose gels of the appropriate percentage using a UV lamp and purified using QIAquick Gel Extraction Kit (QIAGEN #28704) according to the manufacturer's instructions. After purification, DNA was ethanol-precipitated (1/10 volume 5 M Na-acetate pH 5.2, 1 µl glycogen (2mg/ml); 2.5 volumes 100% ethanol), washed in 70% ethanol and dissolved in the appropriate amount of sterile H₂O. All isolated fragments were stored at -20°C until needed.

5.1.3 Transformation of bacteria for plasmid amplification

5.1.3.1 Transformation of chemically competent cells

Chemically competent E.coli XL-1/blue cells were used for routine plasmid amplification. For special applications e.g. after ligation of three fragments XL-10 GOLD cells were chosen.

50 µl of chemically competent cells were thawed on ice and then transferred to a chilled 14 ml Falcon round bottom tube. They were gently mixed with either 100ng plasmid-DNA (0,5 to 1 µl) or 1 to 3 µl ligation reaction mixture and chilled on ice for approximately 30 minutes followed by a 30 second heat shock in a water bath at 42°C. The reaction was chilled again for 2 minutes on ice and 450 µl 37°C warm LB-medium was added. The reaction mixture was incubated 45 to 60 minutes at 37°C and 200 rpm.

Selection of positive clones was carried out by plating various amounts of the transformed bacterial culture onto LB-Agar dishes containing the appropriate selection antibiotic and incubation overnight at 37°C in an incubator. Positive clones were selected using wooden sticks and they were transferred into 15 ml Falcon tubes containing 4 ml LB-medium plus appropriate antibiotic.

5.1.3.2 Transformation of electrocompetent cells

Electrocompetent E.coli XL-1/blue cells were used for special applications e.g. after ligation reactions of blunt end fragments.

Approximately 100 µl cell suspension were used for the transformation. They were thawed on ice and 1 to 3 µl ligation mixture were added. Mixture was gently stirred and then transferred to a chilled electroporation cuvette. Electroporation was done with 2,5 kV and 400 Ω. Immediately, 800 µl 37°C warm LB-medium were added to the cell suspension and the reaction was incubated for 1h at 37°C. Selection of positive clones was done as described in Section 5.1.4.1.

5.1.4 Plasmid purification

All plasmids were isolated by using plasmid purification Kits (QIAprep® Spin Miniprep Kit #27106, Invitrogen Pure-Link™ High Pure Plasmid Cat No K2100-26) according to the manufacturer's instructions. Purified plasmids were eluted with sterile H₂O and stored at -20°C. DNA concentration was determined by spectrophotometric measurement using a Nanodrop ND-1000 spectrophotometer (peqlab Biotechnology). Spectral absorbance at 260 nm was used for calculation and ratio between of OD_{260nm}/OD_{280nm} served as purity control. Ratios obtained were in the range between 1,8 and 2,1.

5.1.5 Isolation of genomic DNA from murine tissue

Approximately 5 to 10 mg tissue were incubated in 500µl tissue lysis buffer (10 mM Tris pH 8.0, 100mM NaCl, 15 mM EDTA, 0,5% SDS, 0,5 mg/ml Proteinase K) at 56°C on a shaker (Thermomixer, Eppendorf) overnight at 400 rpm.

Next day, sample is thoroughly mixed until no cell clumps are visible anymore and 500 µl PCI buffer (phenol pH 8.0 : chloroform : isoamylalcohol 25:24:1 (v/v)) are added. The reaction mixture is gently mixed for 20 seconds and then spun at maximum speed (13 000 rpm, Eppendorf centrifuge) for 5 minutes at ambient temperature. The upper aqueous phase is transferred to a fresh tube and 500 µl PCI buffer are added again. The procedure is repeated and the aqueous phase is transferred to a fresh tube. 500 µl CI buffer (chloroform: isoamylalcohol

24:1 (v/v)) are added, the extraction is done again by mixing for 20 seconds and subsequent centrifugation for 5 minutes at 13000 rpm. Finally, the upper phase is transferred to a fresh tube and the DNA is precipitated by addition of 500 µl 2-propanol. After mixing the solution, it is centrifuged for 15 min at 13000 rpm and 4°C. The supernatant is discarded and 500µl 75% ethanol are added to wash the DNA pellet. After removal of ethanol by centrifugation for 5 minutes at 4°C and 13000 rpm, the pellet is shortly air-dried and then re-solubilized in 30 to 100 µl Tris-EDTA buffer pH 8.0. For complete solubilization the samples are kept overnight at 4°C. Next day, they are ready to use or can be stored for longer periods at 4°C.

Generally, all pipetting steps should be carried out with care to avoid shearing forces. Buffers and materials used should be free of DNases.

5.1.6 RNA isolation with Qiazol™ Lysis Reagent

For most experiments the purity of the RNA obtained after Qiazol™ isolation is sufficient. If not, it is possible to further purify the RNA by DNase treatment and purification via the Qiazol RNeasy Mini purification kit (see section 5.1.7).

5.1.6.1 RNA isolation from tissue samples

Tissue samples, that were instantaneously frozen in liquid nitrogen after dissection, are suitable for the isolation of RNA from liver. Briefly, 10 mg of frozen tissue is transferred into a 2mL RNase/DNase-free reaction tube containing 1 ml Qiazol™ Lysis reagent (Cat No: 79306) and a stainless steel bead (Qiagen, 5mm, Cat No. 69989). The samples are lysed by vigorous shaking in the TissueLyser™ (Qiagen) for 90 sec at a frequency of 30 Hz. The lysate is incubated for three minutes at room temperature to release nucleoprotein complexes and then transferred into a fresh RNase/ DNase-free safety lock-reaction tube containing 200 µl chloroform. The mixture is vortexed for 15 sec and then centrifuged for 15 min at 12000 x g. The upper aqueous solution, containing mainly RNA, is carefully removed and transferred into a fresh reaction tube. For precipitation of the RNA 500 µl 2-propanol are added and the sample is mixed by inverting the tube. After 10 min incubation at room temperature the RNA can be pelleted by centrifugation for 10 min at 12000 x g. The supernatant is aspirated and the pellet is washed once with 1 ml 75% ethanol. The solvent is discarded and the pellet is carefully air-dried and resolubilized in a suitable amount of water (30 µl are fine in most cases). The solubilisation is facilitated by incubation at 55°C for 10 min on a Thermomixer (Eppendorf). The samples should be stored until further use at -80°C.

5.1.6.2 RNA isolation from cell samples

Adherent cells are stimulated according to experimental needs. The medium is removed and the cell monolayer is washed once with sterile PBS. The buffer is aspirated and 1mL Qiazol™ Lysis reagent is added/ 10cm plate (or 250 µl per well on a 6-well plate). The cells are scraped with a sterile cell scraper and transferred into DNase/RNase-free reaction tubes. The cells are incubated for 5 min at room temperature and are vortexed vigorously until no cell clumps are visible. The obtained cell lysate can either be stored until further use at -80°C or the RNA can be isolated as described in Section 5.1.6.1 starting with steps that follow tissue lysate preparation.

5.1.7 RNA isolation with RNeasy Mini purification kit

This protocol is suitable for applications, where genomic DNA impurities in RNA preparations are critical to be removed. Tissue samples are transferred into a 2 mL reaction tube equipped with 600 µl RLT buffer and 6µl β-mercaptoethanol and is lysed for 2 min at 30 Hz using the TissueLyser. The obtained lysate is transferred to a Qias shredder column and via centrifugation at 13000 rpm for 2 min the membranes of cell organelles are sheared, DNA is released and also sheared.

To the eluate 600µl 70% ethanol are added and the solution is gently mixed by turning the reaction tube. The reaction mixture is transferred to a RNeasy column (maximum 700 µl at once) and spinned for 1 min at 13000rpm. (RNA isolated using Qiazol™ Lysis reagent can be used for this procedure. In this case the RNA sample is diluted with 350µl RW1 buffer and applied onto the RNeasy column.) The flow-through is discarded and the column is washed with 350 µl RW1 buffer for 5 min. The buffer is removed by centrifugation.

To the dry column 80 µl DNase buffer (10µl DNase and 70µl RDD buffer) are added directly and the digest is incubated for 30 min at ambient temperature. Subsequently, 350 µl RW1 buffer are added and co-incubated for another 2 min. The column is washed twice with 500µl RPE buffer. Finally, the RNA is eluted in 30 µl RNase free water

5.1.8 Evaluation of RNA quality and quantification

To examine the degree of degradation after RNA isolation a 1% Agarose gel is poured with RNase-free reagents. RNA samples are denatured using formaldehyde/ formamide. To 10 µl RNA denaturation buffer 500 ng RNA sample are added and the samples are incubated for 10 min at 65°C.

RNA denaturation buffer (per sample):

- 0,5 µl ethidium bromide (0,1%, Roth, Cat No. 2218.2)
- 0,5 µl 10 x MOPS buffer
- 5µl formamide
- 1,75 µl formaldehyde
- 1,7µl loading dye (Fermentas, #R0611)
- 0,55 µl RNase free water

After denaturation samples are loaded onto the agarose gel and separated for at least 40 min. The quality of the RNA can be determined visually by examination of the ration between 28S to 18S ribosomal RNA, which should be 2:1. Since the mRNA represents only 1% of total cellular RNA it is not possible to directly examine its degradation status.

The amount of RNA was determined spectrophotometrically at 260 nm using the Nanodrop device. Furthermore, the ratio 260nm/280nm was determined to measure protein impurities. The value should be between 1,8 and 2,1.

5.1.9 cDNA synthesis

For the synthesis of cDNA 500ng purified RNA are used, routinely. The RNA is adjusted to a volume of 9µl/sample with RNase/DNase-free water and 1µl oligo(dT)₁₈ primers (Fermentas #K1612) is added per sample. The reaction mixture is vortexed and incubated for 5 min at 70°C for primer annealing at the polyA tails. Samples are chilled for at least 2 min at 4°C and then a reaction mixture is prepared according to the manufacturer's instruction (Fermentas).

Reverse Transcriptase Reaction Mixture (per sample):

- 4 µl 5 x reaction buffer
- 2µl 10 mM dNTP mix
- 1 µl Ribolock™ Ribonuclease Inhibitor

The samples are mixed with the buffer and incubated for 5 min at 37°C, followed by addition of 2µl M-MuLV reverse transcriptase (20u/µl). One control reaction without reverse transcriptase is performed. In the following quantitative PCR reaction, this sample will be important to estimate the amount of genomic DNA that was still present in the RNA isolation.

After 1 hour incubation at 37°C the cDNA synthesis is determined by heat inactivation of the reverse transcriptase for 10 min at 70°C. The cDNA can be stored at -20°.

5.1.10 Quantitative Real-Time PCR

The cDNA samples obtained under 2.1.9 were diluted ten-fold with DNase/RNase free water and per reaction 5µl of this solution were used. A master mix was prepared containing 10µl Platinum® Quantitative PCR Supermix, (Invitrogen Cat. No. 11730-025) 3,6 µl DNase/RNase free water, 0,4µl ROX dye (Invitrogen, Cat. No. 12223-012) and 1µl Taqman® probe per individual reaction. Technical duplicates of all samples were performed. The Taqman probes used were obtained from Applied Biosystems and are listed in Table XXX:

Table 9: Taqman® probes used for qPCR experiments

Probe	Number
ApoB	Mm01545159_m1
ACC1	Mm01304279_m1
caveolin1	Mm00483057_m1
CPT1α	Mm00550438_m1
CD36	Mm00432403_m1
FABP-1	Mm00444340_m1
FAS	Mm00662319_m1
Glucokinase	Mm00439129_m1
G6Pase	Mm00839363_m1
Hes-1	Mm00468601_m1
Hes-2	Mm00456108_g1
Hes-3	Mm00468603_m1
Hes-5	Mm00439311_g1
Hes-6	Mm00517097_g1
Hes-7	Mm00473576_m1
IκBa	Mm00477798_m1
MTTP	Mm00435015_m1
GR	Mm00433832_m1
PDK4	Mm00484152_m1
PP1 regulatory inhibitor su3c	Mm01204084_m1
PGDH	Mm00503037_m1
PEPCK	Mm00440636_m1
PPARα	Mm00440939_m1
PPARγ	Mm00440945_m1

As negative control water only was used and to determine the contamination with genomic DNA a cDNA sample that was not treated with reverse transcriptase was also routinely examined.

20µl PCR reaction were transferred per well onto a MicroAmp™ Optical 96-well reaction plate (Applied Biosystems, Cat. No. 4316813) and quantitative PCR was done on a 7300 Real Time PCR System (Applied Biosystems).

5.2 Cell Biology

Cell cultivation of all cells lines was carried out in incubators at 37°C, 95% humidity and 5% CO₂. Aseptic techniques were always used to maintain cells or for cell culture experiments.

5.2.1 Cell line treatment and transfection

5.2.1.1 Human Embryonic Kidney cells

Human embryonic kidney cells (HEK 293 cells) were maintained and extended in Dulbecco's Modified Eagle Medium with high glucose (DMEM) (Gibco Cat. No. 41966-052), 10% fetal calf serum (FCS) and 1 x penicillin/ streptomycin.

Transient transfections were done with the Ca₃(PO₄)₂-method according to Sambrook and Russle using a modified protocol: the cells were plated at a concentration of 1,16 x 10⁵ cells/ ml the day before the experiment on a 12-well plate. Prior to transfection medium was exchanged and 500µl fresh medium/plate were applied again. Per well between 800ng and 2,5 µg total DNA were used for transfections and each condition was done in triplicates. For this purpose, the appropriate amount of DNA was diluted in sterile water and 12,6 µl 2,5 M CaCl₂ were added to reach a final volume of the solution of 126µl. To facilitate ion exchange on the DNA from Mg²⁺ to Ca²⁺ the reaction mixture was incubated for at least 5 min at 37°C.

Subsequently, 126µl HBSS buffer (pH 7.05) were added dropwise to the reaction while mixing the reaction. After incubation for exactly one minute 504 µl DMEM medium (37°C) were transferred to the solution, the transfection solution was mixed well and 190µl of it were transferred per 12-well immediately. After 3 to 4 hours very fine Ca₃(PO₄)₂ crystals were visible microscopically.

Transfection was done overnight and the following day, medium exchange to normal growth medium or stimulation was carried out.

5.2.1.2 HepG2 hepatocytes

Human HepG2 hepatocytes were maintained and extended in a mixture of DMEM and F-12 medium (1:1 (v/v)) including 10% FCS and 1 x penicillin/ streptomycin. Medium composition decreased the accelerated cell growth of HepG2 cells in pure DMEM and preserved the hepatocyte characteristics of the cells.

For transfections HepG2 cells were plated at a concentration of 3×10^6 cells/ml on 6-well plates. After 6 to 8 hours cells were attached and transfection was done using a $\text{Ca}_3(\text{PO}_4)_2$ method with triplicates of each experimental condition per transfection. Total DNA amounts between 1,5µg and 3µg were routinely used. DNA was transferred to a reaction tube and 400µl 0,25M CaCl_2 was added. The solution was mixed and 400µl 2xBBS buffer were added in drops to it while mixing the reaction. After 20 min incubation at room temperature 200µl of the reaction mixture were used per well. Transfection was allowed to complete overnight and the next day medium exchange to DMEM/ F-12 or stimulation was done, respectively.

5.2.1.2.1 H4IIE rat hepatocytes, Hepa1C1 wt cells and 293A cells

H4IIE cells were maintained in MEM medium (Gibco Cat No. 31095-052) with 10% FCS, 1% NAA and 1% penicillin/ streptomycin. 293A cells and Hepa1C1 wt cells were cultivated in D-MEM medium supplemented with 10% FCS, 1% NAA and 1% penicillin/streptomycin.

5.2.2 Harvest of transfected cells

Cells were harvested 48 to 72h after transfection. The medium was discarded and the cells were washed once with PBS. Subsequently, harvest buffer (25 mM Gly-Gly pH 7,8, 15 mM MgSO_4 , 4 mM EGTA, 0,1 mM DTT, 0,01% Triton X-100) was added to the wells. Typically, for one well on a 12-well plate 150µl harvest buffer were used. Cells were incubated for 5 min on a shaker to facilitate detachment from the dish and the lysate was transferred to a 1,5ml reaction tube. Lysis of the cell was facilitated by pipetting the suspension several times. Insoluble debris was removed by centrifugation for 3 min at 13000 rpm and the supernatant was transferred to a fresh tube. The lysate can be used directly for reporter gene assays or stored at -20°C .

5.2.3 Measurement of luciferase activity

Luciferase assays are used to investigate a specific promoter activity driving the expression of the firefly luciferase gene. Luciferase is an enzyme catalysing a reaction in which beetle luciferin is transformed into oxyluciferin by oxidative decarboxylation thereby emitting photons.

Under the assay conditions the substrate luciferin is available in excess, consequently the amount of light emitted is proportional to the amount of firefly luciferase in the lysate.

For the determination of luciferase activity in lysates of transfected cells, 30 µl of this lysate are transferred into a well on a black 96-well-plate. The lysate is diluted with 100 µl assay buffer (25 mM Gly-Gly pH 7.8, 20 mM K₃PO₄, 15 mM MgSO₄, 4 mM EGTA, 2 mM ATP, 1,6 mM DTT) and the plate is placed into a luminometer (Mithras 940 Luminescence) equipped with a dispenser. Automatic injection of 100 µl luciferin buffer (0,32 mg/mL luciferin, 25 mM Gly-Gly pH 7,8, 15 mM MgSO₄, 4 mM EGTA) starts the reaction.

Light emission is measured at a wavelength of 560 nm and as blank value harvest buffer (5.2.2) is used. Biological triplicates of all samples are done and each value is normalized against β-galactosidase values (5.2.4.).

5.2.4 Measurement of β-galactosidase activity

Transfection efficiency is monitored by co-transfection of a plasmid constitutively expressing β-galactosidase. For this purpose the vector pCMV β-galactosidase is used at various amounts. The β-galactosidase activity directly correlates with the amount of DNA incorporated during transfection, therefore it is a good measure to control transfection efficiency. It is important to test whether any experimental condition e.g. stimulation has an influence on the expression of β-galactoside to exclude variations.

For the assay a buffer including the substrate ortho-nitrophenyl-β-galactopyranosid (ONPG) is prepared (1M Na₂HPO₄, 1mM MgCl₂, 10 mM KCl, 1mg/ ml ortho-nitrophenyl-galactopyranosid) and to 5 ml of this buffer 13,5 µl beta-mercaptoethanol are added prior to use. Into a clear 96-well plate (Costar Cat No. 13631) 50 µl cell lysate/ well is transferred and 50 µl/ well ONPG buffer is added. As a blank value only harvest buffer is transferred into three wells. The plate is incubated until a clear yellow color is visible in the samples and the signal to noise ratio is higher than 5:1. The absorption is measured at 405 nm, the maximum absorption of the ortho-nitrophenylat ion.

5.3 Biochemistry

5.3.1 Preparation of Protein Extracts from liver samples using PGC buffer

Protein extracts are prepared with PGC lysis buffer. A 1,5 ml reaction tube is equipped with 1 ml PGC lysis buffer, protease inhibitors and a stainless steel bead and incubated on ice. Into the ice-cold buffer approximately 30 mg frozen liver tissue are transferred and the sample is immediately homogenized in the TissueLyser ® (Qiagen) for 2 min at 30 Hz. The extracts are

incubated for 20 min on ice and the lysate is transferred to a fresh tube. The lysate is spun for 15 min at 13000 rpm. If a fat layer appears at the surface after centrifugation, it is discarded without perturbing the lysate. The lysate is transferred to a fresh reaction tube and a determination of the protein concentration is carried out as described in Section 5.3.3. All samples are adjusted to a concentration of 1 mg/ml protein with 2 x SDS buffer. These samples are incubated for 5 minutes at 95°C for denaturation and can be directly used for SDS-PAGE and immunoblotting. If not used immediately, the denaturated samples are stored at -20°C. The original lysates before denaturation should be kept at -80°C.

5.3.2 Preparation of Protein Extracts from liver samples using SDS lysis buffer

Approximately 20 mg snap-frozen liver tissue samples are transferred to a 2 ml SafeLock ® tube equipped with 1 ml SDS lysis buffer (at room temperature so the SDS cannot precipitate) and a stainless steel bead. Protease inhibitors are not necessary when using this buffer. Immediately, homogenize the samples for 2 minutes or until no tissue clumps are visible at 30 Hz employing the Qiagen Tissue Lyser. After homogenisation, samples are incubated for 5 minutes at room temperature and the lysate is transferred to a fresh tube. Subsequently, the debris is removed by centrifugation for 10 minutes at 13000 rpm and room temperature. The supernatant is transferred to a fresh tube and incubated for 5 to 10 minutes at 95°C. The protein concentration is determined using the 2D-Quant Kit (see Section 5.3.4), since the high amount of SDS interferes with the protein determination of the BCA™ Protein Assay Kit.

A part of the original lysates is adjusted with SDS lysis buffer to 1 mg/ml. Original lysates and adjusted samples can be stored at -20°C.

5.3.3 Protein determination with the BCA™ method

The assay is done in a 96-well format to allow the simultaneous measurements of up to 42 samples. First a standard curve from 2 µg to 10 µg protein in duplicates is transferred to the plate using BSA (2mg/ml, Pierce Cat. No. 23209). Then between 2 µl and 8 µl of protein lysates with unknown protein concentration are added to separate wells. The protein concentration, however, should lay within the range of the standard curve. If necessary, dilutions of the original protein lysate can be prepared using 0,9% saline for dilution. Next working reagent is prepared by mixing BCA™ reagent A with BCA™ reagent B in a ratio of 50:1 (v/v). Per sample 200 µl working reagent are transferred with a multistep pipet onto the plates and the reaction mixture is incubated for 5 min at 37°C.

5.3.4 Protein determination with the 2D-Quant Kit

The 2D Quant Kit (Amersham Biosciences Europe, 80-6483-56) is used for determination of protein samples containing high SDS concentrations (1% SDS and more). The procedure works by quantitatively precipitating proteins while leaving interfering substances in solution. The assay is based on the specific binding of copper ions to protein. Precipitated proteins are resuspended in a copper-containing solution and unbound copper is measured with a colorimetric agent. The color density is inversely related to the protein concentration. Accurate estimation of protein concentration is achieved by comparing to a standard curve. For the standard curve BSA (2mg/ml) is used.

For the assay between 3 and 10µl protein lysates are used and proteins are precipitated following manufacturer's instructions. Samples are done in duplicates.

The absorbance of samples and standards is read at 480 nm in a spectrometer (Ultrospec, Pharmacia) using water as reference. Subsequently the standard curve is generated by plotting the known protein concentration against the absorbance. Absorbance values of unknown samples should lie in the same range, extrapolation is not advisable.

5.3.5 SDS-PAGE

For SDS-page, proteins are diluted in 2xSDS sample buffer (120 mM Tris pH 6.8, 200 mM DTT, 4% SDS, 20% glycerol, 0,01% bromophenol blue) and denatured by boiling for 5 min. Protein lysates are examined using SDS polyacrylamide gel-electrophoresis (SDS-PAGE) as introduced by Laemmli using discontinuous gels. Proteins are first focused in the low-percent collection gel and subsequently separated in the separation gel. For the separation gel different concentrations of acrylamide were used. Routinely, 10cm gels were poured as shown in Table 12. During polymerisation the gel is overlayed with 2-propanol.

On top of the separation gel, 3 ml collection gel are added (2,1 ml water, 0,38 ml Tris-HCl pH 6,8, 0,5 ml 30% acrylamide mix, 30µl 10% SDS, 30µl 10% ammonium persulfate, 3 µl TEMED). Protein amounts between 10 and 50µg were subjected to separation on 10 ml gels in SDS electrophoresis buffer (1,92 M Glycin; 0,25 M Tris , 0,45% HCl; 30 mM SDS).

Table 10: Composition of polyacrylamide gels with different concentration of acrylamide

	8% gel	10% gel	12% gel
Water	4,6 ml	4 ml	3,3 ml
30% acrylamide mix	2,7 ml	3,3 ml	4 ml
1,5 M Tris (pH 8,8)	2,5 ml	2,5 ml	2,5 ml
10% ammonium persulfate	100µl	100µl	100µl
10% SDS	100µl	100µl	100µl
TEMED	6 µl	4µl	4µl

After electrophoretic separation gels were either stained with Coomassie or subjected to immunoblotting (Section 5.3.6). For Coomassie staining gels were briefly washed with water and then fixed in fixation buffer (25% 2-propanol, 10% acetic acid) for 1h and gentle shaking. The gels were washed twice with water and stained using PageBlue™ protein staining solution (Fermentas Cat. No. R0571) overnight. Excess staining was removed by washing the gel several times with water.

5.3.6 Immunoblotting

Proteins are electrophoretically transferred to nitrocellulose membranes, which has been equilibrated with transfer buffer (1,92 M Glycin; 0,25 M Tris, 20% methanol) overnight at 30V and 4°C. The slow transfer facilitates especially efficient blotting of larger proteins. After transfer membranes are washed briefly in water and the transfer was examined by Ponceau S staining (Sigma, Cat. No. P7170) for 5 min. Ponceau S is removed and membrane is washed twice with water followed by 1h incubation in blocking buffer (5% non-fat powder milk (Roth #T145.2)) dissolved in TBST buffer (20mM Tris pH 7.5, 140 mM NaCl, 0.1% Tween-20®) for 1 hour. Primary antibodies were used as indicated in Table 11. Subsequently, membranes were washed three times with TBST buffer for 15 min each. Secondary antibodies (conjugated to horse radish peroxidase (HRP)) were used at a dilution of 1:2000 to 1:5000 and were applied in blocking buffer for 45 min to 1h. Membranes were rinsed again three times for 15 min. To detect specific bands the enhanced chemiluminescence system (ECL™) Western Blotting Detection Reagent (Amersham Cat. No. RPN2106) was used, followed by the exposure to Hyperfilm™ ECL films (Amersham Cat. No. RPN3103K). Exposure times varied between the different antibodies used.

Table 11: Primary and secondary antibodies for immunoblot

antibody	Source	species	Dilution
CREB clone NL 904	Upstate 05-767	rabbit monoclonal	1:2000
P-CREB (Ser-133)	05-807 (Upstate)	mouse monoclonal	1:2000
FLAG M2 HRP	A 8592 Sigma	mouse monoclonal	1:1000
GR M-20	sc-1004 Santa Cruz	rabbit polyclonal	1:2000
Hes-1	Tetsuo Sudo, Japan	rabbit polyclonal	1:1000
I κ B α H-4	sc-1643 Santa Cruz	mouse monoclonal	1:500
MKP-1	sc-1102 Santa Cruz	rabbit polyclonal	1:500
p300	sc-584 Santa Cruz	rabbit polyclonal	1:1000
PPAR γ H-100	sc-7196 Santa Cruz	rabbit polyclonal	1:1000
VCP	ab11433 Abcam	mouse monoclonal	1:10000
anti-mouse IgG, HRP	170-6516 BioRad	goat	variable
anti-rabbit IgG, HRP	170-6515 BioRad	goat	variable

5.3.7 Isolation of hepatic lipids

The lipids are extracted with chloroform/methanol (2:1 v/v) from frozen liver tissue. Frozen liver samples are cut on dry ice with a scalpel and weighed. The weight should be approximately 100 mg and it is annotated since the amount of triglycerides will be normalized with the initial organ mass. The liver tissue is transferred into a 2 ml polypropylene tube equipped with 2 ml chloroform/methanol. The tissue is homogenized with an Ultraturrax until no big tissue clumps are visible. To extract the lipids, samples are incubated for 20 min at room temperature on a rotating wheel. The tissue suspension is pelleted at 4000 rpm for 10 min and the supernatant is transferred to a fresh tube. The organic layer is extracted twice against 0,9% sodium chloride and the aqueous solution is aspirated carefully. Finally, 50 μ l of the organic layer are transferred to a fresh tube and 10 μ l of Triton-X 100/ chloroform (1:1 v/v) are added. The reagents are mixed and the solvent is evaporated. The residue containing the hydrophobic contents of the liver is resuspended in 50 μ l water and stored at -20°C until further use.

5.3.8 Isolation of hepatic glycogen

Frozen liver samples are cut into 100 to 200 mg big pieces and the exact weight is determined. The liver is transferred into a reaction tube equipped with 1 ml 30% (w/v) KOH and a stainless steel bead. Homogenization of the samples is facilitated in the TissueLyser® (Qiagen) for 2 minutes at 30 Hz. For complete tissue disruption the lysate is incubated for 30 minutes at 95°C with shaking in a Thermomixer (Eppendorf). The debris is removed by centrifugation for 5

minutes at 13000 rpm and the supernatant is transferred into a 15 ml reaction tube. The glycogen is precipitated by addition of 1,5 ml 95% ethanol and subsequent centrifugation at 3000 x g for 20 minutes. The pellet is washed once with 1 ml ethanol and after air-drying the pellet for 5 minutes it is resolubilized in 0,5 ml water and incubated for 30 minutes at 37°C. After vigorous mixing, the insoluble material is removed by centrifugation for 5 minutes at 3000 x g. The supernatant is transferred to a fresh tube and can be stored at -20°C until further use.

5.3.9 Colorimetric Assays

5.3.9.1 Determination of triglyceride levels

The triglyceride measurement is a colorimetric assay in which the amount of glycerol liberated from triglycerides is determined enzymatically. Since the stoichiometric ratio between glycerol and triglycerides is one, the test allows the quantification of the amount of substance *n*. For the measurement, the serum triglyceride determination kit from Sigma (Cat No: TR0100) was used.

Practically, 4 µl of isolated hepatic triglycerides per sample (see Section 5.3.7) are transferred to a 96-well plate. As a positive control glycerol (2,5 mg/ ml, Sigma, Cat No G7793) is used and as negative control water. All samples are transferred in duplicates. 100 µl Free Glycerol Reagent is added per well and the plate is incubated for 5 minutes at 37°C and measured at 540 nm. This measurement reveals the glycerol that has not been released from triglycerides.

A second plate containing the same samples in duplicate is prepared and 100 µl Triglyceride Reagent are added. After incubation for 5 minutes at 37°C the optical density at 540 nm is determined. In this measurement the total amount of glycerol (free or as triglyceride) is determined.

By subtraction of the two obtained values per sample the amount of glycerol stored as triglycerides can be calculated.

5.3.9.2 Digestion of glycogen with Amyloglucosidase and Determination of Glucose liberated from Glycogen

A stock solution of Amyloglucosidase (Sigma, A7420) is prepared by dissolving 0,33 mg enzyme in 0,2 M sodium acetate pH 4.8. Samples with isolated glycogen are thawed and 50 µl of glycogen sample is mixed with 450 µl Amyloglucosidase stock solution. The mixture is incubated for 2 h at 37°C on a Thermomixer (Eppendorf) while shaking the samples. The reaction is stopped by neutralisation with 10 µl 30% (w/v) KOH.

The glucose determination is done with the Glucose (HK) Assay Kit (Sigma, GAHK-20). The kit uses the following reactions:

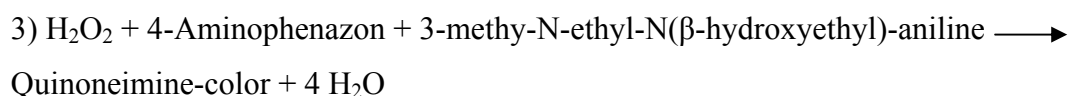
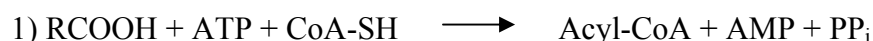


The release of NADH is directly proportional to the amount of glucose in the reaction. NADH is measured spectrometrically at 340 nm. A standard curve with known concentrations of D-glucose is prepared and the glucose content is determined according to the standard curve. The amount of sample used for the reaction varies, the obtained OD-values should lay within the range covered by the standard curve. The test is carried out according to manufacturer's instructions.

5.3.9.3 Determination of Free Fatty Acids

Free Fatty Acids can be determined in serum samples or in lipid extracts (isolation of hepatic lipids, Section 5.3.7). A colorimetric assay from Wako (NEFA C, Cat No: 999-75406) is used for the measurement.

The assay principle is the following (R-COOH any free carbonic acid) catalysed by (1) Acyl CoA synthetase, (2) acyl CoA oxidase and (3) peroxidase.



A standard curve using oleic acid (1 mM, Cat No: 270-76499) is used and 4 µl sample (in duplicates) are used for the measurement. The procedure is carried out according to manufacturer's instructions. OD-values are determined at 550 nm and the amount of free fatty acid is calculated according to standard curve.

5.3.9.4 Cholesterol measurement

For cholesterol measurements serum samples or hepatic lipid extracts (see Section 5.3.7) have been used. The total cholesterol determination kit (Randox Laboratories, Cat No: CH5715) has been employed.

Cholesterol \longrightarrow Cholesten-3-on + H₂O₂ (Cholesteroloxidase)

2H₂O₂ + Phenol + 4-Aminoantipyrin \longrightarrow Chinonimin + 4 H₂O (Peroxidase)

The sample cholesterol concentration is assessed by preparation of a standard curve with cholesterol. The assay is performed in a 96-well format. Briefly, 4 µl sample are mixed with 100µl assay reagent and incubated for 15 minutes at room temperature. Standard and a blank control (water) are treated equally. The optical density is measured at 492 nm and the sample concentration is calculated according to the standard curve.

5.3.10 ABCD Assay

5.3.10.1 General principle

The Avidin-Biotin Conjugation DNA binding assay (ABCD assay) is an *in vitro* method to examine the binding of transcription factors to their respective response elements on the DNA. In a broader sense, also transcriptional cofactor binding can be determined, however a prerequisite is the stability of the transcription complex under the experimental conditions. Either whole cell extracts or nuclear extracts can be investigated depending on the biological problem.

The ABCD-Assay takes advantage of the high affinity binding ($K_D \sim 10^{15} \text{ M}^{-1}$) between streptavidin, a protein isolated from *Streptomyces avidinii*, and biotin. Thus, biotinylated oligonucleotides bearing response elements of transcription factors are bound to streptavidin, which is covalently linked to agarose. The immobilized oligonucleotides are then exposed to protein extracts containing the desired proteins. Unbound proteins are washed away and specifically bound proteins are eluted and subsequently examined via western blots.

5.3.10.2 ABCD Assay for the glucocorticoid receptor

The cell lysates that are used for this assay are prepared from H4IIE cells. H4IIE cells are seeded two days before the assay and at the day of stimulation that should have 80-90% confluency. The medium is removed (MEM + 10% FCS + 1% NAA + 1% P/S) and the cell layer is washed once with serum-free medium (MEM + 1% NAA + 1% P/S). For the assay cells are stimulated with 10 nM Dex or ethanol for 1h in serum-free medium.

For the ABCD assay the following buffers need to be prepared:

Oligonucleotide annealing buffer

10 mM Tris/ HCl

50 mM NaCl
pH 8.0

Oligonucleotide binding buffer

5 mM Tris/HCl
0,5mM EDTA
1M NaCl
pH 7.5

PGC cell lysis buffer for ABCD assay

20 mM HEPES
125 mM NaCl
0,1% NP40
1 mM EDTA
10% (v/v) glycerol

Prior to use protease inhibitors and phosphatase inhibitors I and II are added. The glycerol prevents unspecific binding of proteins to the streptavidin agarose and is therefore recommended for use. However, by increasing the viscosity of the buffer it might on the other hand also decrease the specific binding of proteins to the investigated DNA elements.

DNA oligonucleotides were synthesized and only the sense oligonucleotide beared a biotinylated 5'-end. As a positive control for the assay the consensus glucocorticoid response unit (GRU) as described by Granner (48) was chosen. The binding of GR to the cAMP responsive element (CRE) and the Notch intracellular domain responsive element (RBP) as they occur in the murine Hes-1 promoter sequence were examined. In Table 12 the oligonucleotide sequences that have been investigated for glucocorticoid receptor binding are listed.

Table 12: Oligonucleotide sequences used in the ABCD assay with the glucocorticoid receptor

name	Oligonucleotide sequences of sense and antisense strands
CRE	5' - [Biotag] ATCCTTTTGATTGACGTTGTAGCCTCCGGTGCCC - 3' 5' - GGGCACC GGAGGCTACAACGTCAATCAAAAGGAT - 3'
-440bp/-393bp	5' - [Biotag] ATCCTCTTTACCTTGTTCCCTCCTTTTTTCAATCACTAAATTTGTCT - 3' 5' - AGACAAAATTTAGTGATTGAAAAAAGGAGGAACAAGGTAAAGAGGAT - 3'
-392bp/-346bp	5' - [Biotag] TGGCCTATATCTGTTCAAAATATTTTTCAAATGAACTTATTATACAAA - 3' 5' - TTTGTATAATAAGTTCATTTGAAAAATATTTTGAACAGATATAGGCCA - 3'
-345bp/-297bp	5' - [Biotag] GTAGTTATATTGCATGCAGCAAGAACAATAAAAACCAAAGGCCTGGCC - 3' 5' - GGCCAGGCCTTTGGTTTTTATTGTTCTTGCTGCATGCAATATAACTAC - 3'
-296bp/-261bp	5' - [Biotag] ACAAAAGAAATAGACTAGACTAAACTAAGCAAAGC - 3' 5' - GCTTTGCTTAGTTTTAGTCTAGTCTATTTCTTTTGT - 3'
-260bp/-225bp	5' - [Biotag] CCAGAGGAAAGAGTTAGCAAAGGGTTAAATCCTTT - 3' 5' - AAAGGATTTTAACCCTTTGCTAACTCTTTCCTCTGG - 3'
random	5' - [Bio-Tag] AAAAAAAAAAAAAAAAAAAAAAAAAAAAAAAAAA - 3' 5' - TTTTTTTTTTTTTTTTTTTTTTTTTTTTTTTTTT - 3'
Consensus GRU	5' - [Biotag] TTACGTTGATGGTACAAAATGTTCTAGGGTAC - 3' 5' - GTACCCTAGAACATTTTGTAACCATCAACGTAA - 3'

The oligonucleotides are annealed as such:

5µl biotinylated sense-oligonucleotide (100µM)

5µl antisense oligonucleotide (100µM)

40 µl Annealing buffer

(48)

are mixed and incubated for 5 minutes at 95°C for complete denaturation of the oligonucleotides, followed by a stepwise controlled cooling of 5°C per 2 min until a final temperature of 25°C is reached. Samples are then kept at 4°C. The annealing of the oligonucleotides can be examined using a 3% agarose gel. In the meantime, 60 µl of streptavidin agarose (Invitrogen, Cat No: SA100-04) are equilibrated with 1 ml oligonucleotide binding buffer in a 1,5 ml Eppendorf tube and spinned down for 1 minute at 3000 rpm to remove the binding buffer. The agarose is supplemented again with 500 µl oligonucleotide binding buffer and 48 µl annealed oligonucleotides are added. The slurry is incubated for 1 hour at room temperature on a rotating wheel. The streptavidin agarose is spinned down at 3000 rpm for 3 minutes and the supernatant is discarded. The agarose is used without any further washing steps for protein binding.

During the 1 hour incubation time of biotinylated oligonucleotides to the streptavidin agarose, HEK293 cells are harvested by trypsination, followed by wash steps in PBS and centrifugation

of the cells. For one experimental condition in the ABCD assay typically one 15 cm plate of HEK 293 cells is used. The cell pellet of one plate is resuspended in 1,5 ml PGC-lysis buffer supplemented with protease inhibitors and phosphatase inhibitors. The suspension is incubated on ice for 20 to 30 minutes and vortexed vigorously to facilitate cell lysis. The lysate is centrifuged for 15 minutes at 4°C and 13 000 rounds per minute and 1 ml of the lysate is transferred to the washed agarose. Furthermore, 50 µl of the cell lysate are diluted with an equal volume of 2x SDS buffer and incubated for 5 minutes at 95°C for denaturation. This sample will serve as the input control in the western blot analysis.

The cell lysate is incubated on the agarose for 30 minutes at room temperature. Unbound proteins are removed by washing the agarose beads three times with 600 µl PGC cell lysis buffer including protease inhibitors. The agarose beads are pelleted by centrifugation for 2 minutes at 9000 rpm. The washing fraction is removed completely and 60 µl of 2x SDS buffer are added to each individual sample. The samples are vortexed once and incubated for 5 minutes at 95°C to elute all specifically bound proteins completely. Samples are vortexed again to facilitate complete protein recovery and centrifuged for 5 minutes at 13000 rpm at room temperature. The supernatant contains the released proteins and is stored at -20°C until investigation in western blots.

5.3.11 Chromatin Immunoprecipitation (ChIP-Assay)

The ChIP assay is a method to test the occupation of a certain protein on a DNA sequence *in vivo*. The assay can be performed starting from cultured cells or with tissue lysates.

5.3.11.1 ChIP assay from liver lysates

Approximately 50 mg of snap-frozen liver tissue are homogenized in dry ice powder in a pre-chilled mortar using a pistil. The frozen tissue powder is transferred into a 50 ml reaction tube equipped with 1,5 ml DMA buffer (2,4 mg/ml DMA in triethanolamine pH 8.0) and wrapped with aluminium foil. Since the CO₂ powder will lead to freezing of the DMA solution the whole mixture needs to thaw on ice. After complete thawing the suspension is incubated at room temperature for 30 min to crosslink proteins with each other. The suspension is spinned down for 3 min at 2000 rpm and the supernatant is discarded. The pellet is re-suspended in 5 ml 1% formaldehyde in PBS and incubated for 10 min at room temperature on a rotating wheel to facilitate DNA-protein crosslinking. The tissue is pelleted again by centrifugation for 3 min at 2000 rpm and washed once with 5 ml ice-cold PBS. After removal of PBS the tissue pellet is re-suspended in 1 ml cell lysis buffer (10 mM Tris pH 8,0, 10mM NaCl, 0,2% NP-40) including

protease inhibitors. The mixture is transferred into a pre-chilled Dounce Homogenizer (Size B) and homogenisation is done until no tissue clumps are visible anymore. After incubation for 5 min on ice the solution is transferred to a 2ml reaction tube and spun down for 5 min at 13000 rpm. The pellet is re-suspended in SDS lysis buffer (50 mM Tris-HCl pH 8,1, 10 mM EDTA, 1% SDS) including protease inhibitors and incubated for 10 min on ice. The samples are subsequently sonicated 4 times for 20'' at Duty cycle 30, Output control 3. After another centrifugation step for 10 min at 13000 rpm and 4°C the lysate is transferred to a fresh tube and the pellet is discarded.

The protein concentration of each sample is determined using the 2D Quant Kit (see Section 5.3.5). Afterwards, all samples are adjusted to the same protein concentration using SDS lysis buffer. For the subsequent steps 200µg protein are used and 20µg protein are used for the input control samples.

The solution containing 200µg protein is diluted 10-fold with ChIP dilution buffer (16,7 mM Tris-HCl pH 8,1, 167 mM NaCl, 1,2 mM EDTA, 1,1% Triton X-100, 0,01% SDS) to obtain final SDS concentration of 0,1%. To each sample the 5µg antibody are added and antigen-antibody reaction is done overnight at 4°C on a rotating wheel.

The next day 60µl salmon sperm agarose (Upstate) are added per sample and incubated for 2h at 4°C on a rotating wheel. The suspension is gently centrifuged for 2min at 1000 rpm and the supernatant is discarded. The agarose is washed several times in the following sequence for 5 min per step and between each step washing solution is removed by centrifugation for 2 min at 1000 rpm.

First washing cycle is done once with 1 ml low salt buffer (20 mM Tris-HCl pH 8,1, 150 mM NaCl, 2mM EDTA, 1% Triton X-100, 0,1% SDS) per sample followed by washing once with 1 ml high salt buffer (20 mM Tris-HCl pH 8,1, 500 mM NaCl, 2mM EDTA, 1% Triton X-100, 0,1% SDS). 1ml immuno-complex buffer (10 mM Tris-HCl pH 8,1, 1% deoxycholic acid, 0,25 M LiCl, 1% Igepal-CA 630) are then added and finally, to remove LiCl completely agarose is rinsed twice with 1ml TE buffer (10mM Tris pH 8,0, 1mM EDTA) per sample. After complete removal of TE-buffer, 100µl 10mM DTT per sample are added to the agarose and elution is facilitated by incubation for 30 min at 37°C in a Thermomixer (Eppendorf) at 400 rpm. The elution is repeated and subsequently the eluates are combined.

Input samples containing 20µg protein are thawed and diluted with 100µl 10mM DTT. Samples are de-crosslinked by addition of 4µl 5M NaCl and 2µl 5M NaCl to the input samples, respectively and incubation at 65°C overnight.

Next day, samples are briefly spun down to collect the buffer and then a Proteinase K digest of the proteins is performed by addition of 2µl 0,5M EDTA, 4µl 1M Tris-HCl pH 6,5 and 0,4µl proteinase K per sample. For the input samples the volumes are bisected. Protein digest is done for 1h at 45°C and the DNA is purified using the PCR purification Kit (Qiagen) following the manufacturer's instructions. DNA is eluted with 21µl TE buffer and stored at -20°C until evaluation with PCR.

5.3.11.2 ChIP assay from cultured cells

For each individual condition one 15cm plate is needed with 80 to 90% confluency. Per 25 ml medium 680 µl formalde are used and the cells are incubated for 10 min at 37°C. The medium is removed and the cells are washed once with ice-cold PBS. Cells are harvested in 2ml PBS using a cell scraper and the suspension is transferred into a fresh tube. The cells are pelleted by centrifugation for 5 min at 3000 rpm and the supernatant is discarded. Re-suspension is done in 400µl SDS lysis buffer containing protease inhibitors. Subsequently, the ChIP protocol is done as described in section 2.3.8.1

5.3.11.3 Antibodies used for ChIP Assays

Table13 lists antibodies used for chromatin immunoprecipitation.

Table 13: Antibodies used for ChIP assay

Antibody	Source
CREB	06-863 Upstate
P-CREB	05-807 Upstate
p300 N-15	sc-584 Santa Cruz
acetyl-histone H3	06-599 Upstate
GR P-20	sc-1002 Santa Cruz
normal mouse IgG	sc-2025 Santa Cruz
normal rabbit IgG	sc-2027 Santa Cruz

5.3.11.4 Evaluation by PCR

After isolation of DNA protein complexes and subsequent proteinase K digestion DNA with an average size of approximately 1000 to 2000 bp is available. To examine the amount of immunoprecipitated DNA complexes, a PCR reaction is performed. During this work protein complexes

on the murine Hes-1 promoter, on the rat Hes1 promoter and on the murine PEPCK promoter were used (see Table 14).

Table 14: Specific primers used for the evaluation of ChIP experiments

Promoter	Species	Primer	Sequence
Hes-1	Rat	Forward	5'-CCCAGAGGAGTTAGCAAA-3'
	Rat	Reverse	5'-CGAGTGAAACTTCCCAAA-3'
Hes-1	Mouse	Forward	5'-AGCGGAATCCCCTGTCTACCTCTC-3'
	Mouse	Reverse	5'-ATATCAGCTGGCATTTCGTTTTT-3'
PEPCK	Rat	Forward	5'-GGCCTCCCAACATTCATTAAC-3'
	Rat	Reverse	5'-GTAGCTAGCCCTCCTCGCTTTAA-3'

Per individual PCR reaction 3µl DNA isolated in ChIP experiments, 12,5µl 2x PCR Mix, 7,5µl ultra-pure water, 1µl forward primer (1µM) and 1µl reverse primer (1µM) are used to reach a final volume of 25µl.

The PCR follows the this protocol:

Initial denaturation:	10 min	95°C
35 cycles	30 sec	95°C
	30 sec	56°C (Hes-1 primer), 52°C (PEPCK primer)
	90 sec	72°C
Final elongation	30 sec	95°C
	3 min	72°C
	cool down to 4°C.	

The PCR reaction is interrupted at cycle 28 to 30 and 10µl of the mixture are transferred to a fresh tube. The PCR is completed with the remaining reaction mixture, so that finally per individual reaction two samples at different times of the PCR reaction are available. The samples are diluted with Orange Dye (6-fold, Orange G dye, 50% glycerol, 10 mM EDTA) and are run on a 1,5% agarose gel. The signal intensity obtained directly correlates with the amount of immuno-precipitated protein complexed with the DNA and therefore is a measure for binding affinity under a given experimental condition.

5.3.12 Radioimmunoassay for corticosterone

Serum corticosterone levels were measured using the corticosterone RIA Kit from MP Biomedicals (MP Biomedicals, Cat No #07120102). Serum samples are slowly thawed on ice and briefly spinned to sediment particles for 30'' at 13 krpm. Dilutions of serum are done in Seroid Diluent (included in Kit) depending origin of the sample, e.g. samples from fasted

animals and db/db mice are diluted 1:200, serum samples with low corticosterone levels are diluted 1:25. The assay is carried out in Fiolax tubes (Roth Cat No: 223.1 8x70 mm) according to manufacturer's instructions. Safety rules valid for work with ^{125}I is applied. A standard curve is prepared with stock solutions provided in the Kit. Samples are done in duplicates.

After addition of all reagents following the kit instructions, samples are incubated for 2h at RT. Bound corticosterone is precipitated by centrifugation for 15 min at 2400 rpm at 20°C (Hereaus centrifuge). Supernatant is discarded and remaining radioactivity in residue is measured in a gamma Counter (Master 1277, LKB Wallac) with 1 min count time per sample.

Corticosterone levels are calculated based on the standard curve.

5.4 Animal experiments

5.4.1 Glucose tolerance test

Mice are maintained on a 12 h light/dark cycle and fasted for approximately 15 hours starting at 6 pm. The animals are transferred into fresh cages equipped with fresh water but no food. The following morning, the body weight is determined and the initial blood glucose level is determined by nicking the tail with a razor blade by a horizontal cut at the very end. A blood drop is transferred onto a glucometer stripe and measured.

The mice are then injected intraperitoneally with 10 $\mu\text{l/g}$ body weight of 20% (w/v) D-glucose. The measurement of blood glucose is done by sampling blood from the tail. At 10, 20, 30, 60, 90 and 120 min after injection the value is determined. Immediately after the end, food is provided for the animals.

5.4.2 Insulin tolerance test

Mice are maintained on a 12 hour light/dark cycle and the test is performed with animals fed *ad libitum*. For the insulin tolerance test a stock solution of 0,75 U insulin/ ml is prepared employing Huminsulin® Normal 40 (Lilly) dissolved in 0,9% sodium chloride. The body weight of all animals is determined initially and the blood glucose level is measured by nicking the tail with a razor blade. The blood drop is put onto a glucometer strip and measured.

Per mouse 1,5 U insulin/ kg body weight are injected intraperitoneally. The blood glucose level is monitored after 10, 20, 30, 60 and 120 minutes.

5.5 Generation and production of Adenoviruses

5.5.1 Cloning of adenoviruses

For the generation of adenoviruses, containing shRNA sequences against murine Hes-1 or against murine GR, the BLOCK-iT™ Adenoviral RNAi Expression System by Invitrogen was used. Suitable oligonucleotide sequences were chosen using Invitrogen's website tool BLOCK-iT™ RNAi Designer (<https://rnaidesigner.invitrogen.com/rnaiexpress/setOption.do?designOption=stealth>). Selected oligonucleotides are targeted against the murine Hes-1 sequence with the accession number NM_008235 and for GR accession number X04435. Oligonucleotides used to specifically target either GR or Hes-1 are listed in Table 15 and 16.

Table 15: shRNA sequences for RNA interference with murine Hes-1.

Hes 1		Oligonucleotide sequence	selection
shRNA	forward	CACCGGATGCACCTTAAGAAAGATAGCGAACTATCTTTCTTAAGTGCATCC	invitrogen
	reverse	AAAAAGGATGCACCTTAAGAAAGATAGTTCGCTATCTTTCTTAAGTGCATCC	
shRNA	forward	CACCGGAAATACCGCGCCGGCTTCA CGAA TGAAGCCGGCGCGGTATTTCC	invitrogen
	reverse	AAAAAGGAAATACCGCGCCGGCTTCA TTCG TGAAGCCGGCGCGGTATTTCC	
shRNA	forward	CACCGCGACACCGGACAAACCAACGAA TTTGGTTTGTCCGGTGTCTG	invitrogen
	reverse	AAAAAGCGACACCGGACAAACCAATTCG TTTGGTTTGTCCGGTGTCTG	
shRNA	forward	CACCGCACTGCATTTGTATATATTTCAAGAGAATATATACAAATGCAGTGC	promega
	reverse	AAAAAGCACTGCATTTGTATATATTTCTCTTGAAATATATACAAATGCAGTGC	
shRNA	forward	CACCGGATTGCGCCTTTGTATTATTCAAGAGATAATACAAAGGCGCAATCC	promega
	reverse	AAAAAGGATTGCGCCTTTGTATTATCTCTTGAAATATACAAAGGCGCAATCC	
shRNA	forward	CACCGCAGACATTCTGGAAATGATTCAAGAGATCATTTCCAGAATGTCTGC	promega
	reverse	AAAAAGCAGACATTCTGGAAATGATCTCTTGAAATCATTTCCAGAATGTCTGC	
shRNA	forward	CACCGGCCAATTTGCCTTTCTCATTTCAAGAGATGAGAAAGGCAAATTTGGCC	promega
	reverse	AAAAAGGCCAATTTGCCTTTCTCATCTCTTGAAATGAGAAAGGCAAATTTGGCC	

Indicated in red are the specific sequences targeting the murine Hes-1

Table 16: Oligonucleotides encoding for shRNAs targeting the murine GR

name		sequence	Selection
shRNA1	forward	CACCAGAAATGACTGCCTTACTATTCAAGAGATAGTAAGGCAGTCATTTCT	D. Habermehl
	reverse	AAAAAGAAATGACTGCCTTACTATTCAAGAGATAGTAAGGCAGTCATTTCT	
shRNA2	forward	CACCGGAGATACAATCTTATCAAGCCGAAGCTTGATAAGATTGTATCTCC	invitrogen
	reverse	AAAAGGAGATACAATCTTATCAAGCTTCGGCTTGATAAGATTGTATCTCC	
shRNA3	forward	CACCGGTGTTATATGCAGGATATGACGAATCATATCCTGCATATAACACC	invitrogen
	reverse	AAAAGGTGTTATATGCAGGATATGATTCGTCATATCCTGCATATAACACC	

Indicated in red are the specific sequences targeting the murine GR

The nucleotides were annealed and cloned into the pENTR™/U6 vector plasmid (Invitrogen) according to manufacturer's instructions. Positive clones were identified with as restriction enzyme analysis as such:

Subsequently, pENTR™/U6 constructs containing shRNA sequences were recombined with the vector plasmid pAd/BLOCK-iT™ Dest (Invitrogen). This vector contains the viral DNA sequence of adenovirus serotyp 5, whereas the genes E1 and E3 , that are important for replication of the virus, are deleted. At the 5'-end of the viral genome recombination sequences are included and at this site the pENTR™ vector recombines in such a way that the U6 promoter, the shRNA sequence and a PolIII termination signal are integrated into the newly formed plasmid. During recombination, a chloramphenicol resistance gene is excised and positive clones therefore are resistant against kanamycin but chloramphenicol sensitive.

With colony PCR positive clones are confirmed and subsequently they are propagated for preparation of plasmid DNA.

The viral vector is linearized by restriction with PacI and transfected into 239A cells using Lipofectamine according to manufacturer's instructions. 6 to 8 days after transfection viral plaques are visible on the cell monolayer and cells start to detach from the cell culture dish. If several plaques are identified, cells are harvested. In the first virus propagation after transfection, usually not all cells are transfected or subsequently infected by the virus. It is therefore advisable to harvest the virus ten to twelve days after transfection.

5.5.2 Virus harvest by Freeze-and-Thaw-Method

293A cells that have been transfected with plasmids containing viral DNA or infected with functional viruses are harvested, when cells start to detach from the cell culture dish. For this purpose, the cell culture medium, in which the cells were maintained during viral infection is

purpose, the cell culture medium, in which the cells were maintained during viral infection is used for washing cells from the plate to achieve high viral titers. Cell suspensions from up to 20 15cm plates are collected and the cells are pelleted for 10 min at 4000 rpm. The supernatant is discarded and the cell pellet is resuspended in 2 to 3 ml PBS-TOSH buffer and transferred to a 15 ml Falcon tube (only use polypropylene tubes!). The tubes are snap-frozen in liquid nitrogen for 2 min and then thawing is facilitated in a 37°C water bath. Thawing is accelerated by vigorous mixture of the suspension using a vortex. This step is crucial, since the ice crystals destroy the cell membranes thereby releasing the viruses. The Freeze-and-Thaw cycle is repeated three times. Subsequently, the cell lysate is centrifuged for 15 min at 4000 rpm and 4°C. The supernatant contains the virus particles and can be kept until cesium chloride purification at -80°C. The cell pellet is discarded.

The storage of virus-containing supernatants after Freeze-and-Thaw cycles at -80°C is not critical for the stability of the adenoviruses, probably because proteins in these solution contribute to viral stabilisation.

5.5.3 Virus production

For the production of adenoviruses for mouse experiments 40 to 80 cell culture dishes with a diameter of 15 cm are used. 239A cells are maintained in D-MEM medium containing 10% FCS; 1% non-essential amino acids and 1 x penicillin/ streptomycin until they reach a confluency of 70 to 80%.

After transfection of adenoviruses and the first virus harvest it is advisable to transfect a maximum of 10 15 cm plates with 10µl of crude virus lysate (obtained after Freeze-and-Thaw cycle). After three to four days cell detachment should be visible, otherwise, transfection should be repeated.

5.5.4 Cesium chloride gradient

Crude virus lysates are thawed on ice and the viral solution is diluted with PBS-TOSH buffer to a final volume of 18 ml. This solution should contain the virus of 20 plates.

Before the gradient is poured the pH of all solutions used should be adjusted to pH 7.2. 40 ml centrifuge tubes (Beckmann Polyallomer 25mm x 89 mm) are filled with 9 ml 4M cesium chloride and carefully covered by a second layer with 2,2M cesium chloride. Finally, the virus-containing solution should be added slowly to generate a third layer. In the end, three distinct layer should be distinguishable. Between each step gradient tubes should be weighed and balanced by adding the appropriate solution (different cesium chloride solutions have different density and therefore different masses). The virus is purified by ultracentrifugation (Beckmann

ultracentrifuge XL-70) for 2h with a swing bucket rotor (SW28 rotor) at 24000 rpm and 4°C. The virusband appears between the 4M and 2,2M cesium chloride layer and is removed by carefully plunging the tube with 2ml syringe equipped with a cannula (BD Microlance 3, 18G x 1 ½’’). The obtained virus band is diluted with the same volume of a saturated cesium chloride solution and transferred into a 12 ml centrifuge tube (Beckmann Polyallomer 14mm x 89 mm). The maximum volume should not exceed 7 ml. The solution is gently overlayed by 4M cesium chloride (2-3 ml). Subsequently, 2 to 3 ml 2,2M cesium chloride are added dropwise to result in third distinct layer and the step gradient is centrifuged for 3h at 35000 rpm and 4°C in a swing bucket rotor (SW41 Ti rotor). After the second purification step, a bluish-fluorescent band should appear between the 4M and 2,2M layers. The virus is isolated again by plunging the tube with a 18 gauge needle.

To remove the high salt concentration the virus is dialyzed three times against 1l PBS containing 10% glycerol (v/v) using a dialysis membrane with a 15 kDa cut-off (Spectra/Por® Biotech, MWCO 15’000, 10 mm diameter). The first two steps are done 1h each and the third dialysis is done overnight. The next day, the virus is transferred into a 2ml cryo-vial and aliquots for virus titration etc. are separately frozen to avoid repeated freezing and thawing.

5.5.5 Virus titration

Titration of adenoviruses is done using the Tissue Culture Infectious Dose₅₀ (TCID₅₀) Assay. For this purpose 293A cells are harvested and a cell suspension with a concentration of 10⁵ cells/ml is prepared in D-MEM medium containing 2% FCS (v/v) and 1-fold penicillin/streptomycin.

Cells are seeded into a 96-well plate with 100µl/well using a multistep pipet.

Virus dilutions from 10⁻² to 10⁻¹² are prepared in D-MEM medium with 2% FCS and penicillin/streptomycin and 100 µl of a certain virus dilution are added per well before the 293A cells are attached. Ten wells are used per virus dilution. Usually, the first concentration applied to the plate is 10⁻⁵. As a negative control 16 wells are treated with 100µl D-MEM medium (2%FCS, penicillin/streptomycin) only. Cells are incubated for 10 days at 37°C, 95% humidity and 5% CO₂. Each virus titration is done twice on 96-well plates.

Ten days after infection wells are examined for plaque formation microscopically. The virus titer is calculated using the formula

Titer $T_a = 10^{1+(s-0.5)}$ for 100µl; where s is the sum of all positive wells starting from the dilution 10⁻¹. Ten positive wells correspond the value of 1 for the individual virus dilution. To obtain the virus in ifu/ml T_a has to be multiplied with 10.

5.6 Buffers

PBS 10x:

30 mM KCl; 10 mM KH_2PO_4 ; 1,37 M NaCl; 90 mM Na_2HPO_4 ; pH-Wert 7,0

SDS-running buffer 10x:

1,92 M Glycin; 0,45% HCl; 30 mM SDS; 0,25 M Trizma Base

TBE 10x:

45 mM Borsäure; 10 mM EDTA; 45 mM Trizma Base

TBS 10x:

1,37 M NaCl; 200 mM Trizma Base

TE 10x:

1 mM EDTA; 10 mM TrisCl pH 7,5

transfer buffer 10x:

1,92 M Glycin; 0,25 M Trizma Base

HBSS:

5.3 mM KCl, 0.441 mM KH_2PO_4 , 4.17 mM NaHCO_3 , 138 mM NaCl, 0.338 mM Na_2HPO_4

protease inhibitor mix

0,05% Aprotinin; 1 mM DMSO; 0,05% Leupeptin; 50 mM PMSF; 50 mM NaF; in Ethanol

phosphatase inhibitors (100X)

200 mM imidazole, 100 mM NaF, 115 mM Na-molybdate, 100 mM Na –ortho-vanadate, 400 mM Na-tartrate,

6x Orange G Probenpuffer:

10 mM EDTA; 70% Glycerol; Orange G (1 Spatelspitze)

5.7 Plasmids

Table 17: Lists of plasmids used

Plasmid name	origin	purpose
pGVB mHes-1 LUC -467/+46 bp	R. Kageyama (135)	transfection
pGL2 mHes-1 LUC -194bp/+160bp	D. Ndiaye (209)	transfection
wt PKA	McKnight(210)	transfection
mut PKA	McKnight(210)	transfection
pCMV bGal	A.Vegiopoulos	transfection
GAL4DBD	M. Conkright	transfection
GAL4GR	M. Conkright	transfection
GAL4CREB	R.Screaton	transfection
pCMX VP16 CREB	Nicola Rieser (unpublished)	transfection
pCMX VP16 KID	R. Screaton	transfection
pCMX VP16 KIX	L.Canettieri	transfection
pCMX VP16 bZIP	L.Canettieri	transfection
pCMX VP16	R. Screaton	transfection
pENTR/U6	Invitrogen	generation of adenovirus
pAd BLOCK-iT/DEST	Invitrogen	generation of adenovirus

6 Appendix

6.1 Abbreviations

11 β HSD1	11- β -hydroxysteroid dehydrogenase
ABCD	avidin-biotin conjugated DNA
ACC1	acyl-CoA carboxylase 1
ADP	adenosine-nucleotide diphosphate
Angptl	angiopoietin-like
ATF1	activating transcription factor 1
ATP	adenosine nucleotide triphosphate
AUC	area under the curve
BSA	bovine serum albumin
cAMP	cyclic adenosine monophosphate
Cav1	caveolin
CBP	CREB binding protein
cDNA	complement desoxyribonucleic acid
ChIP	chromatin immunoprecipitation
CI	chloroform:isoamylalcohol
CMV	cytomegalovirus
CO ₂	carbon dioxide
CoA	coenzyme A
CPT1 α	carnitine palmitoyl transferase 1 α
CRE	cAMP response element
CREB	cAMP response element binding protein
CREM	cyclic AMP responsive element modulator
CT	computer tomography
DBD	DNA binding domain
DMA	dimethyladipimide
DMEM	Dulbecco's Modified Eagle Medium
dNTP	deoxyribonucleotide
DOI	diet-induced obesity
DTT	dithiothreitol
DUSP-1	Dual Specific Phosphatase
EDTA	ethylenediamine tetraacetic acid
EGTA	ethyleneglycol tetraacetic acid
FABP-1	fatty acid binding protein
FAS	fatty acid binding protein
FFA	free fatty acids
FKBP52	FK506 binding protein 52
FLAG	artificial peptide sequence used as protein tag
GC	glucocorticoids
GFP	green fluorescent protein
GK	glucokinase
GLUT2	glucose transporter 2
GLUT4	glucose transporter 4
Gly-Gly	glycylglycin
GR	glucocorticoid receptor
GR _{dim}	glucocorticoid receptor bearing a mutation in the DNA binding domain

GRE	glucocorticoid response element
GTT	glucose tolerance test
HAT	histone acetyltransferase
HBSS	HEPES buffered saline solution
HEK	human embryonic kidney
HEPES	(4-(2-hydroxyethyl)-1-piperazineethanesulfonic acid)
Hes-1	Hairy and Enhancer of Split 1
HFD	high fat diet
HRP	horse radish peroxidase
Hsp70	heat shock protein 70
Hsp90	heat shock protein 90
ifu	infective units
IGF-1	insulin-like growth factor 1
IgG	immunglobulin G
IRS	insulin receptor substrate
ITT	insulin tolerance test
KID	kinase inducible domain
KOH	potassium hydroxide
LBD	ligand binding domain
LB-medium	Luria Bertani medium
L-GRKO	liver-specific glucocorticoid receptor knockout
LPL	lipoprotein lipase
LUC	luciferase
MKP-1	mitogen activated protein kinase phosphatase 1
MOI	multiplicity of infection
MOPS	3-(N-morpholino)-propanesulfonic acid
MR	magnetic resonance
MTTP	microsomal triglyceride transfer protein
NAA	non-essential amino acids
NADH	nicotinamid adenosine dinucleotide, reduced form
NADPH	nicotinamid adenosine dinucleotide phosphate, reduced form
NAFLD	Non-Alcoholic Fatty Liver Disease
NASH	Non-Alcoholic Steatohepatitis
NEFA	non esterified fatty acids
NIDDM	Non-insulin dependent diabetes mellitus
NZB	New Zealand Black
NZO	New Zealand Obese
OD	optical density
ONPG	ortho-nitrophenyl- β -D-galactopyranosid
PBS	phosphate buffered saline
PCI	phenol:chloroform:isoamylalcohol
PCR	polymerase chain reaction
PDE	phosphodiesterase
PEPCK	phosphoenol-pyruvate carboxykinase
PGDH	phosphogluconat dehydrogenase
PI 3-K	phosphoinositide 3-kinases
PKA	protein kinase A
PKC	protein kinase C
PKI	protein kinase inhibitor
POD	peroxidase
PP1	protein phosphatase 1

PP2A	protein phosphatase 2A
PPAR	peroxisome proliferation-activating receptor
rpm	rounds per minute
RT-PCR	real time polymerase chain reaction
SCD1	stearoyl CoA desaturase 1
SDS	sodium dodecylsulfate
SDS-PAGE	sodium dodecylsulfate polyacrylamide gel electrophoresis
shRNA	short hairpin RNA
TBP	TATA box binding protein
TBS	Tris buffered saline
TGs	triglycerides
TRIS	tris(hydroxymethyl)aminomethane
UV	ultraviolet
VCP	Valosin-containing protein
VLDL	very-low density lipoprotein
wt	wildtype
w/v	weight per volume

6.2

Figures

Figure 1.1: Glucagon signaling and transcriptional activation of target genes.	17
Figure 1.2: Signal transduction in insulin action.....	20
Figure 3.1: Generation of an adenovirus constitutively expressing an shRNA sequence targeting the murine GR.	26
Figure 3.2: Analysis of shRNA-induced GR depletion in the murine liver.	28
Figure 3.3: Target gene analysis in wildtype mice after GR depletion.	30
Figure 3.4: Target gene analysis in db/db mice after GR depletion.	31
Figure 3.5: Hes-1 expression is up-regulated after GR knockdown.....	32
Figure 3.6: Starvation-induced fatty liver and hepatic Hes-1 expression.....	34
Figure 3.7: Hes-1 expression in db/db mice – a standard model of fatty liver.....	35
Figure 3.8: Hepatic Hes-1 expression in New Zealand Obese mice.	36
Figure 3.9: Hepatic Hes-1 levels diet-induced obesity.....	36
Figure 3.10: Serum glucocorticoid levels in different mouse models.	38
Figure 3.11 Glucocorticoid treatment leads to weight loss.	39
Figure 3.12: Chronically elevated glucocorticoid inhibit hepatic Hes-1 expression.....	42
Figure 3.13: The Glucocorticoid receptor is necessary for starvation induced Hes-1 down-regulation. ...	43
Figure 3.14: Adenoviral vector encoding rat Hes-1.	44
Figure 3.15: Transient Hes-1 expression in C57Bl/6J mice.....	46
Figure 3.16: Transient Hes-1 expression in db/db mice improves the metabolic phenotype.....	49
Figure 3.17: Evaluation of Hes-1 expression in C57BL/6J mice after three weeks dexamethasone treatment.	53

Figure 3.18: Rescue of hepatic Hes-1 after glucocorticoid treatment prevents fat accumulation in the liver.....	53
Figure 3.19: Transient Hes-1 knock down using adenoviruses.....	54
Figure 3.20: De-regulation of Hes-1 expression in response to adenoviral injection.	55
Figure 3.21: Hes-1 is depleted in primary hepatocytes.	56
Figure 3.22: PPAR γ and Cav1 are up-regulated after Hes-1 depletion in primary hepatocytes.	56
Figure 3.23: Glucocorticoids inhibit Hes-1 expression in vitro by dephosphorylation of CREB.	59
Figure 3.24: Promoter Analysis of proximal Hes-1 promoter region (-440bp to -4bp).	60
Figure 3.25: The glucocorticoid associates <i>in vivo</i> with the Hes-1 promoter.	62
Figure 3.26: The GR occupies to binding sites on the Hes-1 promoter.	62
Figure 3.27: MKP-1 mice are protected against GC-induced glucose in tolerance.	64
Figure 3.28: In MKP-1 $-/-$ mice improved glucose tolerance does not depend on Hes-1.	66
Figure 3.29: Domain structure of CREB and CBP.....	67
Figure 3.30: The VP16 does not interact with either GAL4DBD or GAL4GR.	68
Figure 3.31: GR interacts via the bZIP domain with CREB.	69
Figure 3.32: Glucocorticoids inhibit CREB activity under basal and activated conditions.	71
Figure 3.33: p300 abolishes GC-dependent inhibition of CREB activity.	72
Figure 3.34: Glucocorticoid treatment leads to disruption of P-CREB/p300 transactivation complex on the <i>Hes-1</i> promoter.	73
Figure 4.1: Glucocorticoid mediated repression of Hes-1 transcription.	82

6.3 Tables

Table 1: Serum lipid parameters 13 days after Dexamethasone injection.....	39
Table 2: Organ weight parameters and blood glucose in dexamethasone injected C57BL/6J mice	40
Table 3: Lipid parameters at day of sacrifice.	41
Table 4: Body weight and blood glucose parameters of L-GRKO mice.....	43
Table 5: Body weight and blood glucose at start and end of experiment.....	45
Table 6: Body weight and blood glucose parameters at day of sacrifice	47
Table 7: Gene expression data from db/db mice treated with Hes-1 virus or control	50
Table 8: Weight parameters at day of sacrifice	65
Table 9: Taqman® probes used for qPCR experiments	89
Table 10: Composition of polyacrylamide gels with different concentration of acrylamide	95
Table 11: Primary and secondary antibodies for immunoblot	96
Table 12: Oligonucleotide sequences used in the ABCD assay with the glucocorticoid receptor	101
Table 13: Antibodies used for ChIP assay	104
Table 14: Specific primers used for the evaluation of ChIP experiments	105
Table 15: shRNA sequences for RNA interference with murine Hes-1.....	107

Table 16: Oligonucleotides encoding for shRNAs targeting the murine GR.....	108
Table 17: Lists of plasmids used	112

7 Bibliography

1. Unger, R.H., and Orci, L. 2001. Diseases of liporegulation: new perspective on obesity and related disorders. *Faseb J* 15:312-321.
2. Mokdad, A.H., Marks, J.S., Stroup, D.F., and Gerberding, J.L. 2004. Actual causes of death in the United States, 2000. *Jama* 291:1238-1245.
3. Fagot-Campagna, A., Pettitt, D.J., Engelgau, M.M., Burrows, N.R., Geiss, L.S., Valdez, R., Beckles, G.L., Saaddine, J., Gregg, E.W., Williamson, D.F., et al. 2000. Type 2 diabetes among North American children and adolescents: an epidemiologic review and a public health perspective. *J Pediatr* 136:664-672.
4. Petrie, J.R., Cleland, S.J., and Small, M. 1998. The metabolic syndrome: overeating, inactivity, poor compliance or 'dud' advice? *Diabet Med* 15 Suppl 3:S29-31.
5. Pinhas-Hamiel, O., Dolan, L.M., Daniels, S.R., Standiford, D., Khoury, P.R., and Zeitler, P. 1996. Increased incidence of non-insulin-dependent diabetes mellitus among adolescents. *J Pediatr* 128:608-615.
6. Canbay, A., Bechmann, L., and Gerken, G. 2007. Lipid metabolism in the liver. *Z Gastroenterol* 45:35-41.
7. Holloszy, J.O., and Kohrt, W.M. 1996. Regulation of carbohydrate and fat metabolism during and after exercise. *Annu Rev Nutr* 16:121-138.
8. Weigand, K., and Alpert, E. 1981. Human albumin synthesis via an albumin precursor in liver tissue slices. *Experientia* 37:1145-1147.
9. Weinhouse, S. 1952. Factors involved in the formation and utilization of ketone bodies. *Brookhaven Symp Biol* 5:201-216; discussion, 216-221.
10. Booth, R., Gregory, K.W., Malone, E.M., and Robertson, I. 1971. The effect of dietary cholesterol on cholesterol biosynthesis and other processes in mammalian liver. *Biochem J* 122:25P-26P.
11. McCuskey, R.S., McCuskey, P.A., Urbaschek, R., and Urbaschek, B. 1987. Kupffer cell function in host defense. *Rev Infect Dis* 9 Suppl 5:S616-619.
12. McCuskey, R.S., Urbaschek, R., McCuskey, P.A., Sacco, N., Stauber, W.T., Pinkstaff, C.A., and Urbaschek, B. 1984. Deficient Kupffer cell phagocytosis and lysosomal enzymes in the endotoxin-low-responsive C3H/HeJ mouse. *J Leukoc Biol* 36:591-600.
13. Consoli, A. 1992. Role of liver in pathophysiology of NIDDM. *Diabetes Care* 15:430-441.
14. Shulman, G.I. 2000. Cellular mechanisms of insulin resistance. *J Clin Invest* 106:171-176.
15. Kahn, A. 1997. Transcriptional regulation by glucose in the liver. *Biochimie* 79:113-118.
16. Saltiel, A.R., and Kahn, C.R. 2001. Insulin signalling and the regulation of glucose and lipid metabolism. *Nature* 414:799-806.
17. Miles, J.M., and Jensen, M.D. 1993. Does glucagon regulate adipose tissue lipolysis? *J Clin Endocrinol Metab* 77:5A-5B.
18. Siddle, K., and Hales, C.N. 1975. Hormonal control of adipose tissue lipolysis. *Proc Nutr Soc* 34:233-239.
19. Hales, C.N., Luzio, J.P., and Siddle, K. 1978. Hormonal control of adipose-tissue lipolysis. *Biochem Soc Symp* 97-135.
20. Kawai, A., and Kuzuya, N. 1981. Effects of glucocorticoids on hormone-stimulated lipolysis and calcium uptake in the adipose cells. *Horm Metab Res* 13:224-228.
21. Divakaran, P., and Friedmann, N. 1976. A fast in vitro effect of glucocorticoids on hepatic lipolysis. *Endocrinology* 98:1550-1553.

22. Desvergne, B., Michalik, L., and Wahli, W. 2006. Transcriptional regulation of metabolism. *Physiol Rev* 86:465-514.
23. Kornberg, R.D., and Lorch, Y. 1999. Twenty-five years of the nucleosome, fundamental particle of the eukaryote chromosome. *Cell* 98:285-294.
24. Hayashi, R., Wada, H., Ito, K., and Adcock, I.M. 2004. Effects of glucocorticoids on gene transcription. *Eur J Pharmacol* 500:51-62.
25. Urnov, F.D., and Wolffe, A.P. 2001. Chromatin remodeling and transcriptional activation: the cast (in order of appearance). *Oncogene* 20:2991-3006.
26. Zlatanova, J., Leuba, S.H., Yang, G., Bustamante, C., and van Holde, K. 1994. Linker DNA accessibility in chromatin fibers of different conformations: a reevaluation. *Proc Natl Acad Sci U S A* 91:5277-5280.
27. Janknecht, R., and Hunter, T. 1996. Versatile molecular glue. Transcriptional control. *Curr Biol* 6:951-954.
28. Collingwood, T.N., Urnov, F.D., and Wolffe, A.P. 1999. Nuclear receptors: coactivators, corepressors and chromatin remodeling in the control of transcription. *J Mol Endocrinol* 23:255-275.
29. de Ruijter, A.J., van Gennip, A.H., Caron, H.N., Kemp, S., and van Kuilenburg, A.B. 2003. Histone deacetylases (HDACs): characterization of the classical HDAC family. *Biochem J* 370:737-749.
30. Foretz, M., Pacot, C., Dugail, I., Lemarchand, P., Guichard, C., Le Liepvre, X., Berthelie-Lubrano, C., Spiegelman, B., Kim, J.B., Ferre, P., et al. 1999. ADD1/SREBP-1c is required in the activation of hepatic lipogenic gene expression by glucose. *Mol Cell Biol* 19:3760-3768.
31. Foretz, M., Guichard, C., Ferre, P., and Foufelle, F. 1999. Sterol regulatory element binding protein-1c is a major mediator of insulin action on the hepatic expression of glucokinase and lipogenesis-related genes. *Proc Natl Acad Sci U S A* 96:12737-12742.
32. Shimomura, I., Matsuda, M., Hammer, R.E., Bashmakov, Y., Brown, M.S., and Goldstein, J.L. 2000. Decreased IRS-2 and increased SREBP-1c lead to mixed insulin resistance and sensitivity in livers of lipodystrophic and ob/ob mice. *Mol Cell* 6:77-86.
33. Magana, M.M., Lin, S.S., Dooley, K.A., and Osborne, T.F. 1997. Sterol regulation of acetyl coenzyme A carboxylase promoter requires two interdependent binding sites for sterol regulatory element binding proteins. *J Lipid Res* 38:1630-1638.
34. Kingsley-Kallesen, M., Mukhopadhyay, S.S., Wyszomierski, S.L., Schanler, S., Schutz, G., and Rosen, J.M. 2002. The mineralocorticoid receptor may compensate for the loss of the glucocorticoid receptor at specific stages of mammary gland development. *Mol Endocrinol* 16:2008-2018.
35. Aranda, A., and Pascual, A. 2001. Nuclear hormone receptors and gene expression. *Physiol Rev* 81:1269-1304.
36. Yudt, M.R., and Cidlowski, J.A. 2001. Molecular identification and characterization of a and b forms of the glucocorticoid receptor. *Mol Endocrinol* 15:1093-1103.
37. Oakley, R.H., Jewell, C.M., Yudt, M.R., Bofetiado, D.M., and Cidlowski, J.A. 1999. The dominant negative activity of the human glucocorticoid receptor beta isoform. Specificity and mechanisms of action. *J Biol Chem* 274:27857-27866.
38. Yudt, M.R., Jewell, C.M., Bienstock, R.J., and Cidlowski, J.A. 2003. Molecular origins for the dominant negative function of human glucocorticoid receptor beta. *Mol Cell Biol* 23:4319-4330.
39. Pratt, W.B., Morishima, Y., Murphy, M., and Harrell, M. 2006. Chaperoning of glucocorticoid receptors. *Handb Exp Pharmacol*:111-138.
40. Beato, M. 1989. Gene regulation by steroid hormones. *Cell* 56:335-344.
41. Beato, M., Chalepakis, G., Schauer, M., and Slater, E.P. 1989. DNA regulatory elements for steroid hormones. *J Steroid Biochem* 32:737-747.

42. Schaaf, M.J., and Cidlowski, J.A. 2002. Molecular mechanisms of glucocorticoid action and resistance. *J Steroid Biochem Mol Biol* 83:37-48.
43. Konig, H., Ponta, H., Rahmsdorf, H.J., and Herrlich, P. 1992. Interference between pathway-specific transcription factors: glucocorticoids antagonize phorbol ester-induced AP-1 activity without altering AP-1 site occupation in vivo. *Embo J* 11:2241-2246.
44. Cole, T.J., Blendy, J.A., Monaghan, A.P., Krieglstein, K., Schmid, W., Aguzzi, A., Fantuzzi, G., Hummler, E., Unsicker, K., and Schutz, G. 1995. Targeted disruption of the glucocorticoid receptor gene blocks adrenergic chromaffin cell development and severely retards lung maturation. *Genes Dev* 9:1608-1621.
45. Reichardt, H.M., Kaestner, K.H., Tuckermann, J., Kretz, O., Wessely, O., Bock, R., Gass, P., Schmid, W., Herrlich, P., Angel, P., et al. 1998. DNA binding of the glucocorticoid receptor is not essential for survival. *Cell* 93:531-541.
46. Scott, D.K., Stromstedt, P.E., Wang, J.C., and Granner, D.K. 1998. Further characterization of the glucocorticoid response unit in the phosphoenolpyruvate carboxykinase gene. The role of the glucocorticoid receptor-binding sites. *Mol Endocrinol* 12:482-491.
47. Wang, J.C., Stromstedt, P.E., Sugiyama, T., and Granner, D.K. 1999. The phosphoenolpyruvate carboxykinase gene glucocorticoid response unit: identification of the functional domains of accessory factors HNF3 beta (hepatic nuclear factor-3 beta) and HNF4 and the necessity of proper alignment of their cognate binding sites. *Mol Endocrinol* 13:604-618.
48. Stafford, J.M., Waltner-Law, M., and Granner, D.K. 2001. Role of accessory factors and steroid receptor coactivator 1 in the regulation of phosphoenolpyruvate carboxykinase gene transcription by glucocorticoids. *J Biol Chem* 276:3811-3819.
49. Stafford, J.M., Wilkinson, J.C., Beechem, J.M., and Granner, D.K. 2001. Accessory factors facilitate the binding of glucocorticoid receptor to the phosphoenolpyruvate carboxykinase gene promoter. *J Biol Chem* 276:39885-39891.
50. Schoneveld, O.J., Gaemers, I.C., and Lamers, W.H. 2004. Mechanisms of glucocorticoid signalling. *Biochim Biophys Acta* 1680:114-128.
51. Schoneveld, O.J., Hoogenkamp, M., Stallen, J.M., Gaemers, I.C., and Lamers, W.H. 2007. cyclicAMP and glucocorticoid responsiveness of the rat carbamoylphosphate synthetase gene requires the interplay of upstream regulatory units. *Biochimie* 89:574-580.
52. Patti, M.E., and Kahn, C.R. 1998. The insulin receptor--a critical link in glucose homeostasis and insulin action. *J Basic Clin Physiol Pharmacol* 9:89-109.
53. Araki, E., Lipes, M.A., Patti, M.E., Bruning, J.C., Haag, B., 3rd, Johnson, R.S., and Kahn, C.R. 1994. Alternative pathway of insulin signalling in mice with targeted disruption of the IRS-1 gene. *Nature* 372:186-190.
54. White, M.F. 1998. The IRS-signalling system: a network of docking proteins that mediate insulin action. *Mol Cell Biochem* 182:3-11.
55. White, M.F. 1996. The IRS-signalling system in insulin and cytokine action. *Philos Trans R Soc Lond B Biol Sci* 351:181-189.
56. Pessin, J.E., and Saltiel, A.R. 2000. Signaling pathways in insulin action: molecular targets of insulin resistance. *J Clin Invest* 106:165-169.
57. Shepherd, P.R., Nave, B.T., and Siddle, K. 1995. Insulin activates glycogen synthase by a novel PI 3-kinase/p70s6k dependent pathway in 3T3-L1 adipocytes. *Biochem Soc Trans* 23:202S.
58. Shepherd, P.R., Nave, B.T., and Siddle, K. 1995. Involvement of PI 3-kinase in stimulation of glucose transport and recruitment of transferrin receptors in 3T3-L1 adipocytes. *Biochem Soc Trans* 23:201S.

59. Haigh, R.J., Shepherd, P.R., Nave, B.T., and Siddle, K. 1995. The role of phosphatidylinositol 3-kinase activity in insulin-stimulated mitogenesis in 3T3-L1 adipocytes. *Biochem Soc Trans* 23:179S.
60. Alessi, D.R., Deak, M., Casamayor, A., Caudwell, F.B., Morrice, N., Norman, D.G., Gaffney, P., Reese, C.B., MacDougall, C.N., Harbison, D., et al. 1997. 3-Phosphoinositide-dependent protein kinase-1 (PDK1): structural and functional homology with the *Drosophila* DSTPK61 kinase. *Curr Biol* 7:776-789.
61. O'Brien, R.M., and Granner, D.K. 1996. Regulation of gene expression by insulin. *Physiol Rev* 76:1109-1161.
62. O'Brien, R.M., Streeper, R.S., Ayala, J.E., Stadelmaier, B.T., and Hornbuckle, L.A. 2001. Insulin-regulated gene expression. *Biochem Soc Trans* 29:552-558.
63. Matsuzaki, H., Daitoku, H., Hatta, M., Tanaka, K., and Fukamizu, A. 2003. Insulin-induced phosphorylation of FKHR (Foxo1) targets to proteasomal degradation. *Proc Natl Acad Sci U S A* 100:11285-11290.
64. Tran, H., Brunet, A., Griffith, E.C., and Greenberg, M.E. 2003. The many forks in FOXO's road. *Sci STKE* 2003:RE5.
65. Nakae, J., Kitamura, T., Ogawa, W., Kasuga, M., and Accili, D. 2001. Insulin regulation of gene expression through the forkhead transcription factor Foxo1 (Fkhr) requires kinases distinct from Akt. *Biochemistry* 40:11768-11776.
66. Nakae, J., Park, B.C., and Accili, D. 1999. Insulin stimulates phosphorylation of the forkhead transcription factor FKHR on serine 253 through a Wortmannin-sensitive pathway. *J Biol Chem* 274:15982-15985.
67. Shimabukuro, M., Zhou, Y.T., Levi, M., and Unger, R.H. 1998. Fatty acid-induced beta cell apoptosis: a link between obesity and diabetes. *Proc Natl Acad Sci U S A* 95:2498-2502.
68. Shimabukuro, M., Ohneda, M., Lee, Y., and Unger, R.H. 1997. Role of nitric oxide in obesity-induced beta cell disease. *J Clin Invest* 100:290-295.
69. Lipton, S.A., Choi, Y.B., Pan, Z.H., Lei, S.Z., Chen, H.S., Sucher, N.J., Loscalzo, J., Singel, D.J., and Stamler, J.S. 1993. A redox-based mechanism for the neuroprotective and neurodestructive effects of nitric oxide and related nitroso-compounds. *Nature* 364:626-632.
70. Chiu, H.C., Kovacs, A., Ford, D.A., Hsu, F.F., Garcia, R., Herrero, P., Saffitz, J.E., and Schaffer, J.E. 2001. A novel mouse model of lipotoxic cardiomyopathy. *J Clin Invest* 107:813-822.
71. Zhou, Y.T., Grayburn, P., Karim, A., Shimabukuro, M., Higa, M., Baetens, D., Orci, L., and Unger, R.H. 2000. Lipotoxic heart disease in obese rats: implications for human obesity. *Proc Natl Acad Sci U S A* 97:1784-1789.
72. Hotamisligil, G.S., Shargill, N.S., and Spiegelman, B.M. 1993. Adipose expression of tumor necrosis factor-alpha: direct role in obesity-linked insulin resistance. *Science* 259:87-91.
73. Shoelson, S.E., Lee, J., and Goldfine, A.B. 2006. Inflammation and insulin resistance. *J Clin Invest* 116:1793-1801.
74. Yuan, M., Konstantopoulos, N., Lee, J., Hansen, L., Li, Z.W., Karin, M., and Shoelson, S.E. 2001. Reversal of obesity- and diet-induced insulin resistance with salicylates or targeted disruption of Ikkbeta. *Science* 293:1673-1677.
75. Tuncman, G., Hirosumi, J., Solinas, G., Chang, L., Karin, M., and Hotamisligil, G.S. 2006. Functional in vivo interactions between JNK1 and JNK2 isoforms in obesity and insulin resistance. *Proc Natl Acad Sci U S A* 103:10741-10746.
76. Hirosumi, J., Tuncman, G., Chang, L., Gorgun, C.Z., Uysal, K.T., Maeda, K., Karin, M., and Hotamisligil, G.S. 2002. A central role for JNK in obesity and insulin resistance. *Nature* 420:333-336.

77. Shi, H., Kokoeva, M.V., Inouye, K., Tzameli, I., Yin, H., and Flier, J.S. 2006. TLR4 links innate immunity and fatty acid-induced insulin resistance. *J Clin Invest* 116:3015-3025.
78. Angulo, P. 2007. GI epidemiology: nonalcoholic fatty liver disease. *Aliment Pharmacol Ther* 25:883-889.
79. Powell, E.E., Jonsson, J.R., and Clouston, A.D. 2005. Steatosis: co-factor in other liver diseases. *Hepatology* 42:5-13.
80. Adams, L.A., Lymp, J.F., St Sauver, J., Sanderson, S.O., Lindor, K.D., Feldstein, A., and Angulo, P. 2005. The natural history of nonalcoholic fatty liver disease: a population-based cohort study. *Gastroenterology* 129:113-121.
81. Marchesini, G., Brizi, M., Bianchi, G., Tomassetti, S., Bugianesi, E., Lenzi, M., McCullough, A.J., Natale, S., Forlani, G., and Melchionda, N. 2001. Nonalcoholic fatty liver disease: a feature of the metabolic syndrome. *Diabetes* 50:1844-1850.
82. Jacobson, P.B., von Geldern, T.W., Ohman, L., Osterland, M., Wang, J., Zinker, B., Wilcox, D., Nguyen, P.T., Mika, A., Fung, S., et al. 2005. Hepatic glucocorticoid receptor antagonism is sufficient to reduce elevated hepatic glucose output and improve glucose control in animal models of type 2 diabetes. *J Pharmacol Exp Ther* 314:191-200.
83. Liang, Y., Osborne, M.C., Monia, B.P., Bhanot, S., Watts, L.M., She, P., DeCarlo, S.O., Chen, X., and Demarest, K. 2005. Antisense oligonucleotides targeted against glucocorticoid receptor reduce hepatic glucose production and ameliorate hyperglycemia in diabetic mice. *Metabolism* 54:848-855.
84. Liu, Y., Nakagawa, Y., Wang, Y., Sakurai, R., Tripathi, P.V., Lutfy, K., and Friedman, T.C. 2005. Increased glucocorticoid receptor and 11 β -hydroxysteroid dehydrogenase type 1 expression in hepatocytes may contribute to the phenotype of type 2 diabetes in db/db mice. *Diabetes* 54:32-40.
85. Jenson, M., Kilroy, G., York, D.A., and Braymer, D. 1996. Abnormal regulation of hepatic glucocorticoid receptor mRNA and receptor protein distribution in the obese Zucker rat. *Obes Res* 4:133-143.
86. Cole, T.G., Wilcox, H.G., and Heimberg, M. 1982. Effects of adrenalectomy and dexamethasone on hepatic lipid metabolism. *J Lipid Res* 23:81-91.
87. Tomlinson, J.W., Walker, E.A., Bujalska, I.J., Draper, N., Lavery, G.G., Cooper, M.S., Hewison, M., and Stewart, P.M. 2004. 11 β -hydroxysteroid dehydrogenase type 1: a tissue-specific regulator of glucocorticoid response. *Endocr Rev* 25:831-866.
88. Holmes, M.C., Kotelevtsev, Y., Mullins, J.J., and Seckl, J.R. 2001. Phenotypic analysis of mice bearing targeted deletions of 11 β -hydroxysteroid dehydrogenases 1 and 2 genes. *Mol Cell Endocrinol* 171:15-20.
89. Paterson, J.M., Morton, N.M., Fievet, C., Kenyon, C.J., Holmes, M.C., Staels, B., Seckl, J.R., and Mullins, J.J. 2004. Metabolic syndrome without obesity: Hepatic overexpression of 11 β -hydroxysteroid dehydrogenase type 1 in transgenic mice. *Proc Natl Acad Sci U S A* 101:7088-7093.
90. Letteron, P., Brahimi-Bourouina, N., Robin, M.A., Moreau, A., Feldmann, G., and Pessayre, D. 1997. Glucocorticoids inhibit mitochondrial matrix acyl-CoA dehydrogenases and fatty acid beta-oxidation. *Am J Physiol* 272:G1141-1150.
91. Nagao, M., Parimoo, B., and Tanaka, K. 1993. Developmental, nutritional, and hormonal regulation of tissue-specific expression of the genes encoding various acyl-CoA dehydrogenases and alpha-subunit of electron transfer flavoprotein in rat. *J Biol Chem* 268:24114-24124.
92. Bjorntorp, P. 1991. Adipose tissue distribution and function. *Int J Obes* 15 Suppl 2:67-81.

93. Rebrin, K., Steil, G.M., Mittelman, S.D., and Bergman, R.N. 1996. Causal linkage between insulin suppression of lipolysis and suppression of liver glucose output in dogs. *J Clin Invest* 98:741-749.
94. Mittelman, S.D., and Bergman, R.N. 2000. Inhibition of lipolysis causes suppression of endogenous glucose production independent of changes in insulin. *Am J Physiol Endocrinol Metab* 279:E630-637.
95. Bostrom, K., Boren, J., Wettesten, M., Sjoberg, A., Bondjers, G., Wiklund, O., Carlsson, P., and Olofsson, S.O. 1988. Studies on the assembly of apo B-100-containing lipoproteins in HepG2 cells. *J Biol Chem* 263:4434-4442.
96. Vegiopoulos, A., and Herzig, S. 2007. Glucocorticoids, metabolism and metabolic diseases. *Mol Cell Endocrinol* 275:43-61.
97. Tronche, F., Opherck, C., Moriggl, R., Kellendonk, C., Reimann, A., Schwake, L., Reichardt, H.M., Stangl, K., Gau, D., Hoeflich, A., et al. 2004. Glucocorticoid receptor function in hepatocytes is essential to promote postnatal body growth. *Genes Dev* 18:492-497.
98. Opherck, C., Tronche, F., Kellendonk, C., Kohlmuller, D., Schulze, A., Schmid, W., and Schutz, G. 2004. Inactivation of the glucocorticoid receptor in hepatocytes leads to fasting hypoglycemia and ameliorates hyperglycemia in streptozotocin-induced diabetes mellitus. *Mol Endocrinol* 18:1346-1353.
99. Danielsen, M., Northrop, J.P., and Ringold, G.M. 1986. The mouse glucocorticoid receptor: mapping of functional domains by cloning, sequencing and expression of wild-type and mutant receptor proteins. *Embo J* 5:2513-2522.
100. Hammond, S.M., Bernstein, E., Beach, D., and Hannon, G.J. 2000. An RNA-directed nuclease mediates post-transcriptional gene silencing in Drosophila cells. *Nature* 404:293-296.
101. Schwarz, D.S., Hutvagner, G., Du, T., Xu, Z., Aronin, N., and Zamore, P.D. 2003. Asymmetry in the assembly of the RNAi enzyme complex. *Cell* 115:199-208.
102. Finn, P.F., and Dice, J.F. 2006. Proteolytic and lipolytic responses to starvation. *Nutrition* 22:830-844.
103. Birnbaum, M.J. 2003. Lipolysis: more than just a lipase. *J Cell Biol* 161:1011-1012.
104. Yasuhara, M., Ohama, T., Matsuki, N., Saito, H., Shiga, J., Inoue, K., Kurokawa, K., and Teramoto, T. 1991. Induction of fatty liver by fasting in suncus. *J Lipid Res* 32:887-891.
105. Ohama, T., Matsuki, N., Saito, H., Tsukamoto, K., Kinoshita, M., Katsuragawa, K., Okazaki, S., Yamanaka, M., and Teramoto, T. 1994. Effect of starving and refeeding on lipid metabolism in suncus. *J Biochem (Tokyo)* 115:190-193.
106. Angulo, P. 2007. Obesity and nonalcoholic fatty liver disease. *Nutr Rev* 65:S57-63.
107. Fei, H., Okano, H.J., Li, C., Lee, G.H., Zhao, C., Darnell, R., and Friedman, J.M. 1997. Anatomic localization of alternatively spliced leptin receptors (Ob-R) in mouse brain and other tissues. *Proc Natl Acad Sci U S A* 94:7001-7005.
108. Friedman, J.M. 1997. The alphabet of weight control. *Nature* 385:119-120.
109. Anstee, Q.M., and Goldin, R.D. 2006. Mouse models in non-alcoholic fatty liver disease and steatohepatitis research. *Int J Exp Pathol* 87:1-16.
110. Dallman, M.F., Strack, A.M., Akana, S.F., Bradbury, M.J., Hanson, E.S., Scribner, K.A., and Smith, M. 1993. Feast and famine: critical role of glucocorticoids with insulin in daily energy flow. *Front Neuroendocrinol* 14:303-347.
111. Fujimoto, K., Koishi, R., Shimizugawa, T., and Ando, Y. 2006. Angptl3-null mice show low plasma lipid concentrations by enhanced lipoprotein lipase activity. *Exp Anim* 55:27-34.
112. Herzig, S., Hedrick, S., Morantte, I., Koo, S.H., Galimi, F., and Montminy, M. 2003. CREB controls hepatic lipid metabolism through nuclear hormone receptor PPAR-gamma. *Nature* 426:190-193.

113. Leiter, E.H., Reifsnyder, P.C., Flurkey, K., Partke, H.J., Junger, E., and Herberg, L. 1998. NIDDM genes in mice: deleterious synergism by both parental genomes contributes to diabetogenic thresholds. *Diabetes* 47:1287-1295.
114. Leiter, E.H., and Reifsnyder, P.C. 2004. Differential levels of diabetogenic stress in two new mouse models of obesity and type 2 diabetes. *Diabetes* 53 Suppl 1:S4-11.
115. Reifsnyder, P.C., Churchill, G., and Leiter, E.H. 2000. Maternal environment and genotype interact to establish diabetes in mice. *Genome Res* 10:1568-1578.
116. Subrahmanyam, K. 1960. Metabolism in the New Zealand strain of obese mice. *Biochem J* 76:548-556.
117. Coenen, K.R., and Hasty, A.H. 2007. Obesity Potentiates Development of Fatty Liver and Insulin Resistance, but Not Atherosclerosis in High Fat Diet-Fed Agouti LDLR Deficient Mice. *Am J Physiol Endocrinol Metab*.
118. Alberts, P., Ronquist-Nii, Y., Larsson, C., Klingstrom, G., Engblom, L., Edling, N., Lidell, V., Berg, I., Edlund, P.O., Ashkzari, M., et al. 2005. Effect of high-fat diet on KKAY and ob/ob mouse liver and adipose tissue corticosterone and 11-dehydrocorticosterone concentrations. *Horm Metab Res* 37:402-407.
119. Legendre, A., and Harris, R.B. 2006. Exaggerated response to mild stress in rats fed high-fat diet. *Am J Physiol Regul Integr Comp Physiol* 291:R1288-1294.
120. Bernal-Mizrachi, C., Weng, S., Feng, C., Finck, B.N., Knutsen, R.H., Leone, T.C., Coleman, T., Mecham, R.P., Kelly, D.P., and Semenkovich, C.F. 2003. Dexamethasone induction of hypertension and diabetes is PPAR-alpha dependent in LDL receptor-null mice. *Nat Med* 9:1069-1075.
121. Andrews, R.C., and Walker, B.R. 1999. Glucocorticoids and insulin resistance: old hormones, new targets. *Clin Sci (Lond)* 96:513-523.
122. Askari, H., Liu, J., and Dagogo-Jack, S. 2005. Energy adaptation to glucocorticoid-induced hyperleptinemia in human beings. *Metabolism* 54:876-880.
123. Tung, Y.L., Hewson, A.K., and Dickson, S.L. 2004. Glucocorticoid-dependent stimulation of adiposity and appetite by a ghrelin mimetic in the rat. *Eur J Endocrinol* 150:905-911.
124. Gura, T. 2001. Obesity research. Pot-bellied mice point to obesity enzyme. *Science* 294:2071-2072.
125. Masuzaki, H., Paterson, J., Shinyama, H., Morton, N.M., Mullins, J.J., Seckl, J.R., and Flier, J.S. 2001. A transgenic model of visceral obesity and the metabolic syndrome. *Science* 294:2166-2170.
126. Kageyama, R., Ohtsuka, T., and Kobayashi, T. 2007. The Hes gene family: repressors and oscillators that orchestrate embryogenesis. *Development* 134:1243-1251.
127. Sahai, A., Malladi, P., Pan, X., Paul, R., Melin-Aldana, H., Green, R.M., and Whittington, P.F. 2004. Obese and diabetic db/db mice develop marked liver fibrosis in a model of nonalcoholic steatohepatitis: role of short-form leptin receptors and osteopontin. *Am J Physiol Gastrointest Liver Physiol* 287:G1035-1043.
128. Olsson, B., Bohlooly, Y.M., Fitzgerald, S.M., Frick, F., Ljungberg, A., Ahren, B., Tornell, J., Bergstrom, G., and Oscarsson, J. 2005. Bovine growth hormone transgenic mice are resistant to diet-induced obesity but develop hyperphagia, dyslipidemia, and diabetes on a high-fat diet. *Endocrinology* 146:920-930.
129. Ntambi, J.M., Miyazaki, M., and Dobrzyn, A. 2004. Regulation of stearoyl-CoA desaturase expression. *Lipids* 39:1061-1065.
130. Ntambi, J.M. 1999. Regulation of stearoyl-CoA desaturase by polyunsaturated fatty acids and cholesterol. *J Lipid Res* 40:1549-1558.
131. Walker, J.E., and Gordon, E.R. 1970. Biochemical aspects associated with an ethanol-induced fatty liver. *Biochem J* 119:511-516.

132. Kusunoki, M., Tsutsumi, K., Hara, T., Ogawa, H., Nakamura, T., Miyata, T., Sakakibara, F., Fukuzawa, Y., Suga, T., Kakumu, S., et al. 2002. Correlation between lipid and glycogen contents in liver and insulin resistance in high-fat-fed rats treated with the lipoprotein lipase activator NO-1886. *Metabolism* 51:792-795.
133. Iso, T., Kedes, L., and Hamamori, Y. 2003. HES and HERP families: multiple effectors of the Notch signaling pathway. *J Cell Physiol* 194:237-255.
134. Insel, P.A., and Ostrom, R.S. 2003. Forskolin as a tool for examining adenylyl cyclase expression, regulation, and G protein signaling. *Cell Mol Neurobiol* 23:305-314.
135. Takebayashi, K., Sasai, Y., Sakai, Y., Watanabe, T., Nakanishi, S., and Kageyama, R. 1994. Structure, chromosomal locus, and promoter analysis of the gene encoding the mouse helix-loop-helix factor HES-1. Negative autoregulation through the multiple N box elements. *J Biol Chem* 269:5150-5156.
136. Issack, P.S., and Ziff, E.B. 1998. Genetic elements regulating HES-1 induction in Wnt-1-transformed PC12 cells. *Cell Growth Differ* 9:827-836.
137. Truss, M., and Beato, M. 1993. Steroid hormone receptors: interaction with deoxyribonucleic acid and transcription factors. *Endocr Rev* 14:459-479.
138. Scheidereit, C., Geisse, S., Westphal, H.M., and Beato, M. 1983. The glucocorticoid receptor binds to defined nucleotide sequences near the promoter of mouse mammary tumour virus. *Nature* 304:749-752.
139. Payvar, F., DeFranco, D., Firestone, G.L., Edgar, B., Wrange, O., Okret, S., Gustafsson, J.A., and Yamamoto, K.R. 1983. Sequence-specific binding of glucocorticoid receptor to MTV DNA at sites within and upstream of the transcribed region. *Cell* 35:381-392.
140. Chan, G.C., Hess, P., Meenakshi, T., Carlstedt-Duke, J., Gustafsson, J.A., and Payvar, F. 1991. Delayed secondary glucocorticoid response elements. Unusual nucleotide motifs specify glucocorticoid receptor binding to transcribed regions of alpha 2u-globulin DNA. *J Biol Chem* 266:22634-22644.
141. Morin, B., Zhu, C., Woodcock, G.R., Li, M., Woodward, R.N., Nichols, L.A., and Holland, L.J. 2000. The binding site for Xenopus glucocorticoid receptor accessory factor and a single adjacent half-GRE form an independent glucocorticoid response unit. *Biochemistry* 39:12234-12242.
142. Canettieri, G., Morante, I., Guzman, E., Asahara, H., Herzig, S., Anderson, S.D., Yates, J.R., 3rd, and Montminy, M. 2003. Attenuation of a phosphorylation-dependent activator by an HDAC-PP1 complex. *Nat Struct Biol* 10:175-181.
143. Wadzinski, B.E., Wheat, W.H., Jaspers, S., Peruski, L.F., Jr., Lickteig, R.L., Johnson, G.L., and Klemm, D.J. 1993. Nuclear protein phosphatase 2A dephosphorylates protein kinase A-phosphorylated CREB and regulates CREB transcriptional stimulation. *Mol Cell Biol* 13:2822-2834.
144. Wu, J.J., and Bennett, A.M. 2005. Essential role for mitogen-activated protein (MAP) kinase phosphatase-1 in stress-responsive MAP kinase and cell survival signaling. *J Biol Chem* 280:16461-16466.
145. Bazuine, M., Carlotti, F., Tafrechi, R.S., Hoebe, R.C., and Maassen, J.A. 2004. Mitogen-activated protein kinase (MAPK) phosphatase-1 and -4 attenuate p38 MAPK during dexamethasone-induced insulin resistance in 3T3-L1 adipocytes. *Mol Endocrinol* 18:1697-1707.
146. Wu, J.J., Roth, R.J., Anderson, E.J., Hong, E.G., Lee, M.K., Choi, C.S., Neuffer, P.D., Shulman, G.I., Kim, J.K., and Bennett, A.M. 2006. Mice lacking MAP kinase phosphatase-1 have enhanced MAP kinase activity and resistance to diet-induced obesity. *Cell Metab* 4:61-73.
147. Parker, D., Ferreri, K., Nakajima, T., LaMorte, V.J., Evans, R., Koerber, S.C., Hoeger, C., and Montminy, M.R. 1996. Phosphorylation of CREB at Ser-133 induces complex formation with CREB-binding protein via a direct mechanism. *Mol Cell Biol* 16:694-703.

148. Radhakrishnan, I., Perez-Alvarado, G.C., Parker, D., Dyson, H.J., Montminy, M.R., and Wright, P.E. 1997. Solution structure of the KIX domain of CBP bound to the transactivation domain of CREB: a model for activator:coactivator interactions. *Cell* 91:741-752.
149. Radhakrishnan, I., Perez-Alvarado, G.C., Parker, D., Dyson, H.J., Montminy, M.R., and Wright, P.E. 1999. Structural analyses of CREB-CBP transcriptional activator-coactivator complexes by NMR spectroscopy: implications for mapping the boundaries of structural domains. *J Mol Biol* 287:859-865.
150. Lee, J.S., Zhang, X., and Shi, Y. 1996. Differential interactions of the CREB/ATF family of transcription factors with p300 and adenovirus E1A. *J Biol Chem* 271:17666-17674.
151. Imai, E., Miner, J.N., Mitchell, J.A., Yamamoto, K.R., and Granner, D.K. 1993. Glucocorticoid receptor-cAMP response element-binding protein interaction and the response of the phosphoenolpyruvate carboxykinase gene to glucocorticoids. *J Biol Chem* 268:5353-5356.
152. Sheppard, K.A., Phelps, K.M., Williams, A.J., Thanos, D., Glass, C.K., Rosenfeld, M.G., Gerritsen, M.E., and Collins, T. 1998. Nuclear integration of glucocorticoid receptor and nuclear factor-kappaB signaling by CREB-binding protein and steroid receptor coactivator-1. *J Biol Chem* 273:29291-29294.
153. Angulo, P. 2006. NAFLD, obesity, and bariatric surgery. *Gastroenterology* 130:1848-1852.
154. Tsukamoto, H. 2005. Fat paradox in liver disease. *Keio J Med* 54:190-192.
155. Westerbacka, J., Kolak, M., Kiviluoto, T., Arkkila, P., Siren, J., Hamsten, A., Fisher, R.M., and Yki-Jarvinen, H. 2007. Genes involved in fatty acid partitioning and binding, lipolysis, monocyte/macrophage recruitment and inflammation are overexpressed in the human fatty liver of insulin resistant subjects. *Diabetes*.
156. Matsusue, K., Haluzik, M., Lambert, G., Yim, S.H., Gavrilova, O., Ward, J.M., Brewer, B., Jr., Reitman, M.L., and Gonzalez, F.J. 2003. Liver-specific disruption of PPARgamma in leptin-deficient mice improves fatty liver but aggravates diabetic phenotypes. *J Clin Invest* 111:737-747.
157. Yu, S., Matsusue, K., Kashireddy, P., Cao, W.Q., Yeldandi, V., Yeldandi, A.V., Rao, M.S., Gonzalez, F.J., and Reddy, J.K. 2003. Adipocyte-specific gene expression and adipogenic steatosis in the mouse liver due to peroxisome proliferator-activated receptor gamma1 (PPARgamma1) overexpression. *J Biol Chem* 278:498-505.
158. Gavrilova, O., Haluzik, M., Matsusue, K., Cutson, J.J., Johnson, L., Dietz, K.R., Nicol, C.J., Vinson, C., Gonzalez, F.J., and Reitman, M.L. 2003. Liver peroxisome proliferator-activated receptor gamma contributes to hepatic steatosis, triglyceride clearance, and regulation of body fat mass. *J Biol Chem* 278:34268-34276.
159. Schadinger, S.E., Bucher, N.L., Schreiber, B.M., and Farmer, S.R. 2005. PPARgamma2 regulates lipogenesis and lipid accumulation in steatotic hepatocytes. *Am J Physiol Endocrinol Metab* 288:E1195-1205.
160. Bugianesi, E., McCullough, A.J., and Marchesini, G. 2005. Insulin resistance: a metabolic pathway to chronic liver disease. *Hepatology* 42:987-1000.
161. Lewis, G.F., Carpentier, A., Adeli, K., and Giacca, A. 2002. Disordered fat storage and mobilization in the pathogenesis of insulin resistance and type 2 diabetes. *Endocr Rev* 23:201-229.
162. Usami, A., Ueki, S., Ito, W., Kobayashi, Y., Chiba, T., Mahemuti, G., Oyamada, H., Kamada, Y., Fujita, M., Kato, H., et al. 2006. Theophylline and dexamethasone induce peroxisome proliferator-activated receptor-gamma expression in human eosinophils. *Pharmacology* 77:33-37.

163. Hausman, G.J. 2003. Dexamethasone induced preadipocyte recruitment and expression of CCAAT/enhancing binding protein alpha and peroxisome proliferator activated receptor-gamma proteins in porcine stromal-vascular (S-V) cell cultures obtained before and after the onset of fetal adipogenesis. *Gen Comp Endocrinol* 133:61-70.
164. She, Q.M., Zhao, J., Wang, X.L., Zhou, C.M., and Shi, X.Z. 2007. Effect of dexamethasone on peroxisome proliferator activated receptor-gamma mRNA expression in 3T3-L1 adipocytes with the human recombinant adiponectin. *Chin Med J (Engl)* 120:155-158.
165. Vidal-Puig, A.J., Considine, R.V., Jimenez-Linan, M., Werman, A., Pories, W.J., Caro, J.F., and Flier, J.S. 1997. Peroxisome proliferator-activated receptor gene expression in human tissues. Effects of obesity, weight loss, and regulation by insulin and glucocorticoids. *J Clin Invest* 99:2416-2422.
166. Razani, B., Combs, T.P., Wang, X.B., Frank, P.G., Park, D.S., Russell, R.G., Li, M., Tang, B., Jelicks, L.A., Scherer, P.E., et al. 2002. Caveolin-1-deficient mice are lean, resistant to diet-induced obesity, and show hypertriglyceridemia with adipocyte abnormalities. *J Biol Chem* 277:8635-8647.
167. Cohen, A.W., Razani, B., Wang, X.B., Combs, T.P., Williams, T.M., Scherer, P.E., and Lisanti, M.P. 2003. Caveolin-1-deficient mice show insulin resistance and defective insulin receptor protein expression in adipose tissue. *Am J Physiol Cell Physiol* 285:C222-235.
168. Van Nieuwenhoven, F.A., Verstijnen, C.P., Abumrad, N.A., Willemsen, P.H., Van Eys, G.J., Van der Vusse, G.J., and Glatz, J.F. 1995. Putative membrane fatty acid translocase and cytoplasmic fatty acid-binding protein are co-expressed in rat heart and skeletal muscles. *Biochem Biophys Res Commun* 207:747-752.
169. Poirier, H., Degrace, P., Niot, I., Bernard, A., and Besnard, P. 1996. Localization and regulation of the putative membrane fatty-acid transporter (FAT) in the small intestine. Comparison with fatty acid-binding proteins (FABP). *Eur J Biochem* 238:368-373.
170. Abumrad, N.A., el-Maghrabi, M.R., Amri, E.Z., Lopez, E., and Grimaldi, P.A. 1993. Cloning of a rat adipocyte membrane protein implicated in binding or transport of long-chain fatty acids that is induced during preadipocyte differentiation. Homology with human CD36. *J Biol Chem* 268:17665-17668.
171. Coburn, C.T., Hajri, T., Ibrahim, A., and Abumrad, N.A. 2001. Role of CD36 in membrane transport and utilization of long-chain fatty acids by different tissues. *J Mol Neurosci* 16:117-121; discussion 151-117.
172. Febbraio, M., Abumrad, N.A., Hajjar, D.P., Sharma, K., Cheng, W., Pearce, S.F., and Silverstein, R.L. 1999. A null mutation in murine CD36 reveals an important role in fatty acid and lipoprotein metabolism. *J Biol Chem* 274:19055-19062.
173. Llaverias, G., Vazquez-Carrera, M., Sanchez, R.M., Noe, V., Ciudad, C.J., Laguna, J.C., and Alegret, M. 2004. Rosiglitazone upregulates caveolin-1 expression in THP-1 cells through a PPAR-dependent mechanism. *J Lipid Res* 45:2015-2024.
174. Chawla, A., Barak, Y., Nagy, L., Liao, D., Tontonoz, P., and Evans, R.M. 2001. PPAR-gamma dependent and independent effects on macrophage-gene expression in lipid metabolism and inflammation. *Nat Med* 7:48-52.
175. Moore, K.J., Rosen, E.D., Fitzgerald, M.L., Randow, F., Andersson, L.P., Altshuler, D., Milstone, D.S., Mortensen, R.M., Spiegelman, B.M., and Freeman, M.W. 2001. The role of PPAR-gamma in macrophage differentiation and cholesterol uptake. *Nat Med* 7:41-47.
176. Inoue, M., Ohtake, T., Motomura, W., Takahashi, N., Hosoki, Y., Miyoshi, S., Suzuki, Y., Saito, H., Kohgo, Y., and Okumura, T. 2005. Increased expression of PPARgamma in high fat diet-induced liver steatosis in mice. *Biochem Biophys Res Commun* 336:215-222.

177. Kretz, O., Reichardt, H.M., Schutz, G., and Bock, R. 1999. Corticotropin-releasing hormone expression is the major target for glucocorticoid feedback-control at the hypothalamic level. *Brain Res* 818:488-491.
178. Friedman, J.E., Sun, Y., Ishizuka, T., Farrell, C.J., McCormack, S.E., Herron, L.M., Hakimi, P., Lechner, P., and Yun, J.S. 1997. Phosphoenolpyruvate carboxykinase (GTP) gene transcription and hyperglycemia are regulated by glucocorticoids in genetically obese db/db transgenic mice. *J Biol Chem* 272:31475-31481.
179. Blokzijl, A., Dahlqvist, C., Reissmann, E., Falk, A., Moliner, A., Lendahl, U., and Ibanez, C.F. 2003. Cross-talk between the Notch and TGF-beta signaling pathways mediated by interaction of the Notch intracellular domain with Smad3. *J Cell Biol* 163:723-728.
180. Aguilera, C., Hoya-Arias, R., Haegeman, G., Espinosa, L., and Bigas, A. 2004. Recruitment of IkappaBalpha to the hes1 promoter is associated with transcriptional repression. *Proc Natl Acad Sci U S A* 101:16537-16542.
181. Shinozuka, Y., Okada, M., Oki, T., Sagane, K., Mizui, Y., Tanaka, I., Katayama, K., and Murakami-Murofushi, K. 2001. Altered expression of HES-1, BETA2/NeuroD, and PDX-1 is involved in impaired insulin synthesis induced by glucocorticoids in HIT-T15 cells. *Biochem Biophys Res Commun* 287:229-235.
182. Cantarini, M.C., de la Monte, S.M., Pang, M., Tong, M., D'Errico, A., Trevisani, F., and Wands, J.R. 2006. Aspartyl-asparagyl beta hydroxylase over-expression in human hepatoma is linked to activation of insulin-like growth factor and notch signaling mechanisms. *Hepatology* 44:446-457.
183. Stockhausen, M.T., Sjolund, J., and Axelson, H. 2005. Regulation of the Notch target gene Hes-1 by TGFalpha induced Ras/MAPK signaling in human neuroblastoma cells. *Exp Cell Res* 310:218-228.
184. Fu, J., Tay, S.S., Ling, E.A., and Dheen, S.T. 2006. High glucose alters the expression of genes involved in proliferation and cell-fate specification of embryonic neural stem cells. *Diabetologia* 49:1027-1038.
185. Sasai, Y., Kageyama, R., Tagawa, Y., Shigemoto, R., and Nakanishi, S. 1992. Two mammalian helix-loop-helix factors structurally related to Drosophila hairy and Enhancer of split. *Genes Dev* 6:2620-2634.
186. Ishibashi, M., Ang, S.L., Shiota, K., Nakanishi, S., Kageyama, R., and Guillemot, F. 1995. Targeted disruption of mammalian hairy and Enhancer of split homolog-1 (HES-1) leads to up-regulation of neural helix-loop-helix factors, premature neurogenesis, and severe neural tube defects. *Genes Dev* 9:3136-3148.
187. Ohtsuka, T., Ishibashi, M., Gradwohl, G., Nakanishi, S., Guillemot, F., and Kageyama, R. 1999. Hes1 and Hes5 as notch effectors in mammalian neuronal differentiation. *Embo J* 18:2196-2207.
188. Kunisato, A., Chiba, S., Nakagami-Yamaguchi, E., Kumano, K., Saito, T., Masuda, S., Yamaguchi, T., Osawa, M., Kageyama, R., Nakauchi, H., et al. 2003. HES-1 preserves purified hematopoietic stem cells ex vivo and accumulates side population cells in vivo. *Blood* 101:1777-1783.
189. Kumano, K., Chiba, S., Shimizu, K., Yamagata, T., Hosoya, N., Saito, T., Takahashi, T., Hamada, Y., and Hirai, H. 2001. Notch1 inhibits differentiation of hematopoietic cells by sustaining GATA-2 expression. *Blood* 98:3283-3289.
190. Shojaei, F., Trowbridge, J., Gallacher, L., Yuefei, L., Goodale, D., Karanu, F., Levac, K., and Bhatia, M. 2005. Hierarchical and ontogenic positions serve to define the molecular basis of human hematopoietic stem cell behavior. *Dev Cell* 8:651-663.
191. Matsue, M., Kageyama, R., Denhardt, D.T., and Noda, M. 1997. Helix-loop-helix-type transcription factor (HES-1) is expressed in osteoblastic cells, suppressed by 1,25(OH)2

- vitamin D3, and modulates 1,25(OH)₂ vitamin D3 enhancement of osteopontin gene expression. *Bone* 20:329-334.
192. Deregowski, V., Gaggero, E., Priest, L., Rydziel, S., and Canalis, E. 2006. Notch 1 overexpression inhibits osteoblastogenesis by suppressing Wnt/beta-catenin but not bone morphogenetic protein signaling. *J Biol Chem* 281:6203-6210.
193. Ross, D.A., Rao, P.K., and Kadesch, T. 2004. Dual roles for the Notch target gene Hes-1 in the differentiation of 3T3-L1 preadipocytes. *Mol Cell Biol* 24:3505-3513.
194. Soukas, A., Socci, N.D., Saatkamp, B.D., Novelli, S., and Friedman, J.M. 2001. Distinct transcriptional profiles of adipogenesis in vivo and in vitro. *J Biol Chem* 276:34167-34174.
195. Ross, D.A., Hannenhalli, S., Tobias, J.W., Cooch, N., Shiekhata, R., and Kadesch, T. 2006. Functional analysis of Hes-1 in preadipocytes. *Mol Endocrinol* 20:698-705.
196. Kamakura, S., Oishi, K., Yoshimatsu, T., Nakafuku, M., Masuyama, N., and Gotoh, Y. 2004. Hes binding to STAT3 mediates crosstalk between Notch and JAK-STAT signalling. *Nat Cell Biol* 6:547-554.
197. Inoue, H., Ogawa, W., Ozaki, M., Haga, S., Matsumoto, M., Furukawa, K., Hashimoto, N., Kido, Y., Mori, T., Sakaue, H., et al. 2004. Role of STAT-3 in regulation of hepatic gluconeogenic genes and carbohydrate metabolism in vivo. *Nat Med* 10:168-174.
198. Inoue, H., Ogawa, W., Asakawa, A., Okamoto, Y., Nishizawa, A., Matsumoto, M., Teshigawara, K., Matsuki, Y., Watanabe, E., Hiramatsu, R., et al. 2006. Role of hepatic STAT3 in brain-insulin action on hepatic glucose production. *Cell Metab* 3:267-275.
199. Fisher, A.L., Ohsako, S., and Caudy, M. 1996. The WRPW motif of the hairy-related basic helix-loop-helix repressor proteins acts as a 4-amino-acid transcription repression and protein-protein interaction domain. *Mol Cell Biol* 16:2670-2677.
200. Fisher, A.L., and Caudy, M. 1998. Groucho proteins: transcriptional corepressors for specific subsets of DNA-binding transcription factors in vertebrates and invertebrates. *Genes Dev* 12:1931-1940.
201. Nuthall, H.N., Husain, J., McLaren, K.W., and Stifani, S. 2002. Role for Hes1-induced phosphorylation in Groucho-mediated transcriptional repression. *Mol Cell Biol* 22:389-399.
202. Guardiola-Diaz, H.M., Kolinske, J.S., Gates, L.H., and Seasholtz, A.F. 1996. Negative glucocorticoid regulation of cyclic adenosine 3', 5'-monophosphate-stimulated corticotropin-releasing hormone-reporter expression in AtT-20 cells. *Mol Endocrinol* 10:317-329.
203. Alcorn, J.L., Islam, K.N., Young, P.P., and Mendelson, C.R. 2004. Glucocorticoid inhibition of SP-A gene expression in lung type II cells is mediated via the TTF-1-binding element. *Am J Physiol Lung Cell Mol Physiol* 286:L767-776.
204. Focking, M., Holker, I., and Trapp, T. 2003. Chronic glucocorticoid receptor activation impairs CREB transcriptional activity in clonal neurons. *Biochem Biophys Res Commun* 304:720-723.
205. Rosen, L.B., Majzoub, J.A., and Adler, G.K. 1992. Effects of glucocorticoid on corticotropin-releasing hormone gene regulation by second messenger pathways in NPLC and AtT-20 cells. *Endocrinology* 130:2237-2244.
206. Del Monaco, M., Covello, S.P., Kennedy, S.H., Gilinger, G., Litwack, G., and Uitto, J. 1997. Identification of novel glucocorticoid-response elements in human elastin promoter and demonstration of nucleotide sequence specificity of the receptor binding. *J Invest Dermatol* 108:938-942.
207. Chandrasekhar, S., Souba, W.W., and Abcouwer, S.F. 1999. Identification of glucocorticoid-responsive elements that control transcription of rat glutamine synthetase. *Am J Physiol* 276:L319-331.

208. Forman, B.M., and Samuels, H.H. 1990. Interactions among a subfamily of nuclear hormone receptors: the regulatory zipper model. *Mol Endocrinol* 4:1293-1301.
209. Jarriault, S., Le Bail, O., Hirsinger, E., Pourquie, O., Logeat, F., Strong, C.F., Brou, C., Seidah, N.G., and Israel, A. 1998. Delta-1 activation of notch-1 signaling results in HES-1 transactivation. *Mol Cell Biol* 18:7423-7431.
210. Orellana, S.A., and McKnight, G.S. 1992. Mutations in the catalytic subunit of cAMP-dependent protein kinase result in unregulated biological activity. *Proc Natl Acad Sci U S A* 89:4726-4730.